NAA-SR-MEMO-8679
REVISION 1
COPY 149
99 PAGES

SNAP 10A REACTOR DESIGN SUMMARY, REVISION 1

(Title Unclassified)

ATOMICS INTERNATIONAL
A DIVISION OF NORTH AMERICAN AVIATION, INC.

Atomics International Division
Rockwell International

U

CLASSIFICATION LEVEL
(S, C OR U)

DOCUMENT NO.

NAA-SR-MEMO-8679

COVER SHEET

DOCUMENT TITLE

SNAP 10A Reactor Design Summary, Revision 1

AUTHOR

W. W. Davis
J Susnir

THIS IS AN INTERNAL WORKING DOCUMENT AND MAY BE EXPANDED, MODIFIED, OR WITHDRAWN AT ANY TIME. ~~IT IS INTENDED FOR INTERNAL USE ONLY.~~

CLASSIFICATION TYPE
(RD OR DI)

~~THIS REPORT MAY NOT BE PUBLISHED WITHOUT THE APPROVAL OF THE PATENT BRANCH, AEC.~~

U

CLASSIFICATION LEVEL
(S, C OR U)

DO NOT REMOVE THIS SHEET

CONFIDENTIAL SECRET

NAA-SR-MEMO-8679
REVISION 1
SPECIAL DISTRIBUTION

SNAP 10A REACTOR DESIGN SUMMARY, REVISION 1

(Title Unclassified)

Edited By
W.W. DAVIS
J. SUSNIR

RESTRICTED DATA

This document contains restricted data as defined in the Atomic Energy Act of 1954. Its transmittal or the disclosure of its contents in any manner to an unauthorized person is prohibited.

This document contains Secret-Restricted Data relating to civilian applications of atomic energy.

ATOMICS INTERNATIONAL
A DIVISION OF NORTH AMERICAN AVIATION, INC.
P.O. BOX 309 CANOGA PARK, CALIFORNIA

ISSUED: OCTOBER 26, 1964

SECRET CONFIDENTIAL

CONTENTS

CONTENTS

TABLES

TABLES

FIGURES

FIGURES

ABSTRACT

A description of the SNAP 10A reactor subsystem is presented. Design details of the principal assemblies which constitute the reactor subsystem are discussed. System behavior for abnormal conditions such as disassembly during reentry, operation in rain-filled craters, and long-term operation in space are included.

I. INTRODUCTION

The SNAP 10A reactor is intended for use as a primary power source on satellites and other space vehicles. The reactor produces 39.5 thermal kilowatts which are converted to 525 electrical watts through a thermoelectric convertor. Generation of power in space requires a compact system with remote control capabilities, long life, high reliability, and an ability to operate in a space environment characterized by a high vacuum, meteoroid showers and other phenomena not common to terrestrial environments.

The core of the SNAP 10A reactor consists of uranium-zirconium alloy fuel elements clad in stainless steel. The uranium is fully enriched in U^{235} and comprises 10% by weight of the fuel. The fuel material is hydrided to an N_H of 6.35 (6.35×10^{22} atoms of hydrogen/cc) which is slightly less than the hydrogen concentration in cold water, and thus the elements also serve as moderator. The fuel elements are positioned and constrained in the core by upper and lower grid plates. The grid plates are supported by a fixed ring at the bottom and hold-down springs at the top. Beryllium side reflectors are used in the void between the hexagonal fuel element array and the circular reactor vessel. The reactor vessel top head acts both as a vessel closure and restraining structure for the core hold-down springs. The reactor vessel is surrounded by a beryllium structure which functions as the reflector. Four control drums, which form a part of the reflector assembly, provide both the fine and coarse control required for SNAP 10A reactor operation. The lithium hydride shield is positioned directly below the vessel and is contained in a stainless steel casing. A flexible mount is provided to support the LiH within the casing allowing for prelaunch thermal cycling of the system. Control devices such as electric motors, springs, and sensors are attached directly to the reflector assembly. Controlling elements such as timers and reactor controller are located in the instrument compartment.

As described above, the SNAP 10A reactor subsystem (Figure 1) consists of five major subassemblies: the reactor structure, radiation shield, reflector assembly, reactor control equipment and reactor core. Each major subassembly consists of the following components:

A. REACTOR STRUCTURE

1) Reactor vessel
2) Reactor vessel top head

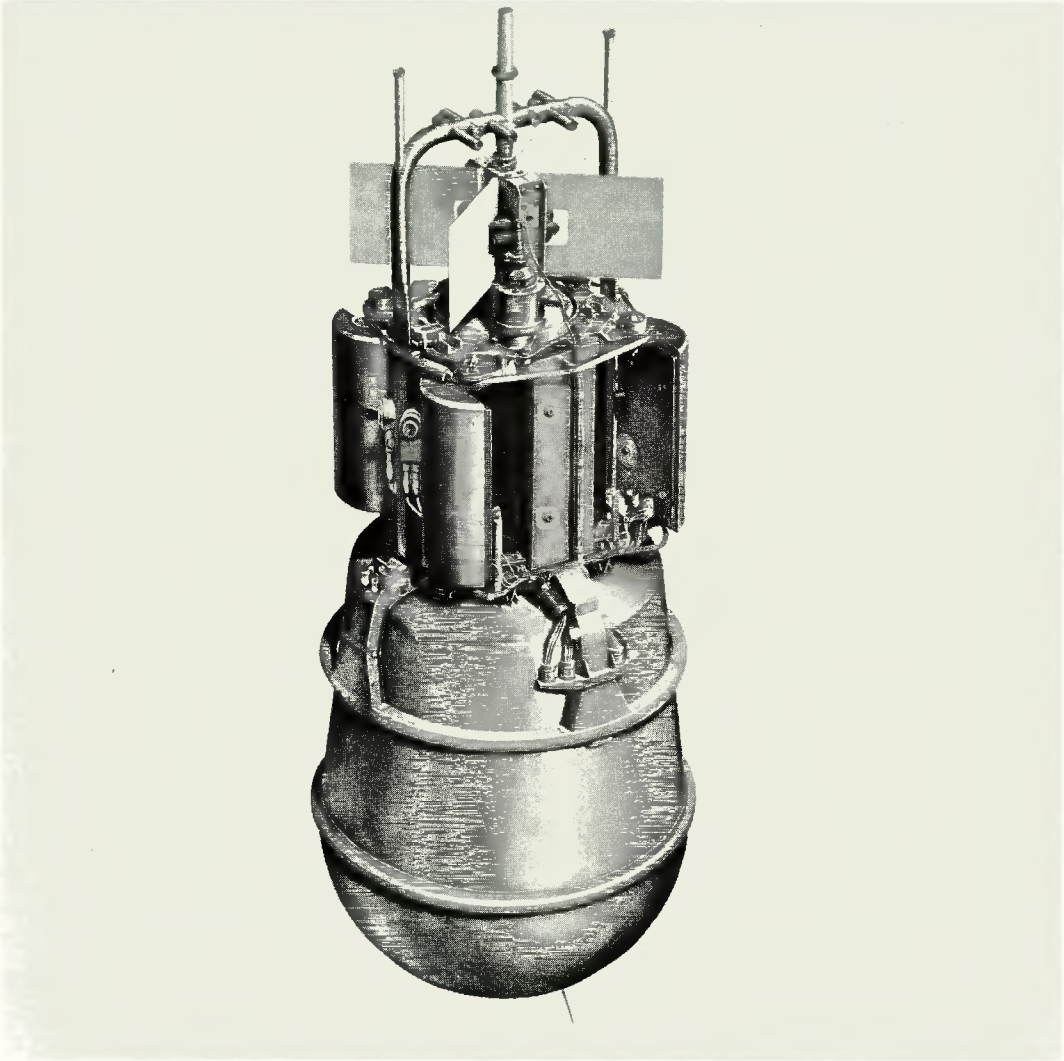

8-1-63 7623-0017

Figure 1. SNAP 10A Reactor and Shield

3) Grid plate support ring
4) Reactor vessel support structure
5) Attachment brackets for pumps, reflectors, etc.
6) Ground safety equipment (shipping sleeve)

B. RADIATION SHIELD

1) Shield casing
2) Shielding material
3) Shield support assembly

C. REFLECTOR ASSEMBLY

1) Main reflector block
2) Control drums
3) Drum drives (gears, bearings, etc.)
4) Actuator motors
5) Position indicators
6) Reflector ejection system (retaining band, springs, actuating devices, etc.)
7) Wiring harness
8) Sensors
9) Ground safety system (void filler blocks)

D. REACTOR CONTROL EQUIPMENT

1) Controller
2) Timer
3) Temperature sensor switches

E. REACTOR CORE

1) Grid plates
2) Fuel elements
3) Core positioning mechanism
4) Internal reflectors

Basic design parameters and nominal operating conditions for the SNAP 10A reactor subsystem are given in Table 1. Nominal operating conditions are defined as those which exist after hydrogen redistribution has been essentially completed or, more specifically, in the period 30 to 90 days after reactor startup. Table 2 gives the shock and vibration environment which components and subassemblies have been designed to withstand.

TABLE 1

SNAP 10A REACTOR DESIGN SUMMARY

Nominal Operating Conditions	
Reactor thermal power (kwt)	39.5
Net electrical power (watt) – Minimum	525
Operating life	1 yr
NaK outlet temperature (°F)	987
NaK inlet temperature (°F)	859
NaK operating pressure (psia)	5
Maximum fuel temperature (°F)	1058
Maximum cladding temperature (°F)	1037
Reactor Design	
Fuel elements	
Number	37
Fuel alloy (wt % U in Zr)	10
Degree of hydriding N_H (10^{22} atom/cm^3)	6.35
Cladding material	Hastelloy-N
Fuel diameter (in.)	1.210
Cladding diameter (OD, in.)	1.25
Cladding thickness (in.)	0.015
Active fuel length (in.)	12.25
Core Vessel	
Material	316 SS
Internal diameter (in.)	8.875
Length (in.)	15.6
Minimum wall thickness (in.)	0.032
Inlet plenum grid plate (lower)	
Material	316 SS
Thickness (in.)	1/2 (sandwich construction)
Outlet plenum grid plate (upper)	
Material	316 SS
Thickness (in.)	1/8
Reflector	
Material	Be
Configuration	Cylindrical sleeve
Nominal thickness (in.)	2
Reflector control elements	
Number	4
Material	Be
Nominal thickness (in.)	2
Internal reflectors	
Material	Be
Cladding	None
Nuclear Parameters	
Average core thermal flux (n/cm^2-sec)	2.5×10^{11}
Mean fission energy (ev)	0.12
Isothermal temperature coefficient at nominal operating conditions (¢/°F)	-0.29
Uranium loading (kg U^{235})	4.75
Effective delayed neutron fraction	0.008
Mean prompt neutron lifetime (μ-sec)	6.5
Burnable poison	
Material	Sm_2O_3
Prepoison reactivity worth ($)†	-1.60
Initial cold excess reactivity ($)†	+3.00
Total lifetime reactivity loss ($)†	-2.58
Xenon equilibrium	-0.17
Samarium burnout	+0.17
Temperature and power defect	-2.25
Hydrogen loss	-0.03
Hydrogen redistribution	-0.20
Burnup and fission product poisons	-0.10
Contingency ($)†	+0.42
Total control drum worth with no shims ($)†	8.60
Total shim capability ($)†	1.26
Shield Parameters	
Material	LiH (cold pressed)
Dimensions	
Maximum diameter (in.)	21.08
Minimum diameter (in.)	17.56
Height (in.)	27.47
Shield casing	
Material	316 SS
Minimum thickness (in.)	0.032
Integrated radiation doses below shield for 1 year of full power operation (fast neutrons and gammas)	
Mating plane (NPU-Booster)	
Center of plane r = o	8.6×10^{12} nvt 7.3×10^{6} r
Inner edge of instrumentation compartment (max) (r = 13-3/4 in.)	1.6×10^{13} nvt 9.6×10^{6} r
Outer edge of instrumentation compartment (max) (r = 24-1/2 in.)	3.8×10^{14} nvt 1.1×10^{7} r
Reference plane (17-1/2 ft below core)	
Center of plane r = 0	2.6×10^{12} nvt 1.9×10^{6} r
Outer edge of plane (max) (r - 30 in.)	3.8×10^{13} nvt 2.8×10^{6} r
Weight Summary	
Reactor core and vessel assembly (lb)	167
Reflector-control assembly (lb)	107
Shield assembly (lb)	217
Electronic equipment (lb)	8
Total nuclear system (lb)	499

†One dollar = 0.008 $\Delta k/k$

TABLE 2

SHOCK AND VIBRATION ENVIRONMENT PARAMETERS OF SNAP 10A REACTOR SUBSYSTEM TESTS

	Shock				Vibration		
	Shape	Axes	Magnitude (g)	Duration (μ sec)	Axes	Magnitude (g)	Frequency (cps)
Assemblies	Half sine wave	Longitudinal	5.5	8	Longitudinal	0.5 in. DA	5 to 12
						3.5	12 to 400
		Lateral and Normal	1.5			7.5	400 to 3000
					Lateral and Normal	0.5 in. DA	5 to 10
						2.5	10 to 250
						5	250 to 400
						7.5	400 to 3000
Components	Half sine wave	Longitudinal	20	6	Longitudinal	1/4 in. DA	5 to 30
						12*	30 to 250
		Lateral and Normal	10			5	250 to 400
						7.5	400 to 3000
					Lateral and Normal	1/4 in. DA	5 to 20
						5	20 to 400
						7.5	400 to 3000

*Instrument compartment components only. Other reactor subsystem components are required to withstand 5g over this frequency range

II. REACTOR STRUCTURE AND CORE

The SNAP 10A reactor structure has been designed to support the reactor core, reflectors, and NaK coolant pump, and to contain the NaK during prelaunch checkout, launch, and orbital operating conditions. Structural behavior under a variety of environmental conditions was considered in establishing the final configuration. Environmental conditions studied are listed below.

a) Accelerations during launch

b) Coolant system pressure

c) Space vacuum

d) Corrosion by NaK

e) Elevated temperature

f) Neutron flux

The reactor structure and core consists of a reactor vessel assembly, 1 top head, 2 grid plates, 6 internal reflectors, 12 hold-down springs, 37 fuel elements, and 4 support legs. The reactor core and vessel (including grid plates) weighs 167 lb. Approximately 7 lb of this is NaK coolant.

The reactor vessel assembly shown in Figure 2 consists of a deep drawn and spun reactor vessel to which a support ring, 2 NaK inlet pipes, and reflector support bracketry are welded. The assembly is constructed entirely of stainless steel, Type 316. The reactor vessel has an inside diameter of 8.875 in. and an overall length of approximately 16 in. It is essentially a right circular cylinder with the lower closure an inverted dome. Wall thicknesses vary from 0.032 in. in the core region to 0.125 in. in areas to which attachments are welded. The fuel elements are supported and positioned in the reactor vessel by the 2 grid plates which are shown in Figures 3 and 4. The diameter of the upper grid plate is 8.830 in.; the lower plate is 8.750 in. in diameter. Each plate is fabricated from Type 316 Stainless Steel. The upper plate is a single piece of material 0.125 in. thick. The lower plate is a brazed assembly consisting of a 0.060-in. thick baffle plate and a 0.060-in. thick orifice plate with spacers between them. The overall thickness of the lower grid plate is 0.500 in. The plates have 37 holes arranged on a 1.260-in. triangular pitch for positioning the fuel elements. The plates are also perforated with 72 holes on a 0.728-in. triangular pitch for coolant flow. The diameter of the flow holes in the upper

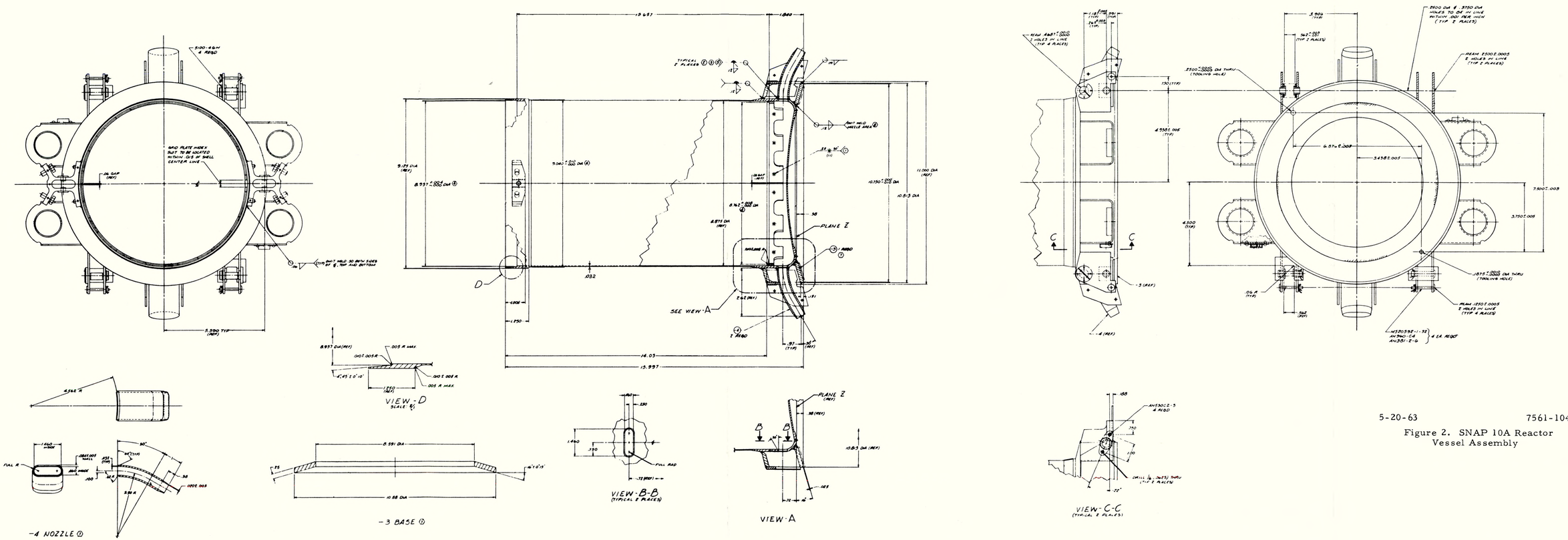

5-20-63 7561-1049

Figure 2. SNAP 10A Reactor Vessel Assembly

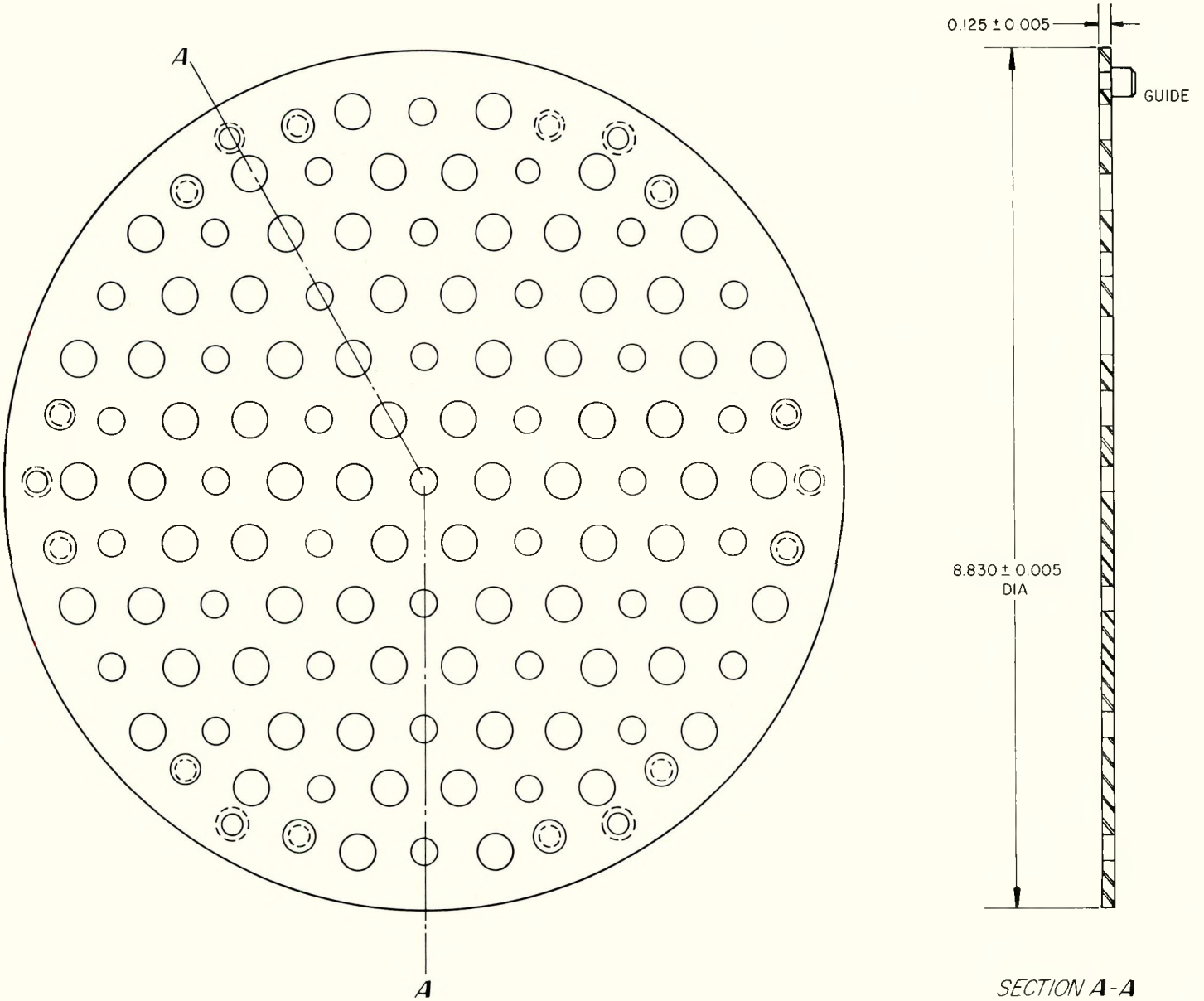

Figure 3. SNAP 10A Upper Gridplate Design

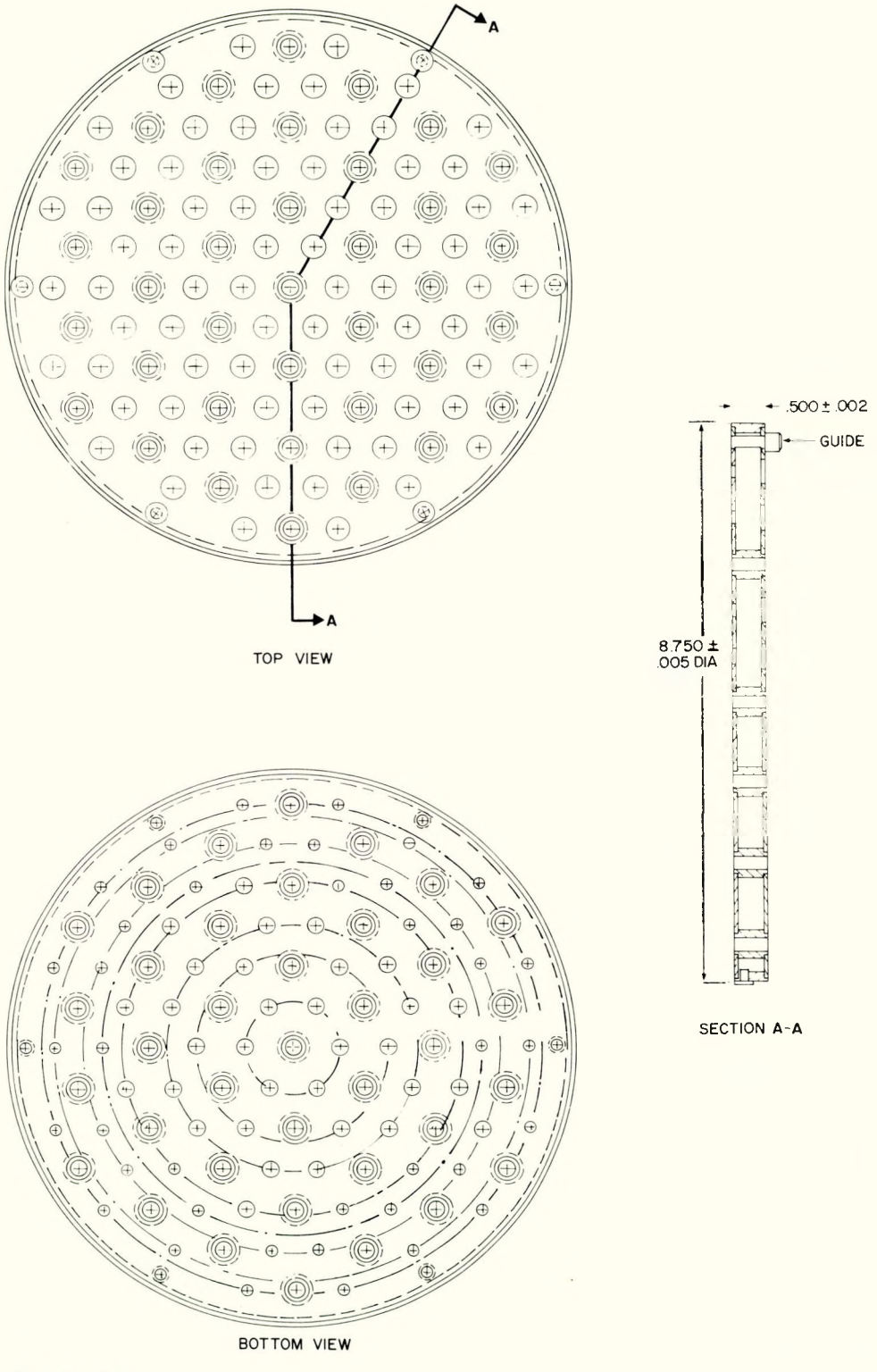

Figure 4. SNAP 10A Lower Gridplate

grid plate, and the baffle plate of the lower grid plate is 0.375 in. The diameter of the flow holes in the orifice plate varies from 0.250 in., surrounding the central fuel element, to 0.188 in. at the outermost ones. Six pins are attached to each plate for positioning of the internal reflectors. Twelve pins are attached to the upper grid plate for location of the core hold-down springs.

Six beryllium internal side reflectors as shown in Figure 5 are positioned between the grid plates; pins in the grid plates mate with holes in the reflectors. The reflectors are 12.455 in. in length and are shaped to fit fuel element and reactor vessel wall contours. The internal reflectors have no major structural function.

The reactor vessel top head, Figure 6, is the final closure for the reactor vessel. It is forged from stainless steel, Type 316. In finished form, it is a 150° cone with a NaK outlet at the center and a flange at the outer edge for attachment to the reactor vessel. The wall thickness of the conical section is 0.095 in. Sockets are forged in the head for locating the core hold-down springs and also for attachment of the pump support outriggers. The flange has an extended lip which is welded to the reactor vessel. This simplifies the final closure operation and provides a configuration which facilitates top head burnoff during atmospheric reentry.

Twelve core hold-down springs are compressed between the reactor vessel top head and the upper grid plate. These springs hold the core in place during launch operations but allow relative thermal expansion between the core and reactor vessel. The springs are fabricated from Rene 41 wire and exert a force of 37.5 lb each as installed. Free and compressed lengths are 0.605 and 0.500 in., respectively.

The reactor is supported on the converter structure by four support legs (Figure 7) formed from 0.032-in. 6AL-4V titanium alloy and welded. The legs are designed to support the reactor structure, with NaK pump and reflectors attached, during launch. The legs permit relative thermal expansion between the reactor and converter structure. The support legs are attached to both reactor and converter structures with blind bolts.

During launch the reactor structure will experience simultaneous accelerations in both longitudinal and lateral directions. For design calculations, three extreme conditions were considered:

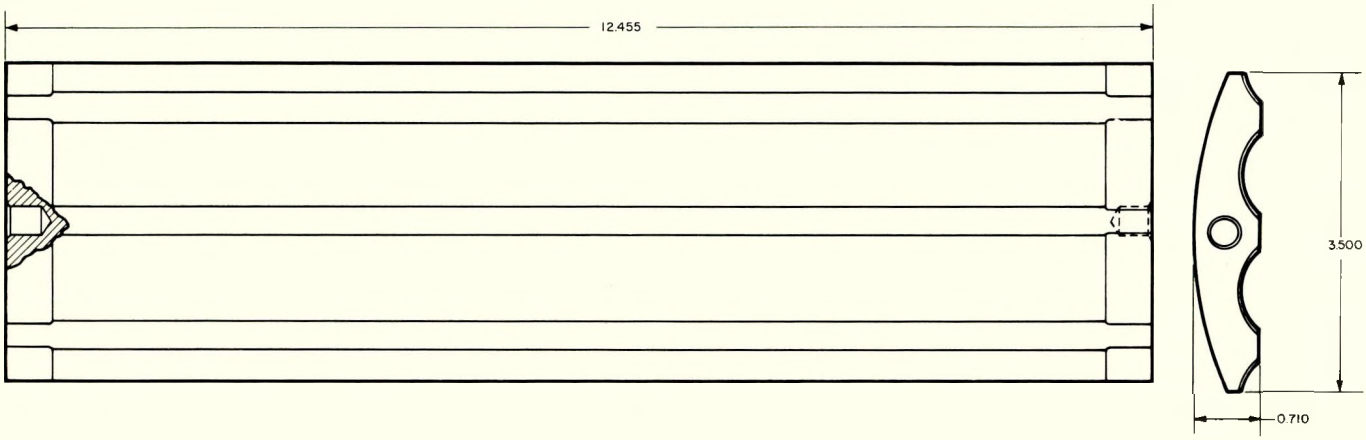

9-30-63

7623-0057

Figure 5. SNAP 10A Reactor Vessel Internal Reflectors

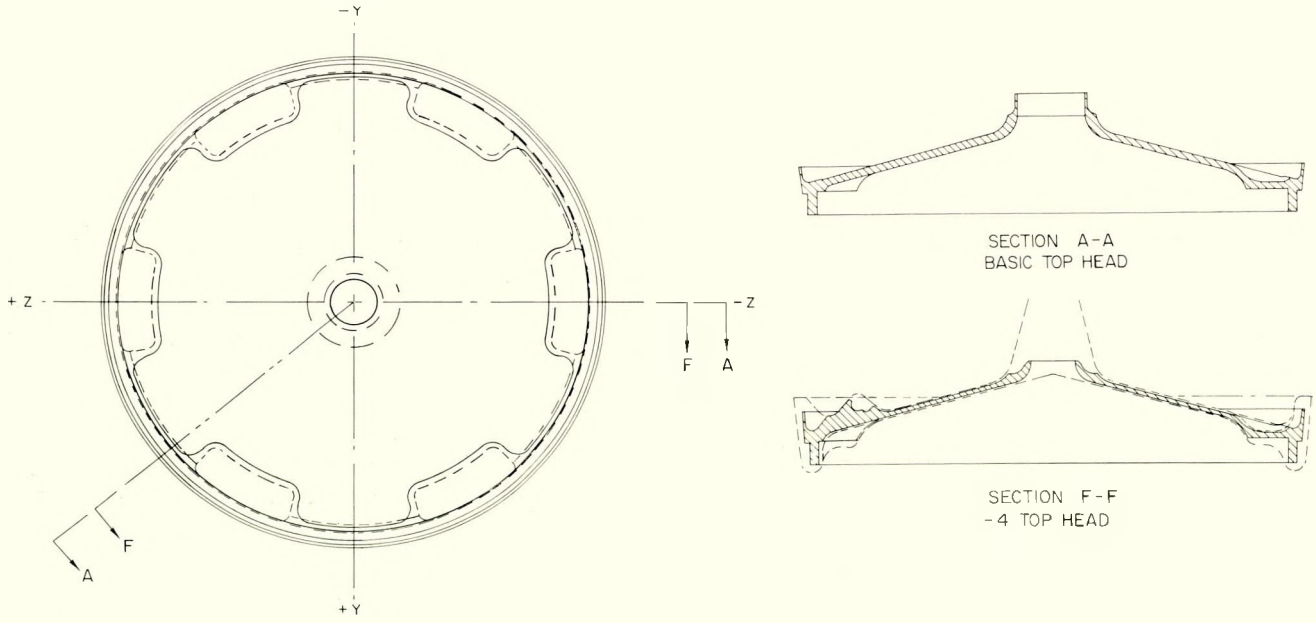

7-15-63

7623-0015

Figure 6. SNAP 10A Reactor Vessel Top Head

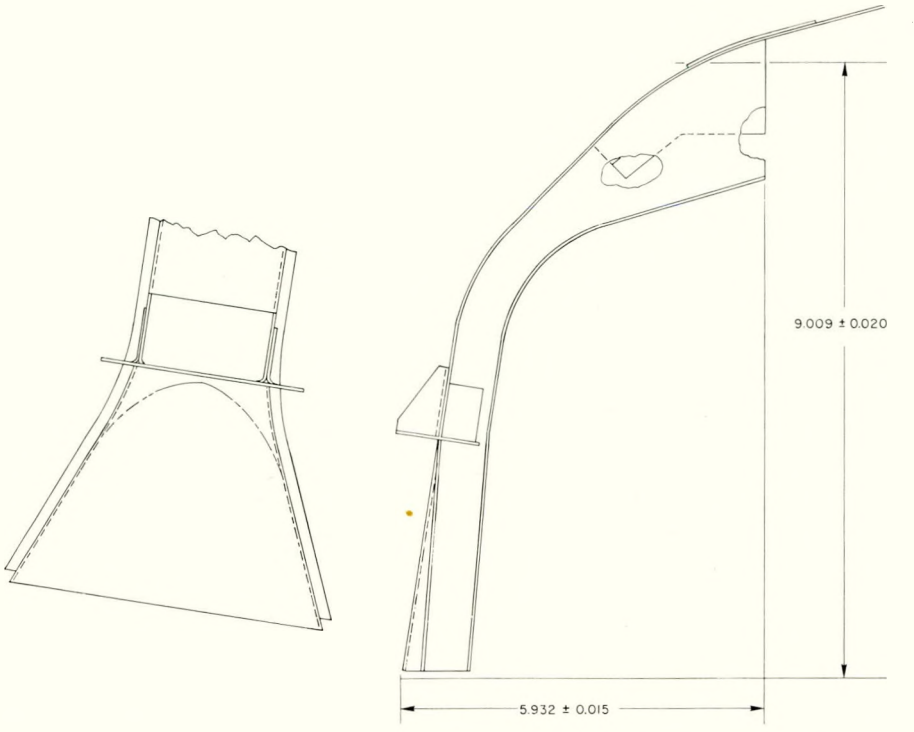

7-15-63 7623-0016

Figure 7. SNAP 10A Reactor Support Legs

a) 7.5 g aft ±1.0 g lateral

b) 2.5 g forward ±1.0 g lateral

c) ±2.0 g longitudinal ±5.0 g lateral

Because the reactor structure is cantilevered on the support legs in the lateral direction, condition (c) has proved to be the most severe mode of loading. The most critical area is the "knee" of the support legs. Stresses calculated on the basis of static loading indicate a factor of safety of about four on the ultimate load-carrying capacity. Because of the low ductility of titanium, a fatigue problem is created by stress concentration in welded areas; the safety margin is very much reduced. Experimental studies, however, have confirmed the integrity of the design. Other critical areas include the blind bolt joints between the legs and the vessel and the attachment between the vessel and reflector positioning bracket. Unlike the support legs, local failure in these two cases would not necessarily jeopardize mission success.

Because launch loading and fabricability impose more stringent design requirements on the reactor vessel and top head than does internal pressure at power operation, the stresses under normal orbital operation conditions are quite nominal. Thermal stresses, even under transient startup conditions, are likewise small. The pressure drop through the entire reactor is 0.17 psi and provides no significant load on the grid plates.

By proper selection of materials, problems created by space vacuum and NaK corrosion have been eliminated. Irradiation damage to the reactor structure during the design lifetime is expected to be negligible since the integrated fast neutron flux is well below the 10^{21} nvt considered to cause problems in austenitic stainless steel. The portions of the reactor exposed to meteoroid bombardment are the top head and the top portion of the vessel where the wall thickness is 0.095 in. For structural reasons, these surfaces are much thicker than required for meteoroid protection.

III. RADIATION SHIELD

The SNAP 10A shield is a shadow shield. Its configuration is determined by the outer extremities of the reactor assembly and the 5-ft-diameter reference dose plane, located 17.5 ft below the bottom of the reactor core. The shield assembly is located directly below the reactor and has a total weight of 217 lb. For normal reactor operation at an average thermal power of 39.5 kw for 1 yr, the gamma dose rate and fast neutron (>0.1 Mev) flux levels at various locations on the reference dose plane and the SNAP 10A-Agena mating plane are listed in Table 3.

TABLE 3

GAMMA AND FAST NEUTRON FLUX LEVELS FOR NORMAL REACTOR OPERATION FOR 1 YR

Plane	Location	Fast Neutrons (n/cm^2/yr at 39.5 kwt)			Gamma Dose Rate (r/yr at 39.5 kwt)
		Radius (in.)	Minimum	Maximum*	
Mating	Centerline	0	8.6×10^{12}	8.6×10^{12}	7.3×10^{6}
Mating	Instrument compartment inner edge	13-3/4	1.3×10^{13}	1.6×10^{13}	9.6×10^{6}
Mating	Instrument compartment outer edge	24-1/2	1.4×10^{14}	3.8×10^{14}	1.1×10^{7}
Mating	Outer edge of plane	30	4.4×10^{14}	7.6×10^{14}	1.2×10^{7}
Reference	Centerline	0	2.6×10^{12}	2.6×10^{12}	1.9×10^{6}
Reference	Outer edge of plane	30	1.0×10^{13}	3.8×10^{13}	2.8×10^{6}

*Maximum neutron dose occurs directly below fine control drums.

The SNAP 10A shield assembly utilizes a cold-pressed lithium hydride shielding material reinforced with stainless steel honeycomb and contained in a Type 316 stainless steel casing. The honeycomb matrix is used to minimize crack propagation and to hold the lithium hydride block together when subjected to thermal gradients. The honeycomb matrix consists of 0.001-in. thick stainless steel foils which divide the shield into 1-in. square cells. The foil contains 1/2-in. perforations on 3/4-in. centers to permit even distribution of the granular hydride prior to cold-pressing. Experience at the Oak Ridge National Laboratories (ORNL) motivated the selection of the cold-pressed honeycombed compact as the form most resistant to cracking under thermal cycling. Figure 8 is a photograph showing the effects of the honeycomb matrix on a typical SNAP 10A shield configuration which has been subjected to thermal cycling. Cold-pressing

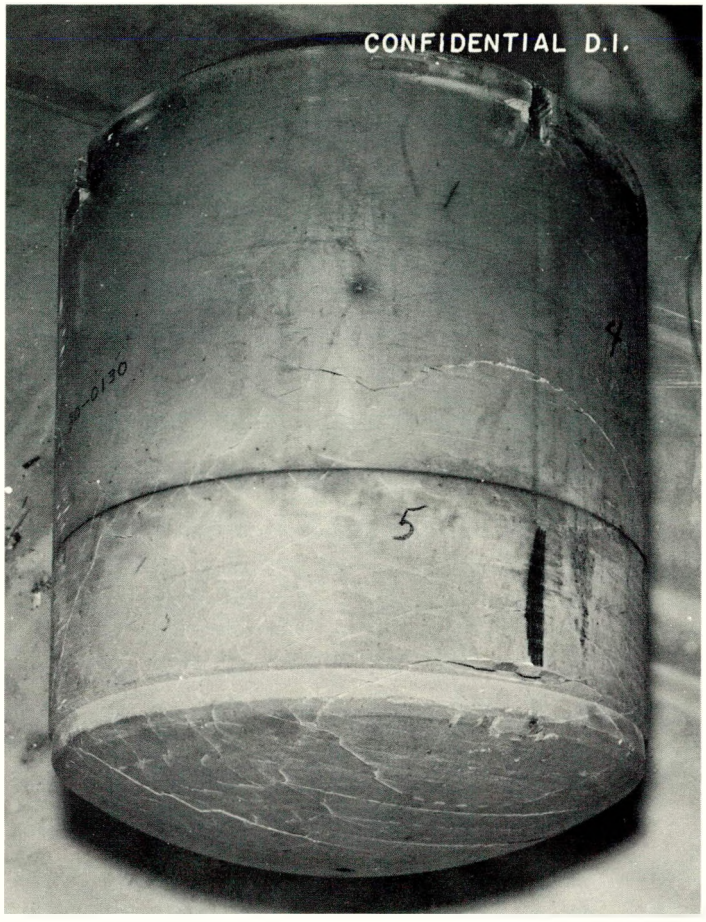

2-28-62 7580-1008

Figure 8. SNAP 10A Shield After Thermal Cycling

with a thick-walled honeycomb matrix results in a lower density shield. The thin, perforated foil presently being utilized offers low resistance to the compacting forces thereby assuring high lithium hydride densities while maintaining sufficient structural integrity of the block.

The compressive and tensile strengths for cold-pressed LiH at room temperature are 10,000 and 1,500 psi respectively. At elevated temperatures, the allowable material stresses are reduced considerably. At an average operating temperature of 800°F the allowable compressive and tensile stress levels, compared to room temperature values, are reduced by a factor of five. (The melting point of lithium hydride is 1240°F.)

To position the hydride against the forward end of the casing during the launch phase, a spring-supporting mechanism preloads the hydride to an equivalent 7.5 g vertical acceleration load. This is the maximum acceleration force

expected during launch. The springs permit expansion of the hydride during prelaunch thermal testing and at operating temperatures. The supporting mechanism consists of eight spring assemblies. The springs are attached to the shield casing and to a parabolic plate below the shield, thus forming a "sling" supporting the shield from below. The support plate was sized in such a manner as to distribute its load uniformly and minimize creep effects in the LiH material. Excessive creep, incurred during prelaunch thermal operation, would cause relaxation of the pretensioning load. Once in orbit, creep of the LiH material has no harmful effect. Below 700°F, LiH will creep less than 1% under a compression load of 350 psi. Above this temperature the creep rate accelerates rapidly resulting in gross deformations. A bearing stress of 28 psi, resulting from the 7.5 g pretensioning load, is present in the vicinity of the parabolic plate. At an average operating temperature of 800°F the lithium hydride expands relative to the casing and induces an additional bearing stress of 25 psi. Thus, the maximum bearing stress on the LiH at operating temperatures is 53 psi. Consequently, creep in the LiH is not a problem.

The pretensioning load from the springs to the hydride is accomplished by eight turnbuckle assemblies. The turnbuckle assembly consists of a threaded eye-bolt which is hooked to the spring, a turnbuckle barrel, and a threaded T-bolt which terminates at a fastening lug brazed to the stainless steel casing. (See Figure 9.) Inconel-X helical coiled springs are utilized to minimize relaxation at temperature. The preload stress in each spring is 59,500 psi. At operating conditions the total maximum stress in the spring caused by both the pretensioning and expansion of the hydride is 89,000 psi at 750°F.

During prelaunch thermal operation, a 3% relaxation occurs in the springs. Relaxation of the springs during long-term temperature operation in orbit is not detrimental and is in fact benefical since relaxation of the springs reduces the bearing load on the lithium hydride.

Thickness and size of the shield casing is based on limiting the membrane stresses due to internal pressure to 90% of yield stress at temperature. For a temperature of 800°F the allowable membrane stress of stainless steel 316 is 20,000 psi. At operating conditions, the shield casing is subjected to an internal pressure of 42 psi. The maximum membrane stress due to pressure at an operating temperature of 800°F is 15,400 psi. (At this temperature a pressure of

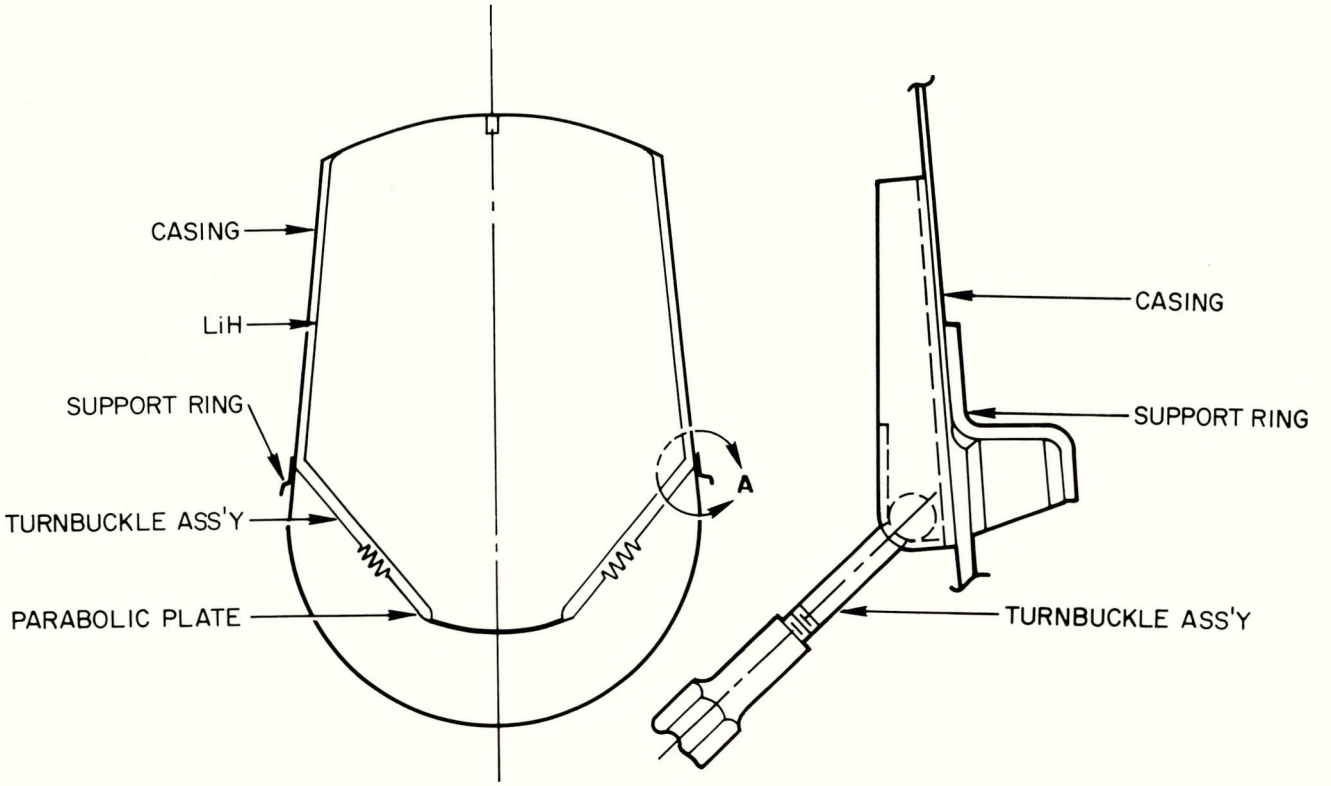

7-10-63 7623-0004

Figure 9. Turnbuckle Assembly

191 psi would be required to rupture the casing.) The minimum wall thickness of the shield casing is 0.032 in. Part of the upper portion, which is exposed to space, is 0.092 in. thick to provide meteoroid protection.

The major contribution of pressure buildup in the shield assembly is the differential expansion between LiH and the stainless steel casing (the coefficient of thermal expansion for lithium hydride is approximately 2-1/2 times that of stainless steel). Lithium hydride expands relative to the casing and compresses the cover gas within the void provided. The casing weight was optimized on the basis of internal pressure and wall thickness, yielding an optimum void volume (Figure 10). The casing length is approximately 32 in. and the lithium hydride length is 27-15/32 in. Maximum and minimum shield diameters are 21-1/8 in. and 17-9/16 in., respectively.

Each shield received by AI must be certified with respect to an outgassing potential. This is to ensure that lithium hydride shields have been properly handled during fabrication and that pressure buildup resulting from outgassing during a long shelf life of the assembly (approximately 1 yr) is minimized.

Certification consists of guaranteeing that the total amount of hydrogen gas which may be evolved during the LiH-H_2O reaction is limited to 0.5 cc of H_2 per square inch of LiH surface area.

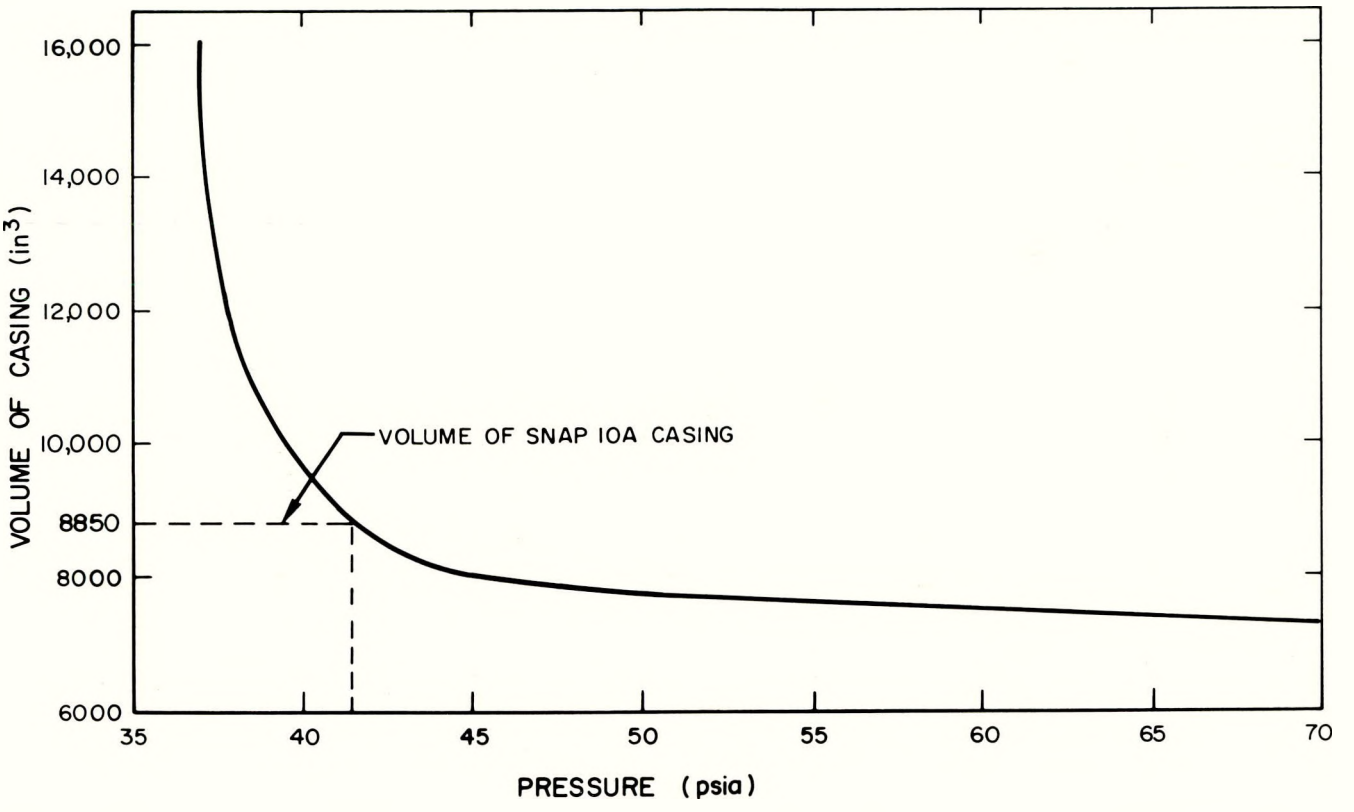

7-10-63 7623-0002

Figure 10. Shield Casing Volume vs Pressure

During prelaunch and orbital operations, the shield casing will be exposed to the steady-state temperature environment described below.

a) The lower end will see the inside of the support structure which will be at an average temperature of 800°F.

b) The upper surface shall see the base of the reactor vessel at approximately 900°F.

c) The lower side shall be adjacent to the power system converter structure which will be at a temperature of 840°F.

d) The upper side area and part of the upper surface shall be exposed to the space environment.

The reactor shield was designed to be removable from the power system by use of bolted attachments. The shield will withstand the thermal cycling encountered during prelaunch testing in a 1 g environment. The maximum vibratory and static loads encountered at launch are +7.5 g, -2.5 g longitudinal in combination with 1 g lateral, or 5 g lateral in combination with 2 g longitudinal. When these loads are present, the shield temperature should not exceed 100°F. During orbital operation, the shield shall function in a zero g space environment and will be subjected to the thermal environment given above. Transient and steady-state temperatures are given in Figure 11. Temperatures are given for the case of no internal heat generation to correlate nonnuclear testing results.

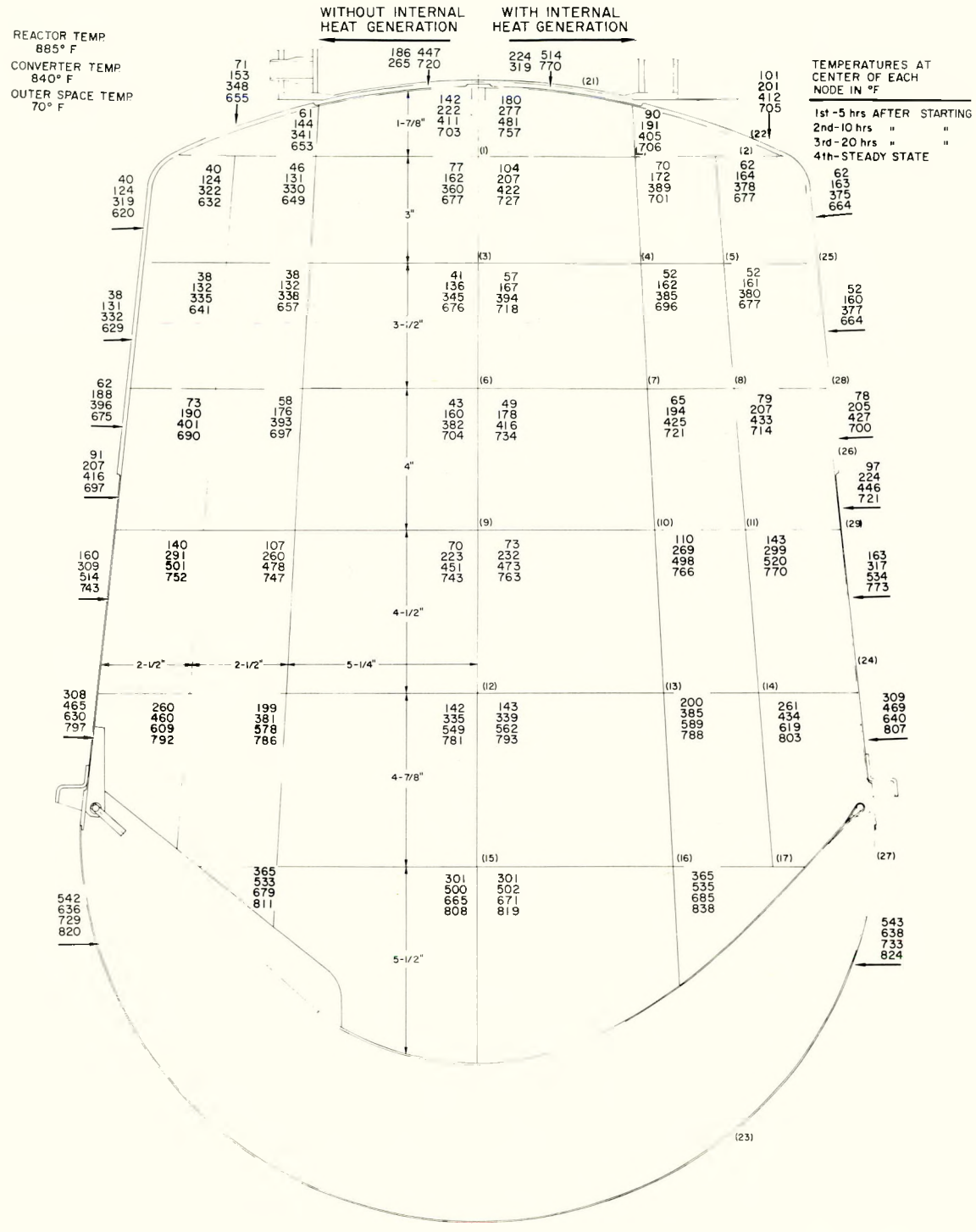

11-21-62

7573-5623D

Figure 11. SNAP 10A Shield Temperatures
(LiH in Pressed Form)

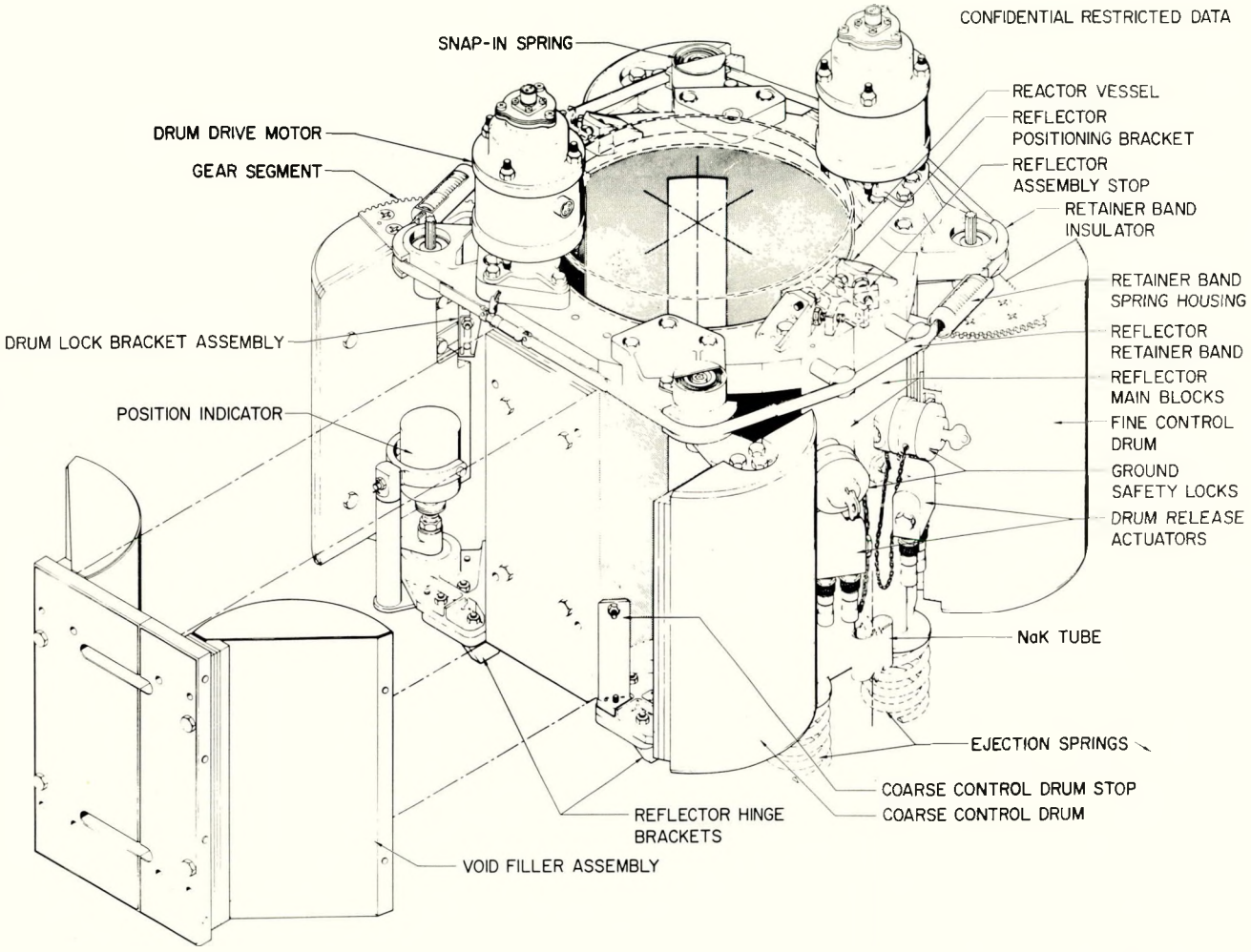

Figure 12. SNAP 10A Reactor Reflector Assembly

IV. REFLECTOR AND SAFETY DEVICES

The control and reflector assembly shown in Figure 12 can be divided into four subassemblies which include the safety devices. These subassemblies overlap in many respects, but are sufficiently distinct to explain the various features of the completed assembly. These subassemblies are the reflector and control assembly, support assembly, ejection assembly, and ground safety assembly.

A. REFLECTOR AND CONTROL ASSEMBLY

The reflector consists of a beryllium sleeve, approximately 2 in. thick, surrounding the reactor core. The inside of this sleeve is a cylinder, while the outside is made up of plane sections approximating a cylinder.

There are four semi-cylindrical cavities, spaced at 90° intervals, in the external surface of the reflector which are utilized for control purposes. Reactor control is provided by four cylindrical segment beryllium drums. The drums are rotated into the semi-cylindrical cavities in the reflector block to vary neutron leakage from the core. In the full in position, the drums are rotated into the reflector block cavities and complete the reflecting sleeve. In the full out position they are rotated 135° from the full in position, leaving a cavity in the sleeve. With the control drums in the full out position, the reactor is adjusted to be $5.60 subcritical at room temperature.

The drums are cut from a cylinder of 3-1/2-in. radius. The bare (unshimmed) drum segment has a maximum thickness of 1.78 in. Each drum may be increased in thickness with as many as three 1/8-in. thick shims which are attached to the back or flat side of the drum. The length of the drums is 10-1/8 in.

When the startup command is received, squibs are fired in actuators adjacent to each control drum. This action pulls a pin, releasing the drum. The two coarse control drums are spring-loaded and, when released, are immediately inserted. This adds $4.30 of reactivity. Fifty seconds after the startup command is received, the two fine control drums take their first step. They then move a half-degree step each 150 sec until reactor operating temperature is reached. It will be approximately 7 hr after startup before criticality is reached, and approximately 2 hr more before operating temperature is reached.

The temperature switch located in the outlet NaK line is set for 1010 ± 10°F and will control the reactor during initial full power operation. When the outlet temperature drops below the set point, the fine control drums will take another step inward. This continues until 72 hr after the startup command, at which time the control system is commanded "off."

The unique features of the coarse control drum package include the snap-in spring, coarse control drum stop, and the drum release system.

The snap-in spring is a flat wire torsion spring, made of Rene 41, which exerts a 10-in.-lb moment on the drum shaft in the full out position and a 5-in.-lb moment on the shaft in the full in position. The lower torque provides a factor of safety of approximately two over the maximum expected bearing friction, and guarantees that the drum will stop in the full in position.

The coarse control drum stop is a stiff Rene 41 cantilever spring which stops the drum in the full in position. It has enough flexibility to stop the drum without causing excessive stress.

The drum release system includes the drum release actuator and drum lock bracket assembly. Each actuator has two M-130 squibs, though either squib firing alone will cause a successful actuation. The squibs fire into a chamber, moving a piston which in turn pulls a pin to release the drum from the full out position. The lock bracketry on the coarse control drum, which engages the lockout pin, incorporates a safety feature which prevents removal of the ground safety lock if the pin is not engaged with the control drum. The safety feature is a spring-loaded clip which is inserted into the locking arm of the ground safety lock when the lockout pin is not properly engaged. The ground safety lock is described in Paragraph IV-D.

The unique features of the fine control drum package include its drum release system, the control drum actuator, position indicator, and gear linkage.

The drum release actuator in the drum release system is identical to the one in the coarse control drum package. Since the brake on the control drum actuator prevents insertion of the drum even though the lockout pin is removed, the spring-loaded safety feature mentioned above for the coarse control drum is not incorporated in the drum lock bracketry on this drum. The bracketry does include a forked slide which may be disengaged to allow 2° of drum movement

with the lockout pin and ground safety lock in place. This permits a check of the control system on the launch pad. During the boost phase, this slide will be engaged to hold the drum immobile.

The control drum actuator is a motor that rotates in finite steps. The windings are each connected in series with a brake on the motor shaft. When a signal is received from the controller, the brake is released and the shaft turns a finite distance. Four motor steps complete one duty cycle and rotate the control drum 0.5° ± 0.1°. Each time the motor is operated, a full duty cycle is completed.

Two gears link the control drum actuator to the control drum. The pinion gear attached to the motor shaft is made of Haynes Stellite 6B, and the gear segment attached to the drum is made of titanium. These gears are matched sets which limit the backlash to 0.1° drum rotation at all times. A Molykote X-15 layer is used to prevent self-welding of the gears.

The position indicator in the fine control drum package is provided for diagnostic instrumentation only. The output voltage of the indicator varies with drum position to give the desired position information. Two ranges of operation are provided; a coarse range indicating position between 0 and 135° and a fine range indicating position between 0 and 30° from the full in position.

B. SUPPORT SYSTEM

The control and reflector assembly is mounted on the reactor in two halves. Each half is supported on two hinges located at the lower end of the assembly. The halves are rotated into position on the hinges until stops located near the top of the reactor are contacted. The complete assembly is then held in position by a retaining band around the upper end of the reflector halves.

Both hinges on a side are of a similar design, although one is restrained against lateral motion while the other is free to allow thermal expansion. Each hinge sits on a 1/4-in. diameter pin attached to the reactor structure. The hinge is held down by a 3/8-in. diameter pin attached to the reactor structure that bears on a cylindrical surface concentric with the 1/4-in. diameter pin. The 3/8-in. diameter pin is an eccentric pin and can be adjusted to obtain the proper clearance in the hinge. Ejection springs, described in Paragraph IV-C, push

upward on the reflector so that the 3/8-in. diameter pin and the cylindrical surface will always be in contact except during launch when maximum accelerations are present. Coatings are used on the hinge to prevent self-welding

Positioning bolts are used on the upper end of the reflector assembly to adjust the position of the assembly. These bolts bear against the stop brackets attached to the reactor vessel. Again, coatings are used to prevent self-welding.

The retaining band is held out from the reflector block by standoffs. Flexible graphite inserts are used between the band and standoffs to minimize self-welding effects. The tension of the band is set at $165 \begin{smallmatrix} +15 \\ -10 \end{smallmatrix}$ lb at ambient conditions. During launch, the band will be heated to a temperature greater than the beryllium reflector, but the springs will maintain sufficient tension to overcome acceleration forces. During thermal acceptance testing and operation, the band will be cooler than the beryllium reflector, but the springs allow stretching of the band without increasing tension in the band to the yield point. Thus, the band is reusable after the thermal cycles expected prior to launch.

The gap between the reflector assembly and reactor vessel is set to prevent contact and possible self-welding or intermetallic diffusion between the reactor and reflector. This gap must be as small as possible to maximize reflector worth. The minimum gap between the reactor and vessel occurs during reactor startup. During startup the beryllium temperature rises much more slowly than the reactor temperature rises. Because the fixed hinges are located 3-1/2 in. off the reactor centerline, the reflector centerline moves with respect to the reactor centerline during thermal cycles. To account for this, the reactor-reflector gap at ambient temperature is largest on the side of the reactor vessel opposite the fixed hinges. At the top of the reactor vessel, opposite the fixed hinges, the minimum gap is 0.072 in. At the bottom the minimum gap is 0.069 in. On the side of the vessel closest to the fixed hinges, the minimum gap at the top is 0.020 in. and at the bottom 0.012 in. When the reactor first reaches full power, the reflector is approximately concentric with the reactor and the gap at the top of the reactor is reduced to a nominal 0.010 in. The minimum gap, which occurs at the bottom next to the fixed hinges, is 0.005 in. As the reflector temperature increases to operating temperature, the gap between the reactor and reflector increases.

C. EJECTION SYSTEM

Reactor shutdown may be effected by ejection of the control and reflector assembly. Ejection is accomplished by compression springs located at the bottom of the reflector halves. When the retainer band is released, the reflector halves are pivoted outward around their support hinges by the spring force.

Prior to ejection of the thermal shield, the reflector halves can be rotated outward at least 7° by releasing the retaining band. After the thermal shield is ejected, the reflector halves can be completely ejected from the reactor. However, the two reflector halves will still be connected to the reactor by the electrical wiring. Seven degrees outward rotation of the reflector reduces reactivity by about $17, and complete reflector ejection reduces reactivity approximately $21.

Two ejection springs are used for each reflector half. These Rene 41 compression springs are located beneath the reflector adjacent to the reflector separation plane. Each spring exerts 100 ± 5 lb on the reflector at room temperature, and 85 ± 5 lb at operating temperature. Since the maximum operating temperature of the ejection springs (900°F) is slightly less than one-half of the absolute melting temperature of the Rene 41, the rate of relaxation of these springs is very slow. At operating temperature the ejection springs initially apply a total moment to each reflector half of approximately 440 in.-lb. This is approximately a factor of two greater than the torque required to break the maximum potential self-welding bonds at the lower support hinge and between the upper positioning bolts and stop bracket. Based on this maximum self-welding bond, and a conservatively high estimate of the spring relaxation rate, it will be at least 100 yr after startup before the ejection springs will relax to the point where they can no longer overcome the self-welding bonds and eject the reflector. The nominal anticipated self-welding bonds are approximately an order of magnitude less than what is referred to above as the maximum bonds. For the case of nominal self-welding, the ejection springs will retain enough force to eject the reflectors even after several thousand years in orbit. This is because the ceramic coatings used to prevent self-welding at the lower support hinge and between the upper positioning bolts and stop bracket are very stable at operating temperatures, and any resulting self-welding will not increase as a function of time.

The hinges which support the reflector are described in Paragraph IV-B. When the reflector rotates outward about 15°, the 3/8-in. diameter pin disengages

from the cylincrical surface allowing the two parts of the hinge to completely disengage. The kinematics of this separation have been verified experimentally. The kinetic energy of the rotating reflector is sufficient to separate the reflector from the ejection springs, as the ejection springs become fully extended. Coatings are used between the ejection springs and the reflector structure to minimize any potential self-welding.

Three distinctly different signals are used to initiate reflector ejection. All three signals activate an electrical device which releases the reflector retainer band. An electrical signal can be provided by (1) ground command through an umbilical prior to liftoff, (2) telemetry, or (3) a failure-sensing device (low converter output voltage). The failure-sensing device starts a 1-minute timer which resets if the malfunction signal is removed. Thus, a momentary voltage fluctuation will not cause an inadvertent shutdown. If the signal persists, a 1-hr delay timer is started. During the 1-hr delay, recording of pertinent data takes place. At the conclusion of the delay period, the timer triggers the electrically actuated band release device (EABRD).

The EABRD consists of a hollow Rene 41 cylinder and an electrical heater which is contained within the cylinder. The cylindrical body is incorporated directly into the retaining band, being attached by special end fittings, and forms an integral part of the band. When a reflector ejection signal is received, voltage is applied to the heater which raises the temperature of the cylinder to about 1700°F. The band tension springs easily pull the body apart in its weakened condition at high temperature, thus severing the band and allowing reflector removal.

Figure 13 shows two views of the finished EABRD before assembly into the retaining band. The EABRD body is machined from a single piece of Rene´ 41; total length, including band end fittings, is 2.3 in. The cylindrical section is approximately 3/16 in. in diameter and has a wall thickness of 0.008 in. It is this thin wall section which separates at high temperature. Normal operating temperature of the EABRD is about 500°F. The heater consists of 32 GA (0.0079 in. diameter) tungsten wire coiled around a ceramic bobbin which is placed inside the cylindrical body.

The EABRD is designed to operate from a 22 to 28 volt dc power source. When operated at the lower end of this range, i.e., at 22 volts, band separation occurs in approximately 15 sec and requires less than 1400 watt-sec of total energy. With an initial operating temperature of 500°F, the maximum current to the heater is 10 amp which occurs initially and then decreases during heating to about 5 amp at separation.

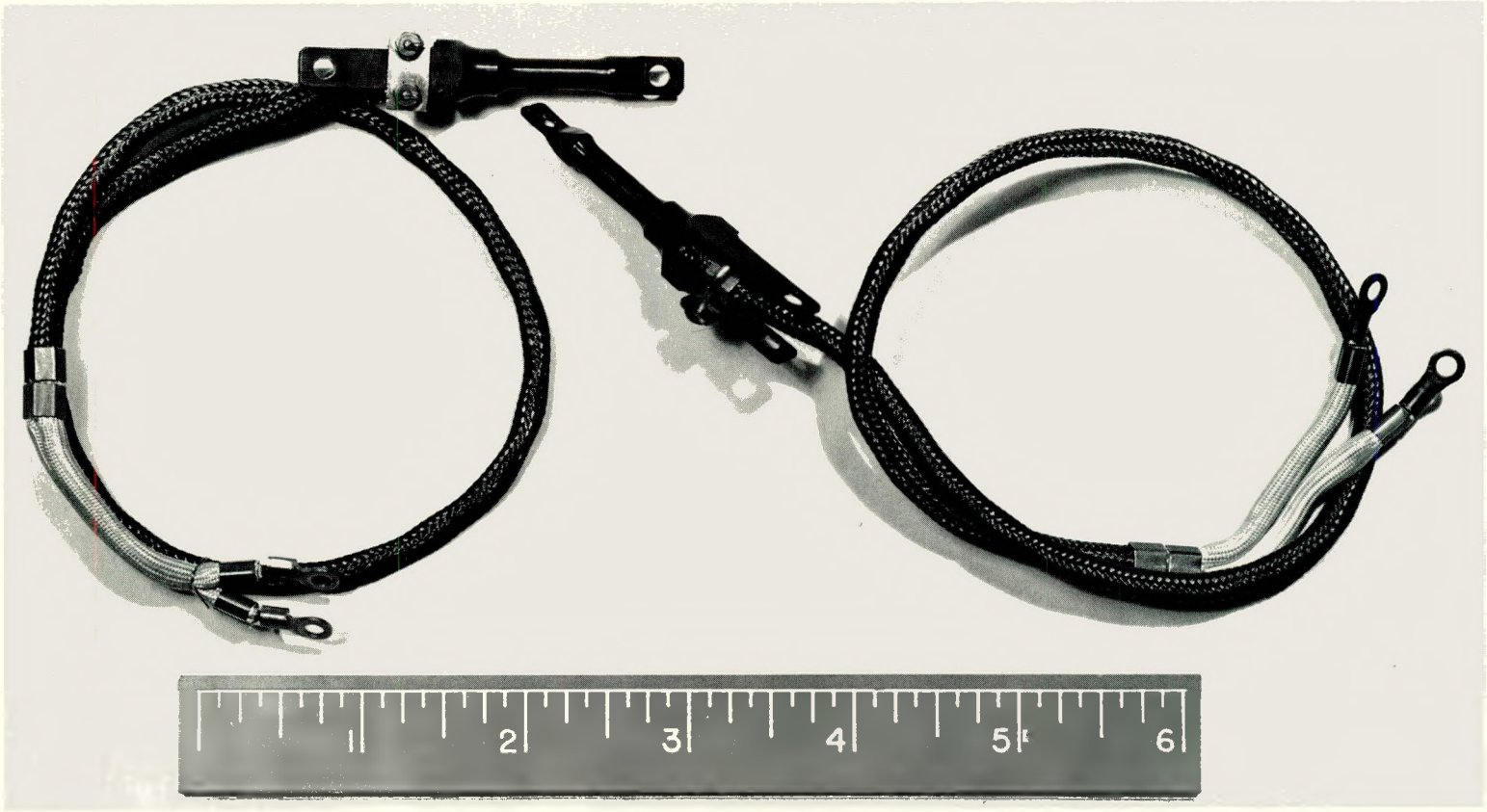

10-16-64

7623-4425A

Figure 13. SNAP 10A EABRD

A thermal-mechanical device is also provided to separate the reflector retaining band in the event the EABRD does not function. This device, called the Temperature Actuated Band Release Device (TABRD), is actuated by a drop in temperature of the NaK in the outlet line adjacent to the reactor. The TABRD, shown mounted in its test stand in Figure 14, is approximately 1 ft in length and works on the principle of differential thermal expansion of two materials. In this design a stainless steel rod moves relative to a molybdenum tube. The two are rigidly joined at one end by a notched stud, which also serves as a shear pin between two overlapping end fittings of the reflector retaining band and a bolt. The notch in the stud is in line with the mating surfaces of the band fittings. While the temperature is increasing, the steel rod, which has a much higher coefficient of thermal expansion than the molybdenum, is allowed to grow freely relative to the tube. On reaching a preset temperature (925 ± 25° F at the NaK line) established by adjustment of the position of a stepped collar on the free end of the rod, an external type snap ring closes behind the step. Thereafter when the temperature decreases below the preset temperature, the stainless steel rod is forced in tension. When the temperature reaches approximately 500° F the tension becomes great enough to break the stud at the notched section and release the retainer band. A temperature drop that will cause the TABRD to release the retainer band can occur in one of two ways: (1) NaK flow stoppage or (2) loss of NaK.

The retainer band is also designed to release upon reentry heating if reflector ejection has not already occurred. The brazed joint in the electrically actuated band release device will melt at about 300,000 ft thereby releasing the reflectors. If for some reason this does not occur, the entire band will melt at about 285,000 ft resulting in reflector ejection.

From a reliability standpoint, the reflector ejection safety devices represent a network of parallel retaining band separation devices with redundant activating mechanisms as shown in the block diagram of Figure 15. This network is further backed up by redundant retaining band failure modes during reentry. In addition, as is discussed in Section IX, if the ejection springs relax beyond the capability of reflector ejection, the reentry aerodynamic forces ensure ejection of the reflector. Furthermore, self-welding of the reflector halves has been minimized by the application of lubricants which have effective lifetimes of thousands of years. Therefore, it is concluded that the combination of shutdown and reentry sequences constitues a safety system which has an extremely high reliability.

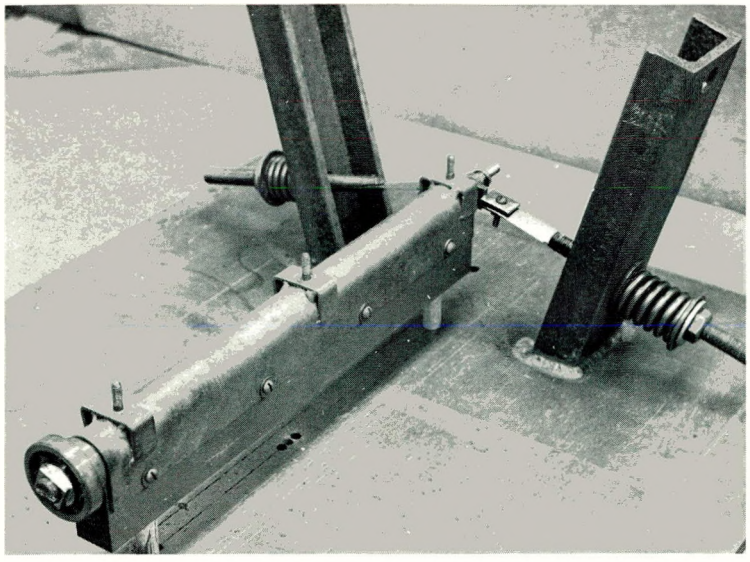

a. Mounted in Test Stand

8-28-63 7622-4501

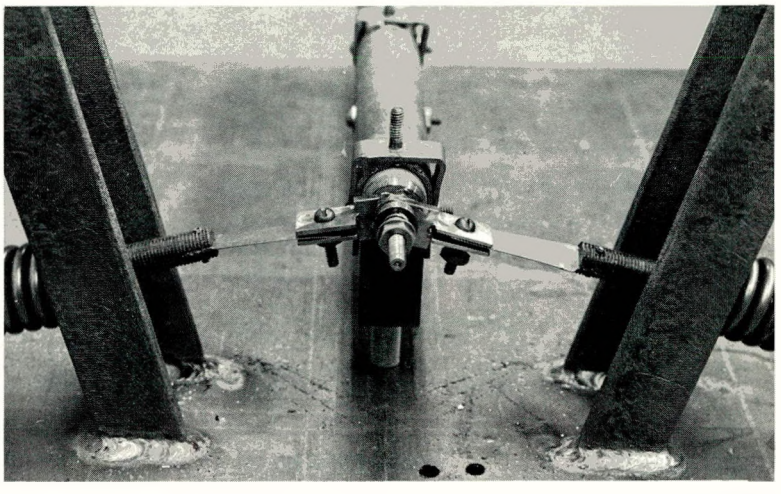

b. Close-up of Top End

8-28-63 7622-4504

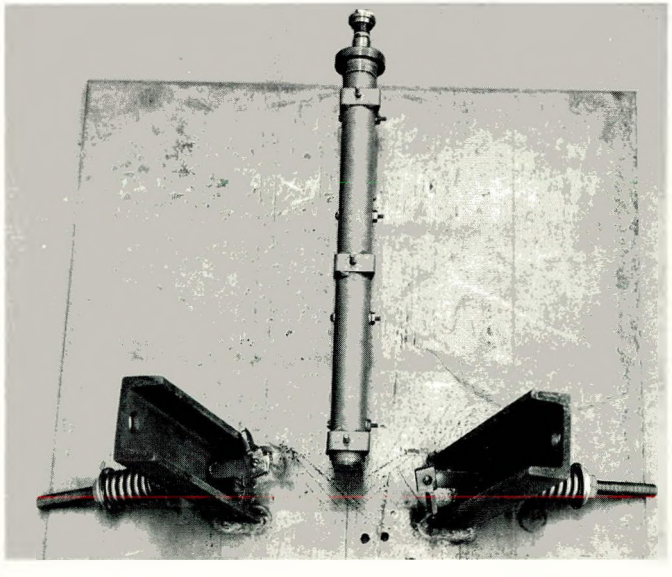

c. After Band Release

8-28-63 7622-4506

Figure 14. SNAP 10A TABRD

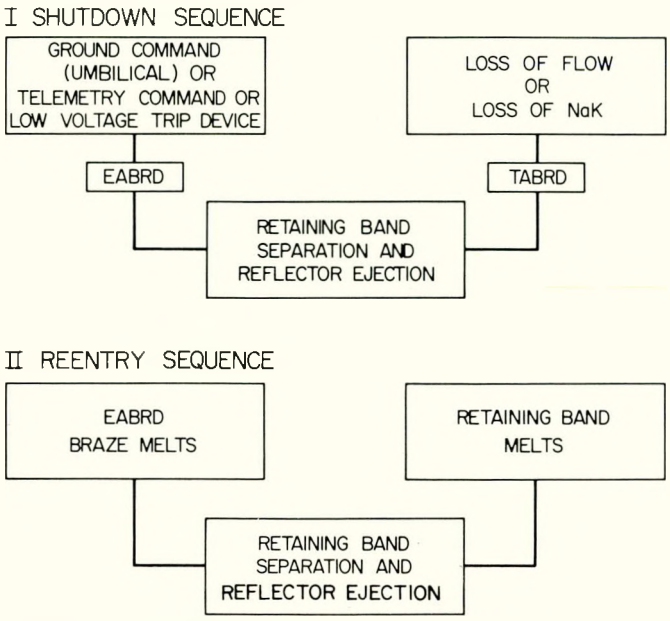

Figure 15. Reflector Ejection Sequences

D. GROUND SAFETY SYSTEM

During handling and shipping operations, when the reflector is not in place around the reactor vessel, a shipping sleeve is installed around the vessel. The shipping sleeve is designed to maintain sub-criticality of the reactor in the event of a shipping accident resulting in total water immersion, internal and external, of the core. The sleeve fits around the reactor core in the position normally occupied by the external reflector as shown in Figure 16.

The sleeve consists, from the reactor vessel outward, of an annular void area 3.75 in. thick, a 1.0 in. layer of boron powder and a protective casing of Type 321 stainless steel. The void area is divided into 132 individual water-tight compartments by 0.01 in. Type 321 stainless steel partitions. The steel occupies 2.75% of the void volume. The boron powder, also incased in 0.01 stainless steel, is compacted to a density of 0.45 gm/cc. Fireproof shipping sleeve materials were selected.

The protective casing is designed to carry all loads, thus minimizing void and boron compartment deformation during an accident. It consists of an 0.25 in. thick shell to which brackets for handling and attachment are welded.

SNAP 10A REACTOR SHIPPING SLEEVE

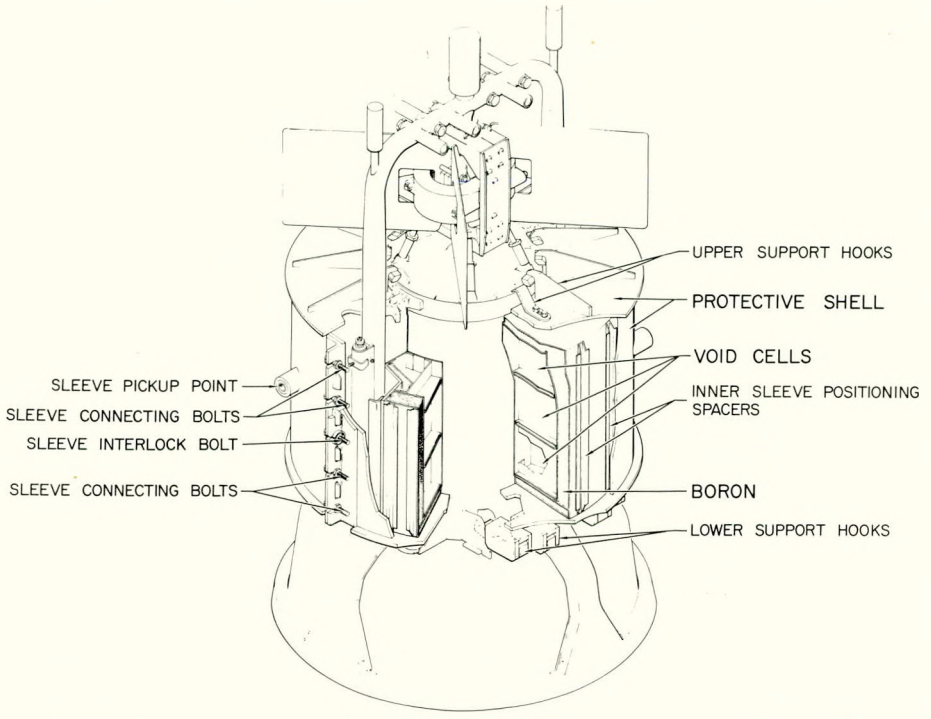

6-27-63 7561-0514

Figure 16. SNAP 10A Shipping Sleeve Assembly

On the inner casing surface, energy-absorbing spacers are attached to position the void and boron compartments.

To permit attachment of the shipping sleeve around the reactor core, the sleeve is made in two identical halves. The halves are flanged and held together by ten toggle bolts. As an interlock, two of these bolts require a special tool for removal.

Four clamps on the bottom of each shipping sleeve half secure the sleeve to the reactor. Two clamps grip the reflector hinge pins and two others grip the base ring. These clamps are adjustable after sleeve attachment, insuring proper axial constraint of the sleeve. Six fixed clamps are attached to the top of each sleeve half. These clamps also provide axial sleeve constraint as well as structural reinforcement in that area.

The SNAP critical assembly (SCA-4B) experiment has verified the capability of the shipping sleeve to prevent criticality of the SNAP 10A flight reactor upon total water flooding or and submersion. Approximately 28 ± 5 center-row compartments could be filled with water, in addition to the flooding and submersion,

and the sleeve would still maintain the reactor subcritical. However, in an accident, the edge compartments would be much more likely to be damaged than those in the center row, and the sleeve will maintain subcriticality with 38 ± 5 edge compartments filled with water.

The shipping sleeve is designed to withstand a 15-ft fall onto a solid rock or concrete surface without significant distortion or without breaking loose from the reactor. When the combined reactor and shipping sleeve are placed in the shipping container, the sleeve is designed to successfully withstand the shocks which would be transmitted to it as a result of a head-on collision (combined velocity 100 mph) between the transport vehicle and another large truck. Such an accident is believed to represent the most severe mechanical test of the shipping sleeve integrity under circumstances which could credibly be followed by immersion of the reactor in hydrogeneous fluids.

A series of drop tests was performed to demonstrate the mechanical adequacy of the shipping sleeve design. Four drops were made. In the first three tests the shipping sleeve was attached to a dummy reactor and dropped from a height of 15 ft onto concrete in three different critical attitudes. In the fourth test, mass mockups of the NaK pump and converter structure were added to the test assembly. This drop was conducted "nose-on," again from a height of 15 ft onto the concrete. During and after tests, the shipping sleeve remained attached to the reactor vessel. In addition, a post-test examination revealed that all void compartments were watertight and that only minor deformation had occurred.

During ground handling operations performed with the reflector in place around the reactor vessel, void filler blocks are attached to the reflector to provide a criticality safeguard. The void filler blocks, shown in Figure 17, are designed to keep the reactor sub-critical under all types of external environmental influences with the beryllium reflector installed on the reactor. The filler blocks partially occupy the four control drum voids in the reflector and thereby positively prevent the drums from moving inward. The filler blocks maintain the reactor subcritical if the reactor is completely submerged in water or other neutron reflecting media. However, if water replaces the NaK in the core, this subcriticality will not be maintained.

The void filler assembly consists of four half-cylinder blocks which partially occupy the voids left in the Be reflector by the outward-rotated control drums, and two rectangular blocks, each of which join two of the half-cylinder

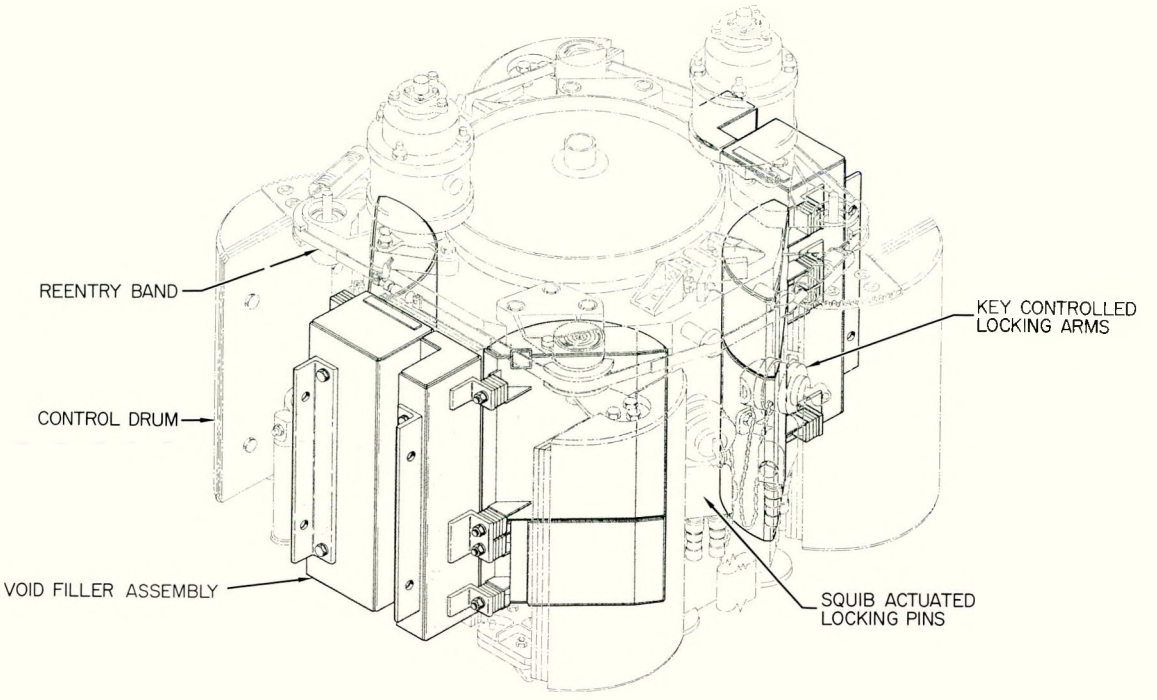

10-21-63 7561-0513C

Figure 17. SNAP 10A Void Filler Assemblies

blocks together. The enclosing structural material is 0.06 in. 304 stainless steel. The outer 1/2 in. of the half-cylinders is packed with natural boron powder to 20% of theoretical density. The remainder of the volume is void (air). The rectangular sections have the void volume on the outside surface and a similar boron layer on the inside (next to the reflector) surface.

Each of the four half-cylinder shells is made in two sections, a long section and a short section. A groove on the back, flat side of the short section assures that this section will clear the control drum adjustment screw when the section is in place. The short section is placed in the drum void. The long section is put into the void above the short section. Each of the rectangular blocks is made in two sections which, when joined, provide a channel for the passage of wiring. The rectangular blocks are secured to the Be reflector with four studs.

Experimental verification tests of the filler block nuclear specifications were performed using simulated void filler blocks and the basic SNAP 10A reactor. The experiments indicated that the present design would maintain the reactor subcritical with full water reflection.

Although the primary design objective of the void filler assembly is to provide nuclear protection against potential environmental sources of reactivity additions, their placement in the drum voids also insures against accidental drum rotation. Keyed safety locks are provided specifically to prevent control drum rotation during ground handling in the latter preflight operational stages when the void filler blocks have been removed. A ground safety lock, shown in Figure 12, is provided for each control drum. These locks are operated with a key and will be removed during the count-down sequence. When installed and locked, an arm positively prevents insertion of the control drums. The locks on the coarse control drums cannot be removed unless the squib-actuated lockout pin is engaged.

Removal of the ground safety locks will be one of the final operations prior to launch. Access holes are provided in the nose cap to allow removal after all squibs have been installed and the nose cap is put in place.

V. REACTOR CONTROL

A. INTRODUCTION

The functions of the control system are (1) to control the rate of reactivity insertion during the startup procedure, (2) to establish operational stability at design levels, and (3) to reduce reactivity to a subcritical condition at termination of the mission.

Because of the small size of the reactor, about 40% of the neutrons born in the fission process will leak away from the core unless it is surrounded by an adequate neutron reflector. Thus, complete control of the reactor is achieved simply and efficiently by varying the effective thickness of the neutron reflector surrounding the core. The reflector is a hollow cylinder of beryllium with a wall thickness of approximately 2 in. Four semicylindrical drums comprise a portion of this cylindrical wall of beryllium. Rotation of the control drums has the effect of varying the thickness of the reflector, thus permitting startup and control of the reactor.

B. SYSTEM OPERATION

After orbit has been established, startup is initiated by a coded telemetry (TM) command. This signal energizes the "on" coils of the startup relays. Switching these relay contacts energizes the controller relay "on" coils, thus switching their contacts and supplying unregulated 28 vdc and plus and minus regulated 28 vdc power to the controller. At the same instant, the control drum squibs are fired and release the drums. Coarse control drum "in" limit switches provide telemetered verification.

The controller starts to drive the two fine control drums in at the rate of 1/2° each 150 sec. The controller will continue to drive the control drums in until the reactor outlet thermal switches close (1010 ± 10°F). These switches are located on the reactor NaK coolant outlet line. This event will occur approximately 9 hr after the start command. For the following 72 hr, during which the reactor reaches equilibrium, the controller is maintained in an active condition. It drives the drums in if the reactor outlet temperature drops below the temperature switch setpoint (the reactor outlet temperature switches open when the temperature drops below the setpoint). Electrical power is then removed to deactivate the controller which can be reactivated by TM command.

Diagnostic instrumentation is provided for status information. Variable position sensors are mounted on the two fine control drums. Limit switches provide "full in" and "full out" status on both the fine and coarse control drum. Limit switches also provide "on" and "off" status on each half of the reflector assembly and on the retaining band.

End of mission can be initiated by a malfunction signal from the converter system or by TM command. The termination signal activates a 1-min timer. This timer will reset to zero if the termination signal is removed before the 1-min period is completed and thus will prevent termination due to short-time malfunction indications. If the termination signal is still present at the end of one minute, this timer activates a 1-hr timer. The purpose of the 1-hr timer is to allow acquisition of diagnostic data prior to reactor deactivation. At the end of the 1-hr period, electrical power is applied to the electrically actuated reflector band release device to break the reflector retaining band. This allows the reflector to be ejected, thereby reducing the reactor to a subcritical condition.

C. CONTROL COMPONENTS

Components comprising the reactor control system are:

1) Controller

2) Controller drum actuators

3) Thermal switches

4) Timer (1-hr and 1-min combined)

These components are described as follows.

1. Controller

The reactor controller is a digital device which provides four sequenced power steps to the control drum actuators every 150 sec when the temperature switches indicate that the reactor outlet temperature is below the temperature setpoint. The controller employs transistorized logic throughout with the exception of the output power switches which are relays. The internal frequency source or time base is a transformer-coupled multivibrator.

The primary reason for the 150-sec time delay period between successive 1/2° drum rotations is to allow time for the reactor temperature to respond to the increase in reactivity. This stepping rate produces a reactor startup time compatible with the reactor characteristics, startup battery capacity, and temperature transient capabilities of the nuclear power system.

2. Control Drum Drive Actuators

The control drum drive actuator is required to rotate the drum in small (1/2°) increments. A stepper motor is used, together with a single 13.8:1 gear set. The motor is a synchronous machine, with a permanent magnet rotor and a 2-phase stator. The rotor and stator are notched to form 50 and 48 teeth on each respectively. The mismatch produces the effect of 200 poles. Therefore, with each change in polarity in the stator windings, the rotor will rotate 1.7°. Each phase of the stator is divided into two windings, which are wound in opposite polarity. This is done to allow simple ON-OFF switching to produce the effect of phase polarity reversal. At any time during actuation two stator windings are always energized. The direction of rotation is determined by the sequence in which the windings are energized. The actuator is designed to perform four steps in order to rotate the drum 1/2°. A 4-step sequence is used to allow the electronic circuits in the controller to return to a stable condition.

A solenoid-actuated brake is mounted in the upper end bell of the actuator, with the solenoid armature spring-loaded against a disc on the rotor shaft. The solenoid winding is in series with the stator, being connected to the common return of the four stator windings. Therefore, the brake is released when power is applied to the actuator and is reapplied when the actuator is deenergized.

3. Thermal Switches

Thermal switching required for control of the SNAP 10A is accomplished by a platinum resistance sensor coupled to an electronic switch. The resistance sensor is placed in a thermal well in the NaK outlet line above the reactor vessel head, and the switching unit is located in the SNAP unit instrument compartment.

Two switches in parallel are used for increased reliability.

4. Timer

The 1-min and 1-hr timer functions are combined in one electromechanical device.

D. POSITION INDICATING DEVICES

The following devices provide position status of various components of the reflector assembly for diagnostic information:

1) Control drum position sensor and demodulator

2) Position switches

These are described as follows.

1. Control Drum Position Sensor and Demodulator

The control drum position indicators are rotary differential transformer devices directly coupled to the drum shafts by zero backlash couplings. Power input to these units is 26 v 400 cycle supplied by a stepdown transformer located in the instrument compartment. The output signals from the position sensors are the inputs to two demodulators. Each demodulator has two 0- to 5-v dc outputs. A coarse scale indicates drum position from 135 to 0° and a fine scale indicates drum position from 30 to 0°.

2. Position Switches

Twelve position switches are used on the reflector assembly. These are:

Coarse Control Drum No. 1 in limit (PnS-1) and out limit (PnS-2)

Coarse Control Drum No. 2 in limit (PnS-3) and out limit (PnS-4)

Fine Control Drum No. 1 in limit (PnS-5) and out limit (PnS-6)

Fine Control Drum No. 2 in limit (PnS-7) and out limit (PnS-8)

+Z reflector assembly position on-off (PnS-15)

-Z reflector assembly position on-off (PnS-16)

+Z reflector band on-off (PnS-17)

-Z reflector band on-off (PnS-18)

These switches are of the high temperature nonsealed single-pole double-throw type. When a second pole is required, two switches are used.

VI. FUEL

The reactor fuel material is a hydrided zirconium-uranium alloy which serves both as fuel and moderator. The alloy contains 10 wt % uranium and is hydrided to a nominal N_H of 6.35 x 10^{22} atoms of hydrogen/cm^3. The uranium is fully enriched in U^{235}. This material is formed into rods of 1.21-in. diameter and 12.25-in. length and is canned in Hastelloy-N cladding tubes. The cladding tubes are 1.25-in. OD and have a wall thickness of 0.015 in. Internal surfaces of the cladding tubes are coated with a 2.0 to 4.0 mil layer of ceramic glass material. This coating acts as a barrier to hydrogen leakage from the fuel. The ends of the fuel elements are sealed with end caps of Hastelloy-N material welded to the cladding tube The end pins which position and hold the elements between the grid plates are an integral part of the end caps. Each fuel element weights 3.4 lb and has an overall length, including end pins, of 12.82 in. The fuel/moderator element is shown in Figure 18.

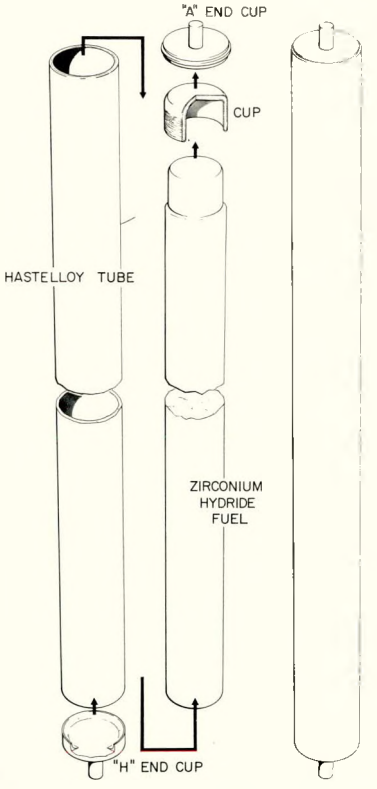

9-28-61 7550-20211

Figure 18. SNAP 10A Fuel Element

Each unclad fuel rod contains approximately 128 grams of U^{235}, 11.8 grams of U^{238}, 24.6 grams of hydrogen, and 1215 grams of zirconium. Total weight is approximately 1380 grams (3.04 lb). [A small amount CRD of carbon (approximately 0.15 wt %) is added as a grain refiner to produce a stronger rod.] The fuel is a hard semibrittle material which has a machined surface and a metallic appearance. All edges of the fuel rod are rounded to prevent damage to the ceramic hydrogen barrier during assembly and handling of the fuel element.

The ceramic glass hydrogen barrier prevents excessive loss of hydrogen from the fuel rod operating in the high temperature and high radiation environment of the reactor core. Integrity of this barrier must be maintained. Hence, handling and shipping of fuel elements must be accomplished with suitable precautions to prevent damage due to excessive shock or vibration.

[The ceramic glass barrier is composed primarily of oxides of aluminum, silicon, titanium, manganese, CRD and barium with smaller amounts of sodium, lithium,

and potassium. This ceramic coating is generally applied in three firings. In the last two firings a small quantity of samarium oxide (Sm_2O_3) is incorporated into the coating. The nominal samarium oxide loading is 8.0 ± 0.8 mg/in. The samarium is a burnable poison. Depletion of this material inserts sufficient reactivity at the proper rate to provide more than 1 yr of stable reactor operation.

One end cap of the fuel element is welded to a cladding tube prior to application of the ceramic barrier. After the ceramic barrier is fired, a fuel rod is inserted into the cladding tube. The cladding tube is then sealed against hydrogen loss by insertion of a ceramic coated blend cap. The hydrogen barrier is made complete by locally heating the cladding tube and blend cap to blend the ceramic surfaces together. Following the blending operation, an end cap is welded to the cladding tube, covering the blend cap. No end play exists between the fuel rod and cladding tube.

A small number (less than 10) of the 37 fuel elements required for a SNAP 10A core loading will have a nominal hydrogen content of 6.0×10^{22} atoms/cm^3 of fuel and/or a Sm_2O_3 loading of 16.0 mg/in. These special elements are used to adjust the excess reactivity and passive control characteristics of the core. They are identical to the standard elements in every other respect.

VII. OPERATING CHARACTERISTICS

The SNAP 10A reactor is similar in nuclear design to the test and developmental reactors which have been developed by, or are presently being operated by, Atomics International for the Atomic Energy Commission.[1,2,3] The SNAP Experimental Reactor (SER) has been extensively tested and its nuclear characteristics determined. After 6000 hr of operation, the SER was disassembled and the SNAP Developmental Reactor (SDR)[3] placed in operation. The SDR logged over 11,000 hr prior to being shut down. These two operating reactors, along with the SCA-4B and SCA-4C critical experiments, have provided a wealth of experimental information regarding nuclear characteristics. In addition, ground operation of the first flight system reactor (FS-1) was recently initiated.

Nuclear characteristics of the SNAP 10A reactor have been determined analytically mainly through use of the AIM-6 multigroup diffusion code with the Los Alamos 16-group cross section library. The AIM-6 code is an expanded version of the WANDA code, incorporating a greater group structure and other features and operations which have been found desirable.[4] The basic AIM-6 calculations have been found by experience to agree reasonably well with SNAP experimental data. Additional nuclear calculations have been made using the ZOOM, CURE, ULCER, and SNG codes.[5,6,7,8] Fast neutron and gamma shielding calculations have been made using the FARSE 2, SCAR 1, and 14-0 codes.[9,10,11]

A summary of SNAP 10A reactor design nuclear, kinetic, shielding, and weight characteristics is presented in Table 1. Most of the nuclear parameter information summarized in Table 1 (Section I) is based on experimental data obtained from SER, SDR, or the SCA critical experiment. The remaining parameters have been calculated using the AIM-6 or other nuclear codes. Calculated radiation dose information only is presented in Table 1; experimental verification of shielding calculational methods is in progress.

Based on the recent FS-1 operation, it appears that the SNAP 10A core loading will require approximately three of the low N_H, high Sm_2O_3 loaded fuel elements. Figure 19 shows the anticipated long-term temperature drift of the SNAP 10A reactor utilizing three of these special elements. The center curve represents the expected temperature behavior when nominal reactivity changes take place. The upper and lower curves illustrate the behavior when the upper and lower limits on the various reactivity changes are assumed to

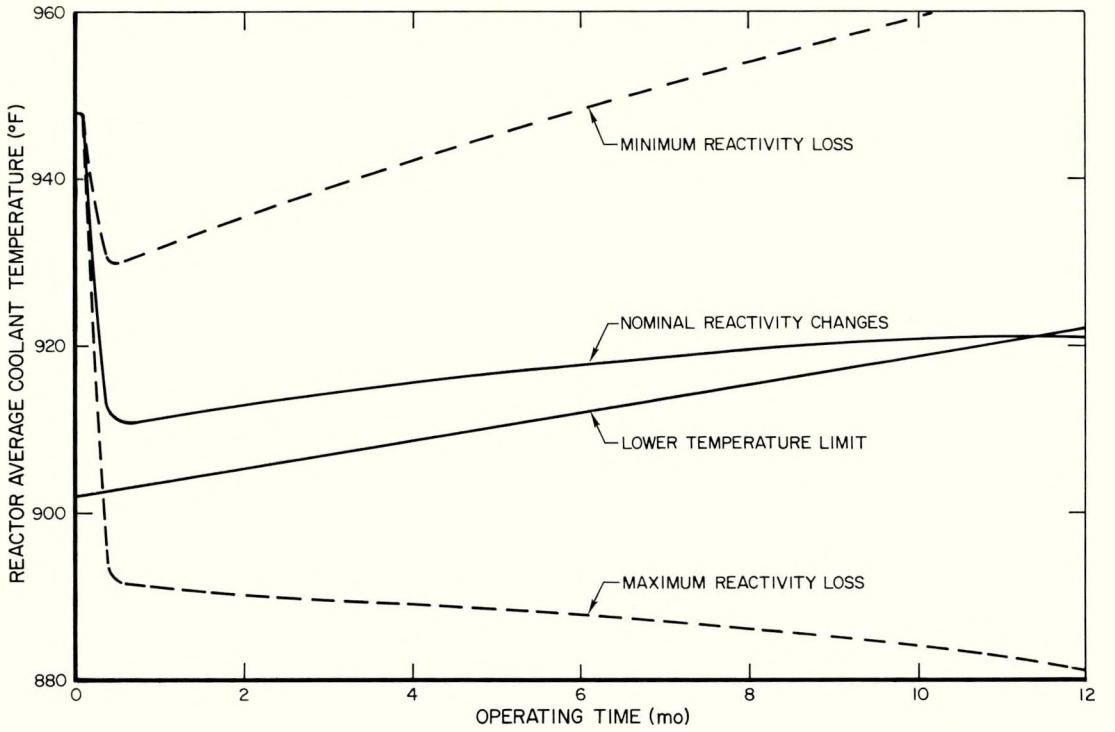

8-5-64 7623-0405B

Figure 19. Long-Term Temperature Drift of SNAP 10A Reactor

occur simultaneously in either the direction of maximum or minimum reactivity loss. The lower temperature limit curve specifies the minimum average coolant temperature which must be maintained in order to produce the required power of 525 electrical watts.

During the first three days of operation, the reactor outlet temperature will be controlled through inward rotation of the beryllium control drums. The reactivity changes due to temperature and power defect, xenon buildup, and partial hydrogen redistribution take place during this period. At the end of 72 hr, control drum movement ceases and the reactor operates on passive control for the remainder of the 1-yr operating period. For the greater part of the first month of operation, system reactivity (and therefore temperature) drops as the negative reactivity effect accompanying hydrogen redistribution rapidly reaches its maximum value. Following completion of hydrogen redistribution, core temperature slowly rises as the positive reactivity insertion caused by samarium prepoison burnout more than balances the reactivity losses due to fuel depletion, fission product accumulation, and hydrogen loss. During the 60-day period following completion of hydrogen redistribution, the core is expected to operate at the nominal full power of 39.5 kw. Other nominal operating conditions are listed in Table 1.

Reactivity values of the SNAP 10A reactor in various normal and abnormal configurations and environments form an extremely important part of the safety analysis. In addition, they govern to a large measure the formulation of safe handling procedures and emergency plans. The reactivity values presented in this section are based on a core loading utilizing three of the low N_H, high Sm_2O_3 loaded fuel elements.

SCA-4C paraffin block experiments have shown that the worth of one human leaning against the reactor surface is approximately 30¢ for reflected cores and about $1.10 for a bare reactor. However, the rigid rectangular blocks do not represent the more flexible contours and appendages of the human body which are present during reactor assembly operations. Additional experiments involving use of a hydrocarbon plastic human mockup, which could be draped over and around the reflected reactor, were performed to obtain effects of a simulated flexible human body.

The mockup was prepared by packing 200 lb of plastic pellets and paraffin into a pair of coveralls. Two long rubber gloves, representing arms, were also filled with the plastic pellets. It was found experimentally that the mockup was worth about $0.85 when leaning against and over the reflected reactor. The total worth increased to approximately $1.95 when "arms" were inserted as far as possible into open drum voids.

The reactivity information summarized in Tables 4 and 5 is therefore based on three separate cases of potential human body reflection:

a) Single human body — standing adjacent

This configuration corresponds to a single person standing against the reactor core or reflector, as the case may be, without any placement of hands in the drum voids. These reactivity values are based on the paraffin block experiments.

b) Single human body reflection — wrap around

This estimate is based on what is believed to be the maximum possible worth of a human body when used intentionally as a reflector. It is therefore considered to be an absolute upper limit for one person. For reflected reactor configurations, results of the human mockup

experiments have been used. With bare reactor cores, human body worths which are 1/3 those of infinite radial water reflection have been chosen to represent an upper reactivity limit.

c) Maximum human body reflection

This case is an extension of b) above, without limit to the number of persons involved (at least three are required). The reactivity worth associated with maximum human body reflection is considered to be equal to the worth of infinite radial water reflection. This is conservative because a human body cannot penetrate into the small spaces and intricate passageways that water can; on the other hand, it does not include axial reflection.

The range of reactivity values provided in Tables 4 and 5 for those cases where human body reflection is involved is based on the various human-reactor configurations discussed above. Additional reactivity information and other nuclear parameters, both analytical and experimental, are given in Tables 6 through 8.

TABLE 4

SNAP 10A REACTIVITY VALUES ($) UNDER VARIOUS ABNORMAL CONDITIONS DURING ASSEMBLY AND SHIPMENT

Condition of Reactor		Reactivity					
On Right Side	On Left Side	In Air	Single Human Standing Adj.	Single Human Wrap Around	Maximum Human Wrap Around	Infinite Water Reflection	
						NaK in Core	H_2O in Core
Sleeve	Sleeve	-18.70	-18.40	-16.70	-12.70	-8.00 ± 1.20	-3.00 ± 0.50
Sleeve	Bare	-19.80	-19.50 -18.70*	-17.80 -12.80*	-6.30	-3.35 ± 2.00	+1.65 ± 2.00
Sleeve	Reflector with void filler blocks	-12.00	-11.70	-10.00	-7.50	-4.60 ± 2.00	+0.40 ± 2.50
Reflector with void filler blocks	Reflector with void filler blocks	-5.00 ± 1.00	-4.70	-4.00	-2.00	-1.25 ± 0.50	+3.75 ± 1.50
Reflector with void filler blocks	Bare	-13.10	-12.80 -12.00*	-12.10 -5.50*	-1.10	+0.85 ± 1.50	+5.85 ± 2.00
Bare	Bare	-21.00	-19.90	-14.00	-1.70 ± 1.00	+1.30 ± 0.80	+6.30 ± 1.50

*Human on bare side

TABLE 5

REACTIVITY VALUES ($) FOR BERYLLIUM-REFLECTED SNAP 10A – NO VOID FILLER BLOCKS

Beryllium Reflected Reactor – All Drums Out No Void Filler Blocks	-5.60
Single human body reflection – standing adjacent	-5.25
Single human body reflection – wrap around	-3.67 ± 1.00
Two human body reflection – wrap around	-1.72 ± 1.00
Maximum human body reflection	-0.73 ± 1.50
Water in core – no water reflection	-0.60 ± 0.80
Infinite water reflection – no water in core	+1.87 ± 2.00
Infinite water reflection and water in core	+6.87 ± 3.00
Agena nose shroud and cap in place (launch config.)	-5.55
Beryllium Reflected Reactor – Two Drums In No Void Filler Blocks	-1.30
Single human body reflection – standing adjacent	-0.95
Single human body reflection – wrap around	+0.63 ± 0.50
Maximum human body reflection	+2.81 ± 1.50
Infinite water reflection – no water in core	+2.23 ± 2.00
Infinite water reflection and water in core	+7.23 ± 2.00
Infinite half plane water reflection (no core water)	+0.46 ± 2.00
Agena nose shroud and cap in place (launch config.)	-1.25

TABLE 6

REACTIVITY VALUES ($) FOR BARE SNAP 10A REACTOR UNDER SEVERAL ABNORMAL CONDITIONS
(See Table 4 for additional bare reactor data)

Bare Reactor – NaK in Core	
Infinite half plane water reflection	-10.00 ± 2.00
Infinite half plane sand reflection 0% H_2O	-15.00 ± 2.00
Infinite half plane sand reflection 30% H_2O	-10.50 ± 2.00
Infinite half plane concrete reflection	-11.30 ± 2.00
Bare Reactor Completely Submerged in Sand – Moisture Content for Criticality – NaK in Core	26%
Bare Reactor – Water in Core, No Water Reflector	-16.00 ± 1.00

TABLE 7

NORMAL SNAP 10A REACTIVITY WORTHS, TEMPERATURE AND POWER COEFFICIENTS

Normal Reactivity Worths		
Material	Worth	Remarks
Hydrogen	64¢ per wt % Hydrogen	Small Changes in Fuel Loading
U^{235}	9.1¢ per wt % U^{235}	Small Changes in Fuel Loading
Zirconium	15.6¢ per wt % Zr	Small Changes in Fuel Loading
NaK (in core and plenums)	+$0.26 ± 0.05	Measured in S10FS-1
Central Fuel Element	$3.15 ± 0.05	SCA-4A Data with Be Reflector
Edge Fuel Element	$1.55 ± 0.05	SCA-4A Data with Be Reflector
Shield	$0.35 (extrapolation)	
Temperature and Power Coefficients		
	Value	Remarks
Fuel Temperature Coef.	-0.075-0.000057T¢/°F	SDR Data
Total Temperature Coef.	-0.29¢/°F	At nominal operating conditions
Power Coefficient	-0.14¢/kw	At 950°F

TABLE 8

OPERATIONAL SNAP 10A REACTIVITY DATA

Condition	Reactivity ($)	Remarks
Reactivity Data for ATF (Bldg 019)		
Be Reflected Reactor (Dry)		
Four Drums In	+2.74	75°F Average Temperature
Three Drums In	+0.59	75°F Average Temperature
Two Drums In	-1.56	75°F Average Temperature
One Drum In	-3.71	75°F Average Temperature
All Drums Out (No Void Fillers)	-5.86	75°F Average Temperature
All Drums Out (Void Fillers)	-5.36	75°F Average Temperature
Required Excess Reactivity at 75°F with NaK	+3.00	All Drums In
Required Zero Power Excess Reactivity at 968°F	+0.92	All Drums In
Bldg 019 Vault Worth	+0.03	
Bldg 024 Vault Worth	+0.02	
Recommended Excess Reactivity In Space at 950°F, Full Power, 72 Hr after Startup	+0.32	

VIII. REACTOR CORE

A. DESIGN

The SNAP 10A reactor core is composed of 37 moderator-fuel elements. These elements are arranged in a triangular array, on 1.26-in. centers, to form a core which is hexagonal in cross section. The overall dimensions of the core are: 8.810 in. across the corners, 7.796 in. across the flats, and 12-1/4 in. in length.

The core assembly is contained in a cylindrical reactor vessel of Type 316 stainless steel. The vessel is 8.875 in. in inside diameter, 15.6 in. in length, and has a minimum wall thickness of 0.032 in. Internal side reflectors of beryllium are used to round out the hexagonal core configuration and fill the void spaces in the reactor vessel.

The elements are positioned in the vessel between grid plates of Type 316 stainless steel. End pins, 0.242 and 0.180 in. in diameter, engage holes in the upper and lower grid plates respectively to position the elements in the core. The lower grid plate is supported by a ring at the bottom of the reactor vessel. The top grid plate is spring-loaded against the vessel top head to permit thermal expansion of the core in the axial direction.

All coolant flow through the core is through the interstices formed by adjacent fuel elements or by elements and the internal side reflectors. Coolant passes through the grid plates by means of 3/8-in. diameter coolant holes drilled to align with the core coolant passages.

An orifice plate located below the lower grid plate was designed to produce the desired flow distribution. The desired flow distribution is one which produces equal coolant temperature rise in all coolant channels and a constant outlet temperature profile across the core. The coolant plenum chambers located above and below the core assembly in the vessel provide mixing space for the coolant.

B. THERMAL AND HYDRAULICS ANALYSIS

1. Core Flow Distribution

Coolant enters the reactor via two diametrically opposed inlet nozzles below the lower grid plate. The velocity of entry is 3.1 ft/sec in a direction

normal to the axis of the reactor. After entering the reactor vessel, the flow decelerates and turns to enter the core. The lower grid plate is made up of two plates: a support plate and an orifice plate. The coolant first flows through the orifice plate which contains 72 holes of diameters ranging from 1/4 to 3/16 in. in steps of 1/64 in., giving five different orifice sizes. The orifice plate was designed to provide a flow distribution to match the radial core power distribution. After passing through the orifice plate, the coolant enters the core through seventy-two 3/8-in. holes in the support plate.

The composite plate provides a rigid but lightweight support for the fuel elements and provides spacing between the orifice plate and the entrances to the coolant channels. If a single plate were used to support and orifice the core, the larger orifices would be partially covered and blocked by the fuel elements.

The core flow area is composed of the 72 orificed coolant channels and 12 extreme peripheral channels to which there is no entry from the lower plenum. The peripheral channels receive flow by crossflow between the fuel elements. NaK leaves the core through seventy-two 3/8-in. diameter holes in the upper grid plate. The flow converges upon the outlet nozzle in the center of the top head, and leaves the reactor at a velocity of 8.0 ft/sec.

Velocities in the coolant channels are governed by (1) the grid plate orifices, (2) the pressure drop in the channels, and (3) the amount of crossflow permitted by the nominal 0.010-in. clearance between fuel elements. Hydraulic tests of core velocity profiles were conducted using salt injection to measure average velocities. Shaping of the core flow was generally achieved, but the amount of crossflow could not be measured by this method. Analysis has shown that crossflow has a significant effect in reshaping the core velocity distribution downstream of the orifices. It is expected that by the time the coolant has traversed half the length of the core, the flow distribution will be nearly uniform. The importance of the core flow distribution upon fuel element temperatures can be assessed by a comparison of two limiting cases. First, in an ideally orificed SNAP 10A core, where the coolant flow profile exactly matches the radial power profile, the maximum fuel temperature in the core would be 1029°F. Second, if no orificing were provided and the velocity distribution were uniform, which corresponds to a 21% increase in the power to flow ratio, the maximum fuel temperature in the core would be 1058°F. These fuel temperatures are based on a coolant inlet temperature of 859°F. These temperatures show what little can be gained by perfect

orificing of the SNAP 10A reactor and, conversely, the effect that a 21% flow deficiency would have on fuel element temperatures. Since the higher of the temperatures is well below current temperature limits, and since the ideal flow distribution may not be achieved, much of the SNAP 10A analysis was based on the higher temperatures attained in a fuel element surrounded by flow-deficient channels.

2. Core Power Distribution

Because of symmetry of the SNAP 10A core and reflector, radial and axial power distributions are expected to be symmetrical about the core center. Local power peaking around the fuel elements is expected to be negligible. There is no significant reflector peaking in either the axial or radial planes. Because of small fractional burnup of fuel and resultant small control system movements, little change of core power profiles is expected during the design life of the reactor. For analysis purposes, axial and radial power distributions can be represented by the following expressions.

a) Axial Power Distribution — Normalized to an average axial power generation rate of 1.0.

$$P(z) = 1.47 \cos (1.48 - 0.241z), \qquad 0<z<12.25 \text{ in.}$$

b) Radial Power Distribution — Normalized to a peak radial power generation rate of 1.0.

$$P(r) = \cos 0.244r, \qquad 0<r<4.03 \text{ in.}$$

3. Fuel Element Temperature Distribution

a. Steady-State Temperatures

The highest fuel element temperatures and temperature gradients are attained in the center fuel element in the core. This element will be in the region of peak radial flux, and will exhibit the highest fuel temperature in the core. It will also produce the highest temperature rise in the adjacent NaK coolant. The latter would not be true for a perfectly orificed core; i.e., the coolant temperature rise would be the same in all channels. However, it is assumed that the flow rate adjacent to the center fuel element lies between the extremes produced by an ideally orificed core and an unorificed core. Temperature profiles in the fuel, clad, and coolant for the two extremes are shown in Figure 20 for a core inlet temperature of 859°F. The coolant profile has the "S" shape typically produced by a cosine axial power distribution. Clad surface temperature

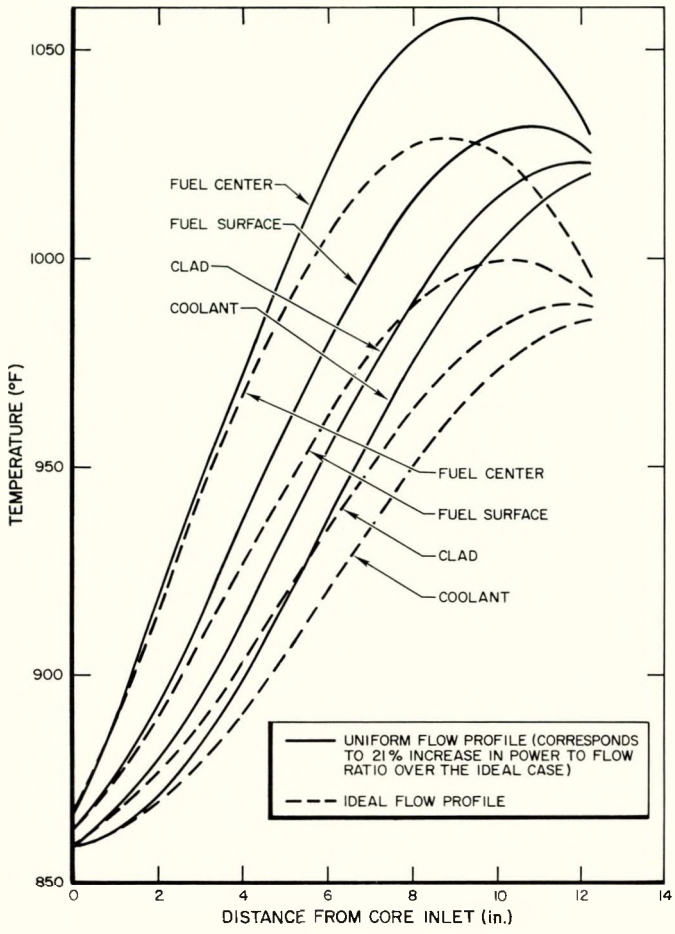

Figure 20. Steady-State Axial Temperature Distribution for Center Fuel Element—Comparison Between Ideal Flow Profile and Uniform Radial Flow Distribution (P = 39.5 kw, Flow 80 lb/min)

10-3-64 7623-0008A

exceeds coolant temperature due to a film drop of 2 to 26°F. Fuel surface temperature exceeds the clad temperature by an average of 15°F due to the temperature drop across the hydrogen-filled gap between fuel and clad. The average fuel temperature, averaged over the length and diameter of the fuel rod, is 983°F for the higher temperature curves of Figure 20. The axial average clad temperature for the same curves is 950°F. These temperatures are used to evaluate the increase in the axial fuel-cladding clearance in Section VIII, B, 4b. At the point of peak fuel temperature, the average temperature across the diameter of the fuel is 1042°F; the adjacent clad temperature is 1008°F. These temperatures were used to evaluate the change in the radial clearance in Section VIII, B, 4b.

b. Temperatures During Startup

From ground to steady-state operating temperatures in orbit, the coefficient of expansion of the fuel clad material exceeds that of the fuel.

Although the fuel-clad clearances increase from ground to operating temperature in orbit, the periods of maximum fuel-to-clad temperature during the startup transient require evaluation. The power, flow, and outlet temperature for the initial startup transient are shown in Figure 21. These curves span a 240-sec period during which the power peaks at 43 kw. Fuel-to-clad temperature excess in the center fuel element reaches a maximum 50 sec after the power peaks. At this time, and at a point 6 in. from the lower end of the fuel rod, the difference between the average fuel and the adjacent clad temperature reaches a maximum of 80°F (407-327°F). (See Figure 22.) At this time, the difference between the axial average fuel and clad temperatures on the centerline fuel elements is 38°F (344-306°F) as compared to the steady-state difference of 29°F.

The minimum axial clearance occurs on an edge-of-core fuel element, 70 sec after peak power. Average fuel and clad temperatures for the core edge fuel element are shown in Figure 23.

To evaluate thermal stresses in the fuel rod, transient radial temperature distributions have been determined for the first 240 sec of the startup transient. Highest thermal gradients occur 7 in. from the lower end of the center fuel rod. Radial temperature distributions in the center element at this elevation are plotted in Figure 24. The temperature gradient increases to a maximum 60 sec after peak power (200 sec after initiation of transient) and thereafter decreases. Peak stress occurs at the fuel surface where the temperature is lowest. Tangential stress at this point is + 960 psi; this value is well below the ultimate tensile strength of the fuel (σ_t> 15,000 psi at the local temperature).

Throughout startup and during steady-state operation, temperatures of the hydrogen barrier and the Hastelloy N clad differ by no more than 7°F. This can be shown by using a peak heat fux of 15,200 Btu/hr-ft^2 corresponding to the 43 kw peak power level during startup. For this heat flux, the temperature difference between the inside surface of the 0.004-in. (maximum) thickness of barrier coating and the outer surface of the 0.0155-in. (maximum) clad thickness is:

$$\Delta T = \frac{Q}{A}\sum\frac{\Delta X}{k}$$

$$= 15{,}200\left(\frac{0.0155}{10.9(12)} + \frac{0.004}{1(12)}\right) = 6.9°F$$

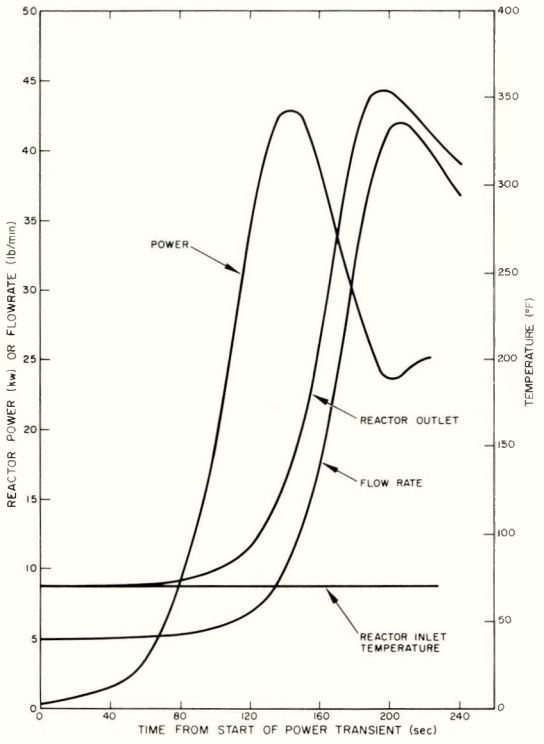

6-16-64 7623-0367

Figure 21. SNAP 10A Reactor Power, Inlet Temperature and Flowrate During Initial Power Transient

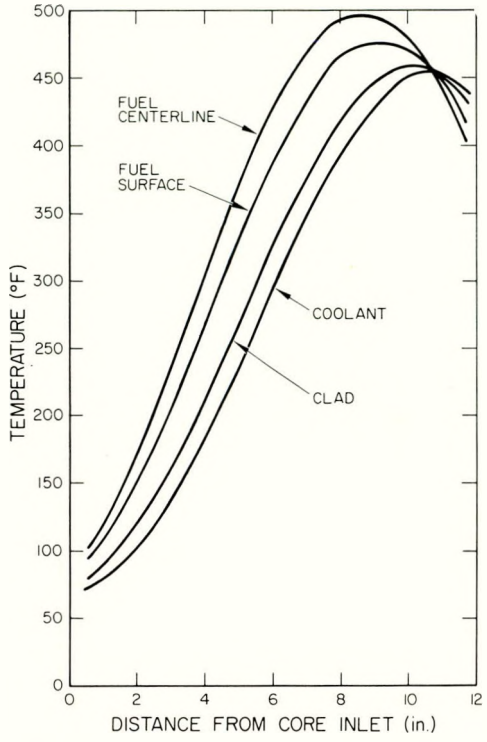

6-16-64 7623-0369

Figure 22. Axial Temperature Profiles in Center Fuel Element 60 Sec After Peak Transient Power

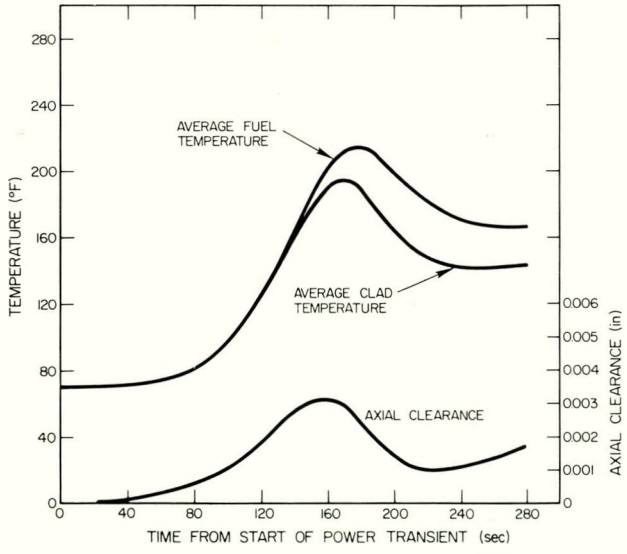

6-16-64 7623-0371

Figure 23. Average Temperature and Axial Clearances for Core Edge Fuel Element During Initial Power Transient

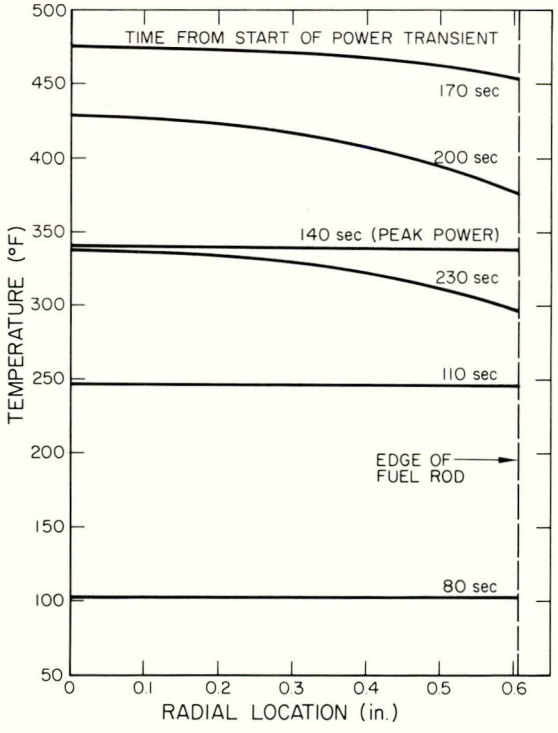

6-16-64 7623-0368

Figure 24 Radial Temperature Profiles in Center Fuel Element at 7 in. Elevation During Initial Power Transient

The difference between the mean barrier and the mean clad temperature does not exceed 4° F.

A relatively severe temperature gradient exists during startup at the junction of the Hastelloy-N clad and the upper end cap. The difference between the average end cap and the clad temperatures, 0.1 in. below the end cap, reaches a maximum of 72° F in the centerline fuel rod 30 sec after the transient power peak. (See Figure 25)

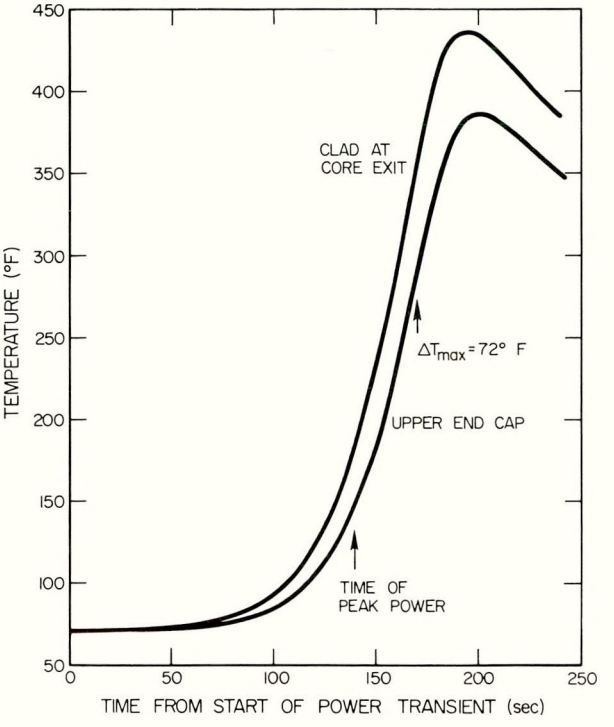

6-16-64 7623-0372

Figure 25. Centerline Fuel Element Upper End Cap and Clad Temperatures During Initial Power Transient

4. Differential Fuel-Clad Expansion

Thermal expansion data for the fuel and clad are illustrated in Figure 26 Note that the clad material expands somewhat more rapidly than does the fuel; the Hastelloy-N exhibits 29% more thermal growth between 70 and 1000° F.

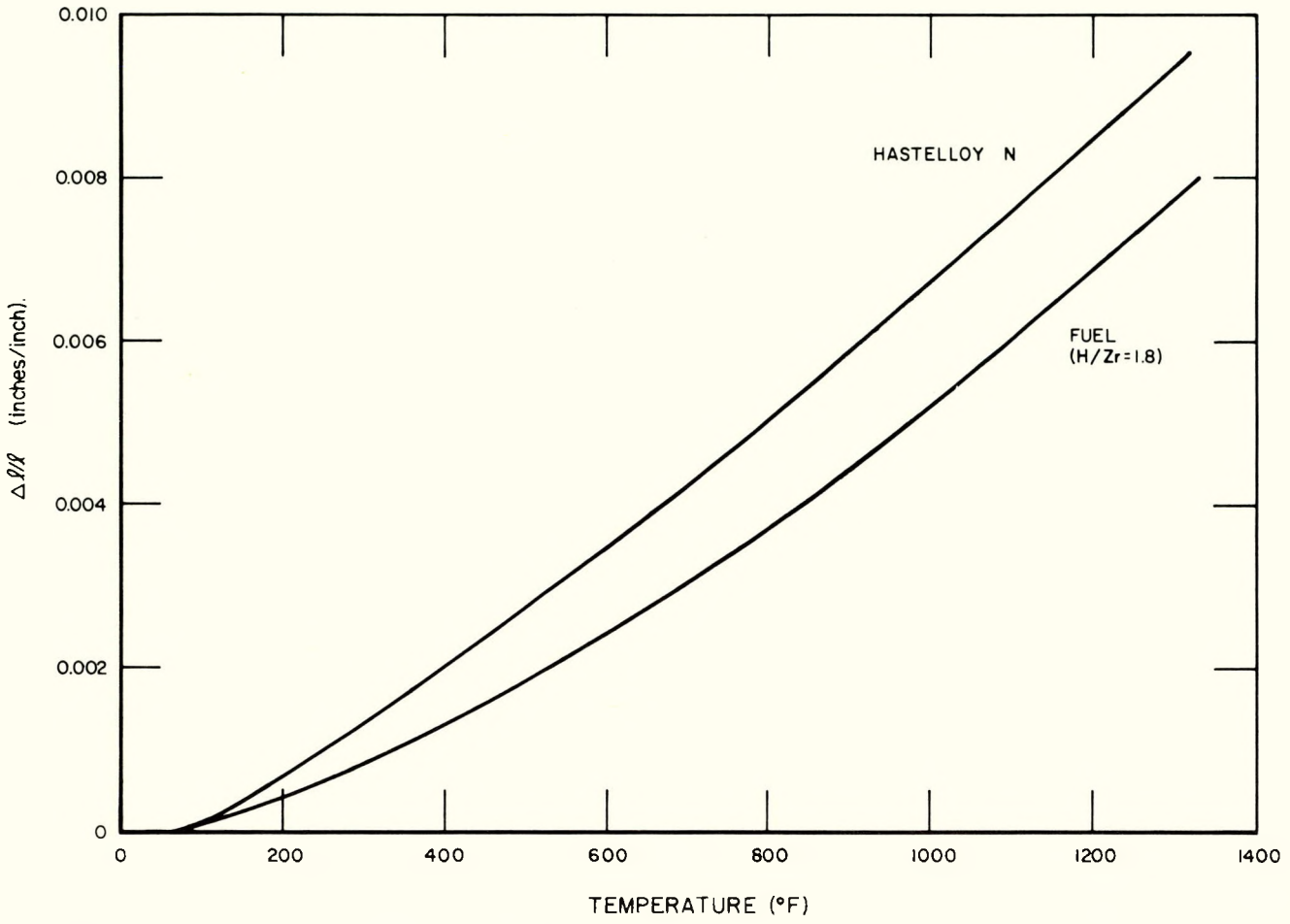

7-10-63 7623-0003

Figure 26. Thermal Expansion of S10A Fuel and Clad Materials

As a basis for evaluating the minimum clearances during operation, the minimum clearances at assembly were chosen. Combination of the fuel diameter and the coated tube ID (with their tolerances) yields a minimum diametric assembly clearance of 0.0035 in. The minimum axial clearance before welding of the end cap is zero.

a. Fuel-Clad Clearances During the Startup Transient

It was noted in Section VIII, B, 3b that the maximum fuel-to-clad temperature difference occurred during startup when the average fuel temperature in the center fuel element was 407°F and the clad temperature was 327°F. This was the worst local condition in the core, occurring 6 in. from the lower end of the fuel rod, 50 sec after the peak power transient. These temperatures produce a net increase in the diametric fuel-clad clearance of 0.0004 in. Using

the axial average temperatures for the edge fuel element discussed in Section VIII, B, 3b, the minimum axial fuel-clad clearance in the core during the startup power transient is 0.0010 in.

b. Fuel-Clad Clearances During Steady-State Orbital Operation

At the point of maximum fuel temperature in the center fuel element, the minimum steady-state diametric clearance between the fuel surface and the clad ID is 0.0015 in. greater than the clearance at assembly. Between room temperature and full power operation of the core, the axial clearance (as determined by the fuel and clad temperatures averaged along the length of the center fuel rod) increases by 0.0159 in. As long as a steady power level and flow rate are maintained, the average and local temperatures of the fuel must exceed the average and local clad temperatures. Therefore, there will always be a positive clearance between the fuel and cladding.

5. Differential Clad-Hydrogen Barrier Expansion

In Section VIII, B, 3b it was stated that the temperature excess of the hydrogen barrier over the clad temperature would not exceed 7°F during the life of SNAP 10A. Thus the assumption of essentially equal clad and barrier temperatures can be applied in determining the differential expansion at any point in the fuel element.

The combination of softening temperature of the barrier and operating temperatures in the fuel element produces compression in the barrier during fabrication and relaxation of barrier stress between launch and operating temperatures. It is desirable to have a compressive prestress in the barrier to minimize tensile stresses produced by launch vibrations. The prestress diminishes during startup, reaching a minimum at the steady-state temperature levels in orbit. The final temperatures are below the softening temperature of the barrier material and well below the range where crystallization takes place.

6. Thermal Stresses in Clad and Barrier at Junction to Upper End Cap

The Hastelloy-N clad and the ceramic barrier are subjected to maximum tensile stresses at the junction of the upper end cap and the clad. These stresses are related to the difference between the average end cap temperature and the adjacent clad temperature. As noted in Section VIII, B, 3b, the maximum temperature difference between the end cap and the clad 0.1 in. away occurs in the

center element and is 72°F (Figure 25). The corresponding maximum tensile stresses in the clad and the barrier are 28,700 and 9,600 psi, respectively.

The yield strength of Hastelloy-N is 40,000 psi at 500°F. Consequently, there is an adequate margin of safety for the clad. Because of the bonding procedure used, a residual compressive stress of approximately 25,000 psi exists in the barrier when the element is heated to 400°F during startup. Therefore, the barrier remains in compression throughout the startup sequence.

Another possible source of internal pressure is heating of the helium which is the cover gas used when the fuel element is loaded. However, when the element is sealed, the internal helium pressure is only 250 microns. The partial pressure of helium in the helium-hydrogen mixture is insignificant.

7. Internal Pressure in the Fuel Element

The principal mechanism of pressure buildup inside the fuel element is the dissociation pressure of hydrogen in equilibrium with the monatomic hydrogen of the fuel. Tangential stress in the clad due to dissociation is plotted against temperature in Figure 27 for an N_H of 6.35 and 0.15 w/o carbon. A conservative approach to internal pressure evaluation is to assume that the local pressure exerted on the clad is a function of the local fuel surface temperature (no hydrogen redistribution). With this definition, the lower curve of Figure 27 represents local clad stress vs local clad temperature. Stress rupture data for Hastelloy-N sheet were extrapolated to 10,000 hr and graphed vs temperature in the same figure.

Comparison of the stress level with the ultimate strength of the clad shows that the maximum allowable clad temperature is 1430°F. Maximum expected clad temperature in the SNAP 10A core is 1037°F. Therefore, rupture of the clad due to internal hydrogen pressure is not a limiting consideration for SNAP 10A conditions.

8. Expansion of the Internal Reflectors and Grid Plates

Due to the high thermal conductivity of beryllium and the high heat transfer coefficients in the core, the internal reflectors will operate at temperatures close to those of the adjacent coolant. Axial expansion of the reflector between 70 and 950°F amounts to 0.107 in. compared to the fuel element expansion of 0.075 in.

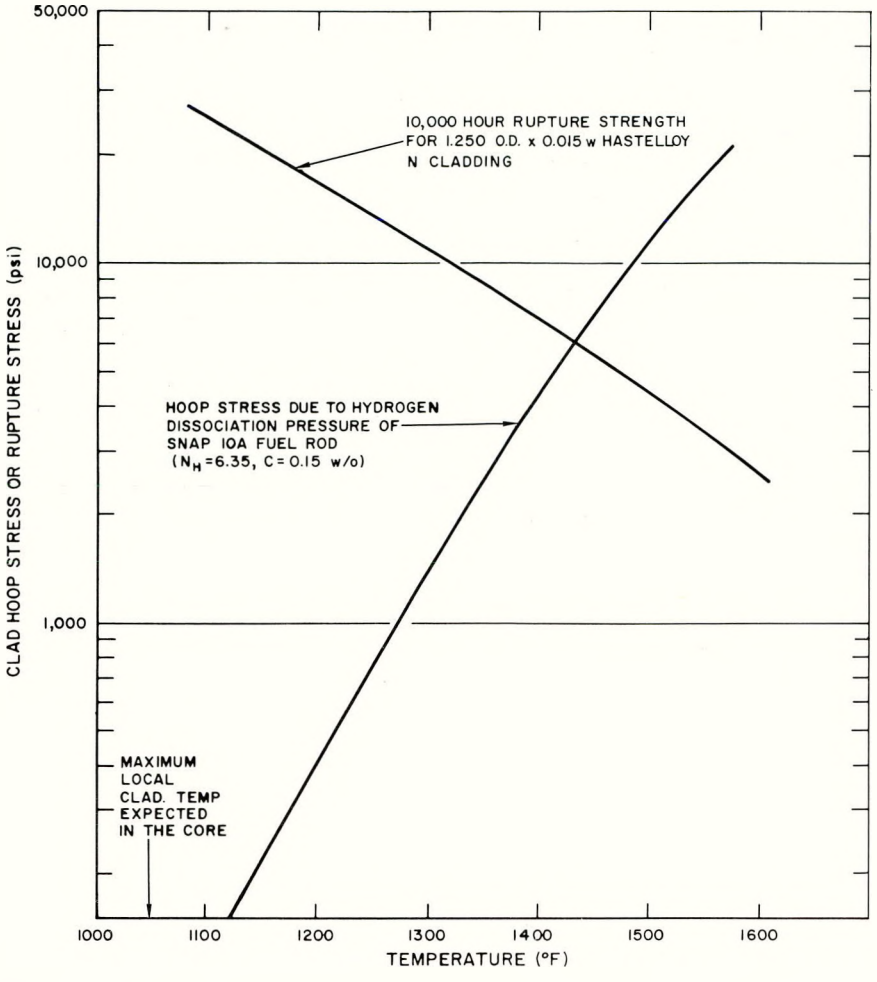

10-4-63 7623-0009

Figure 27. Hoop Stress in the SNAP 10A Reactor Cladding and Long-Term Rupture Data vs Temperature

The lower grid plate, composed of the baffle and orifice plates, will operate at a uniform temperature of approximately 900°F. No thermal stresses will be induced in these plates.

The upper grid plate will have a radial temperature distribution matching the core outlet temperature profile. For an ideally orificed core, the outlet temperatures would be the same for all coolant channels. If a completely uniform velocity profile were to exist, channel outlet temperatures would vary by 80°F, with the center of the plate operating hotter than the periphery. This gradient produces compressive stress on the center of the plate and tensile stresses at the edges, both of which are below 8000 psi. This stress is below yield stress for 316 SS at 1000°F and thus the plate will not buckle.

9. Reactor and Core Pressure Drop

Core pressure drop is made up of a fluid friction loss in the coolant channels plus orifice losses in the openings of the orifice plate and the two support plates. In spite of the fact that the core is orificed, the pressure drop can be fairly well approximated by using superficial uniform velocities based on the total flow areas. These velocities and areas are tabulated in Tables 9 and 11, along with the calculated pressure drop through each section. Velocities are based on a reactor flow rate of 80 lb/min. Pressure drops are based on a smooth tube friction factor and a pressure loss coefficient of 1.73 for submerged, square-edged orifices.

TABLE 9

CALCULATED SNAP 10A PRESSURE DROP USING SUPERFICIAL UNIFORM VELOCITIES BASED ON TOTAL FLOW AREA

	Flow Area ($in.^2$)	Velocity (ft/sec)	Pressure Drop (psi)
Reactor Inlet Nozzle (2)	1.29	3.14	0.051
Baffle Plates (2)	7.96	0.52	0.005
Orifice Plate	2.60	1.56	0.022
Coolant Channels	6.00	0.68	0.010
Reactor Outlet Nozzle	0.52	8.00	0.072
Total for Reactor			0.160

Reactor entrance and exit losses were based on 1.0 and 0.23 velocity head losses for sudden expansion and contraction, respectively. Since these two losses make up 78% of the total pressure drop, accuracy in the total figure must suffer due to inexact knowledge of entry and exit coefficients.

10. Nominal Operating Conditions

During the 60-day period following completion of hydrogen redistribution, the reactor will be in a steady-state operating mode at conditions which are referred to as nominal operating conditions. Table 10 lists the significant core parameters under nominal operating conditions. These parameters are of course not precisely met throughout this interim, but merely reflect the expected average performance during the initial steady-state period. Table 11 summarizes physical properties of the core and its constituents.

TABLE 10

CORE PARAMETERS DURING NOMINAL OPERATING CONDITIONS

Total reactor power (kw)	39.5
Reactor heat to NaK (kw)	37.6
Heat loss from vessel at operating temperatures (kw)	1.90
Core radial peak/average power factor	1.31
Core axial peak/average power factor	1.47
Fuel element peaking factor	1.00
Design NaK flow rate (lb/hr)	4800
Reactor pressure drop (psia)	0.160
Reactor inlet temperature (°F)	859
Reactor outlet temperature (°F)	987
Maximum fuel temperature (°F)	1058
Maximum clad surface temperature (°F)	1037
Nominal core pressure (psia)	5
Minimum core pressure (psia)	2
Maximum core pressure (psia)	10

TABLE 11

CORE MATERIALS – PHYSICAL PROPERTIES (AT 950°F) AND DIMENSIONS

	Material	Density (lb/ft^3)	Specific Heat (Btu/lb-°F)	Conductivity (Btu/hr-ft-°F)
Internal Reflectors	Be	113	0.65	63
Grid Plates	316 SS	495	0.135	11
Fuel	ZrH + 10 wt % U	350	0.15	13
Fuel Element Cladding	Hastelloy-N	538	0.10	10.9
Diffusion Barrier	-	140	0.20	1
Gas Gap	H_2	-	-	0.20
Coolant	NaK-78	46.8	0.209	15

Vapor pressure of NaK at 1000°F (psia)	0.8
Vapor pressure of NaK at 1100°F (psia)	1.7
Heat transfer coefficient at surface of center fuel element (Btu/hr-ft^2-°F)	1500
Core Dimensions (in.)	
Fuel element pitch (triangular arrangement)	1.260 ± 0.003
Fuel element diameter (cladding OD)	1.250 ± 0.002
Clad thickness	0.015 ± 0.0005
Fuel length	12.25 ± 0.002
Diffusion barrier thickness	0.003 ± 0.001
Diametric fuel-clad clearance	0.004 ± 0.0005
Fuel diameter	1.2100 ± 0.0005
ID of coated cladding	1.214 ± 0.001
Flow Areas ($in.^2$)	
Area of 54 tri-cusp channels	3.987
Area of 18 side channels	1.118
Area of 12 unorificed peripheral channels	0.935
Total core flow area	6.04
Area of openings in orifice plate	2.60
Area of openings in baffle plates	7.96
Equivalent diameters (in.)	
Tri-cusp channels	0.151
Side channels	0.075
Core average	0.142
Total active heat transfer area in core (ft^2)	12.35

IX. REENTRY BEHAVIOR

The discussion which follows is restricted to reentry of the SNAP 10A-Agena satellite from orbit. Reentry as a result of failure during the ballistic launch trajectory is not considered herein.

The reentry configuration of the SNAP 10A-Agena, which enters the sensible atmosphere at 400,000 ft after orbital decay is shown in Figure 28. The vehicle velocity vector passes through the vehicle center of mass, and lies below the local horizon. The local horizon is tangent to the atmospheric surface or perpendicular to the radius vector to the center of the earth. Local horizon, flight angle, and aerodynamic restoring force relationship are defined in the figure.

Only that portion of the atmosphere below 400,000 ft is important to reentry heating breakup. The actual atmosphere of the earth is a thin shell wrapped on an oblate spheroid. The earth-atmosphere-orbit relationship is shown in Figure 29 for the proposed 700 nautical mile polar orbit. Considering the SNAP 10A polar orbit, it has been shown that the vehicle orbit can never give constant altitude for all latitudes. Thus, an initial altitude over the pole does not correspond to the same phase of orbit decay as does the same altitude over the equator. However, this effect will not significantly affect the degree of reactor heating and ablation.

The initial point in the orbital decay calculations was taken at 400,000 ft over the North Pole. Trajectory calculations were performed with an electronic digital computer using the computer code RESTORE developed by Dr. V. D. Sanders of Atomics International. The reentry trajectories are shown in Figure 30, together with a reference orbit describing altitude variation due to earth oblateness in the absence of drag forces. The significant events that occur during reentry, as noted on the trajectory in Figure 30 are: (a) transition to continum flow, (b) reactor separation from SNAP 10A system, and (c) SNAP 10A-Agena vehicle separation.

The vehicle enters the atmosphere with an angular rate and arbitrary angle of attack as a result of attitude control. Antenna orientation during system operation requires that the SNAP 10A-Agena make one revolution per orbit, resulting in the reactor always facing outward from the earth. Therefore, the vehicle will enter the atmosphere with some angle of attack with an angular rate. This

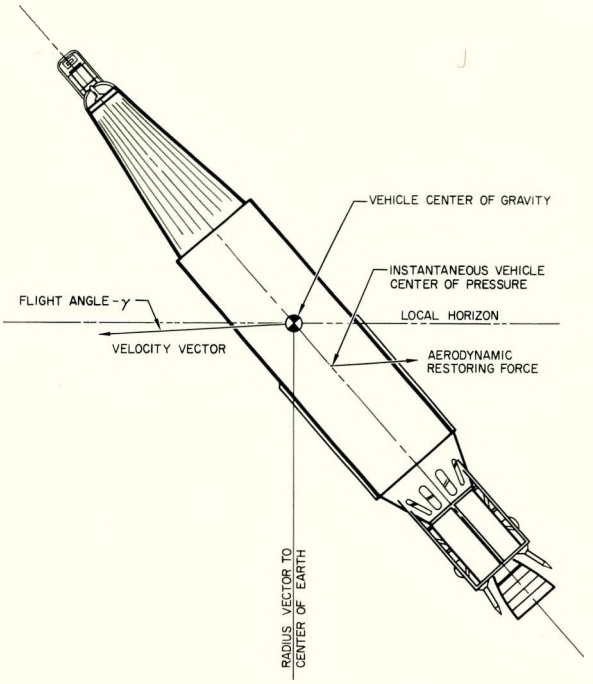

4-13-64 7623-0175

Figure 28. SNAP 10A-Agena Configuration During Reentry

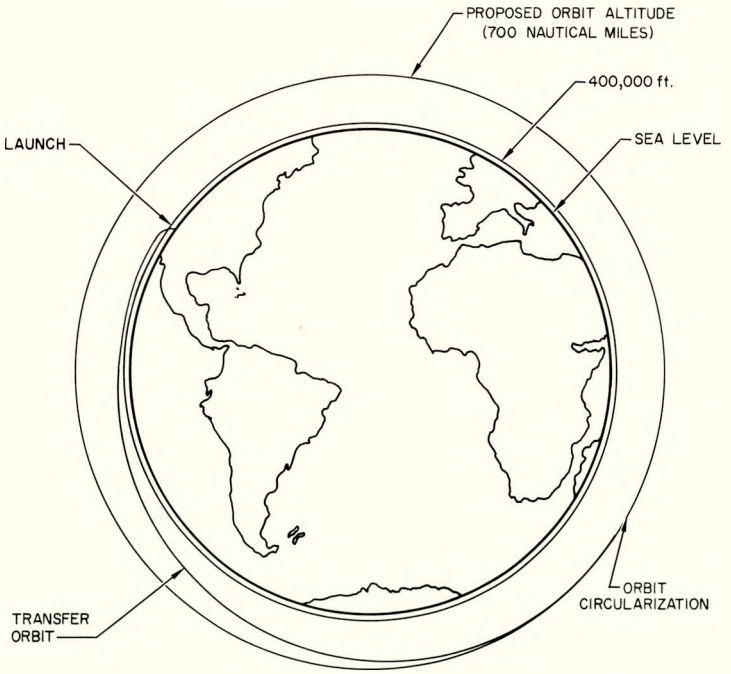

4-13-64 7623-0174

Figure 29. Typical Polar Orbit, SNAP 10A

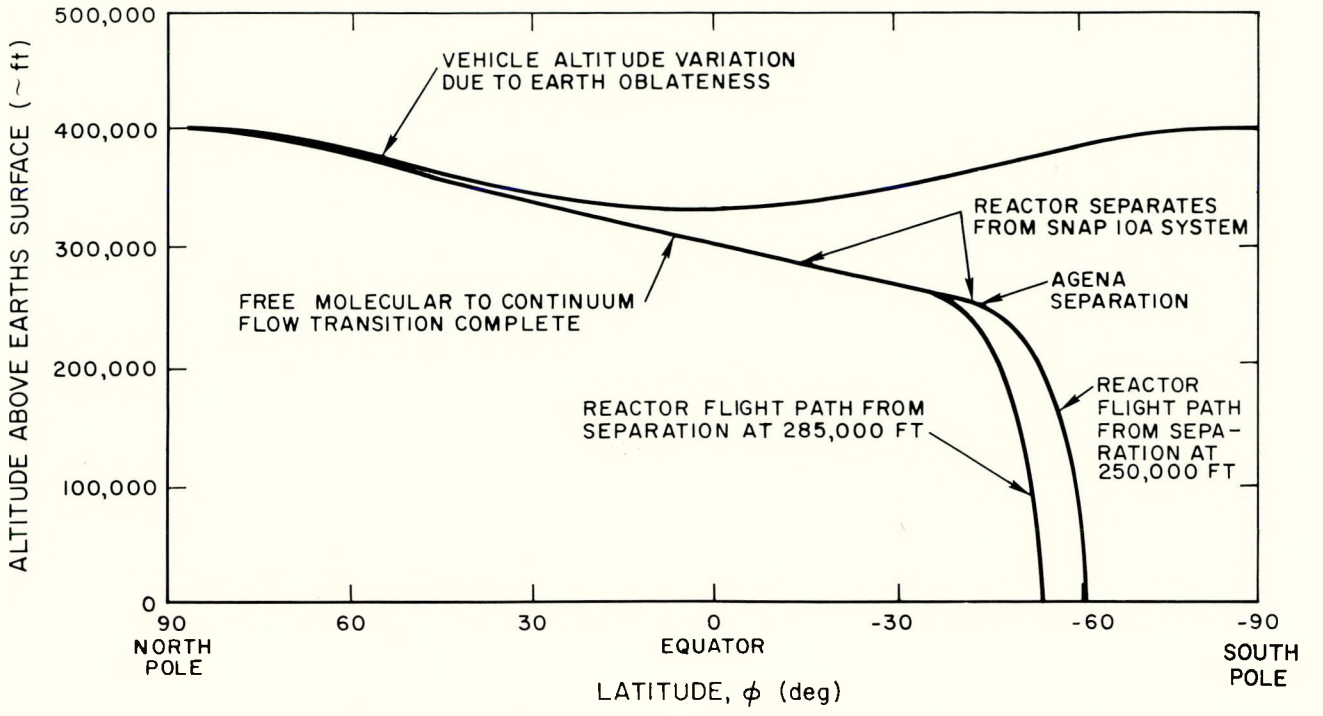

4-15-64 7623-0176-1

Figure 30. SNAP 10A Reentry Trajectory

event is shown in Figure 31 for the nose forward aerodynamic configuration of the SNAP 10A-Agena. The resultant of aerodynamic forces shown by the figure acts through the vehicle center of pressure, thus imposing a moment and forcing the vehicle towards zero angle of attack. The vehicle will oscillate about the center of gravity with the reactor orientated forward due to aerodynamic stability. The SNAP 10A power system achieves aerodynamic stability in the same manner as does the SNAP 10A-Agena vehicle as shown in Figure 31. When separated from the converter structure, the SNAP 10A reactor has neutral aerodynamic stability, and has a tumbling entry mode since there are no restoring aerodynamic forces acting away from the center of mass.

Aerodynamic forces will tend to restore the SNAP 10A-Agena vehicle to a position with the reactor aligned forward along the flight path. The SNAP 10A-Agena vehicle oscillation envelope, cycle frequency and dynamic pressure for this reentry condition are shown in Figure 32 for the case where the initial vehicle angle of attack is 90°. The reduction in oscillation amplitude and increase in frequency is a pseudo-damping effect provided by the increase in

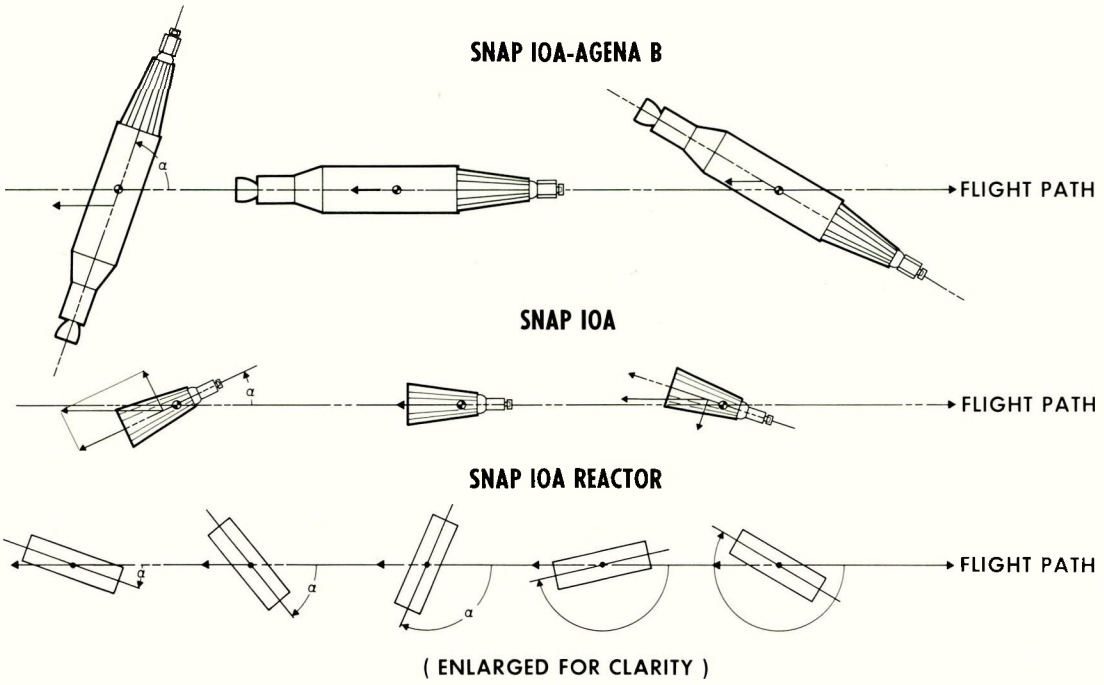

5-2-63 7573-1071

Figure 31. SNAP 10A – Reentry Oscillation

Figure 32. Envelope Dynamic Pressure During Reentry

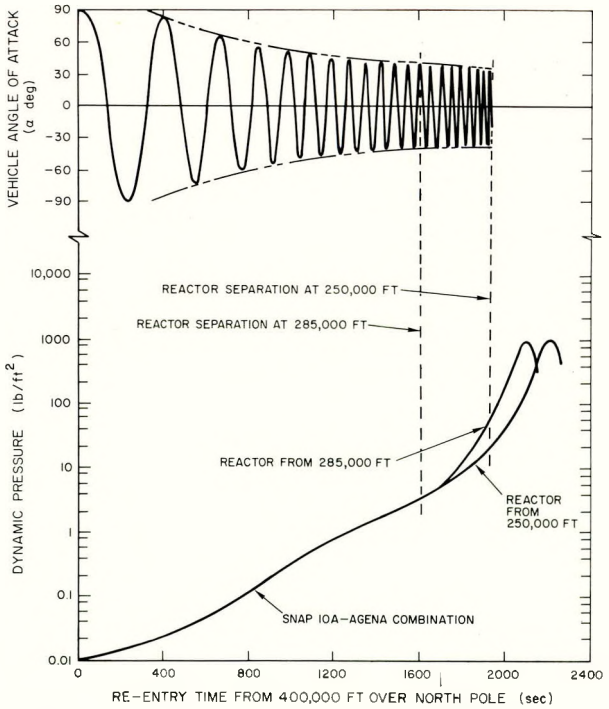

4-15-64 7623-0178

dynamic pressure throughout the orbital decay period to an altitude below significant aerodynamic heating. The increase in dynamic pressure is the result of atmospheric density, which increases monotonically during reentry.

The normal reentry configuration is without the reflector, which is ejected while still in orbit at the end of mission life. Should the reflector still be in place around the reactor at the beginning of reentry, it will shield portions of the reactor support legs from aerodynamic heating and thus delay reactor separation from the converter and vehicle. Because this configuration represents the more pessimistic condition, the detailed reentry analysis reported herein is based on the case where the reflector is not ejected prior to reentry. However, as will be shown, aerodynamic heating will melt the reflector retaining band at an early stage of the reentry, thus initiating reflector ejection and minimizing its effect on reactor separation.

For reentry following the design orbit lifetime of 3800 years, it is conceivable that the reflector ejection springs will have degraded to the point where they will not be capable of causing reflector ejection. However, even under this assumption, there will be sufficient aerodynamic forces to remove the reflector as described below.

The vehicle oscillation about its center of gravity during reentry results in varying degrees of vehicle angular acceleration. Following retainer band separation (caused by aerodynamic heating), the reflector half with a major surface component on the lee side of the reactor, with respect to air flow, will separate from the reactor on the first oscillation of the reactor back toward zero vehicle angle of attack. This reflector half can be visualized on the upper side of the reactor centerline shown in Figure 28. To further illustrate this point, consider an arbitrary point on the oscillation path of the vehicle at a zero vehicle angle of attack. From this angle, the vehicle is accelerated away from the flight path by aerodynamic forces. However, when the vehicle reaches the maximum angle of attack and accelerates back toward the flight path, the reflector on the leeward side of the reactor will continue on a path away from the reactor. The reflector continues in this path because there is no longer a restraining force, from either the retainer band or aerodynamics, which holds the reflector to the reactor or which causes it to deviate, as the reactor does, back toward the flight path. The remaining reflector half separates during the

next segment of the same vehicle oscillation period, in which the vehicle is on the opposite side of the flight path, thus placing the remaining reflector half on the leeward side of the reactor.

As discussed previously (Section IV), possibility of self-welding of the reflector onto the reactor vessel is extremely remote. However, should a strong enough bond form between the beryllium reflector and the reactor vessel, it may not be possible to eject the reflector during reentry. In this case, the reactor will probably impact on earth in an essentially intact condition. The remaining discussion is based on the premise that self-welding of the reflector onto the vessel will not occur.

The probability of reentry occurring with a NaK-filled system depends upon orbit lifetime. However, if NaK is present in the reactor, the combination of surface coatings on the vessel and reflector assures that the NaK will be in a liquid state when reentry commences. The reentry events for a system both devoid of NaK and filled with NaK are described in the following paragraphs.

A. REENTRY OF A SYSTEM DEVOID OF NaK

The reentry trajectories and oscillation behavior shown in Figures 30 and 32, respectively, provided the free-stream flight conditions and spatial orientation of the vehicle with respect to time, or altitude, for correlation of aerodynamic heating on vehicle components. The spherical stagnation point heating rates for a cold wall (temperature equal to 540°R) and vehicle velocity are presented in Figure 33.

1. Reflector Retainer Band-Reflector Ejection

In the event that the reflector assembly is still attached at the time of reentry, the retainer band will be aerodynamically heated to a temperature where separation occurs, releasing the reflector assembly. During reentry the band temperatures oscillate due to the variable aerodynamic heating rate being applied to a changing projected band surface area and to cyclic reactor shadows on the band. By an altitude of 290,000 ft, the retainer band will have cycled through the melting temperature of stainless steel. When the band parts, the reflector halves, being retained only by a cable harness containing electrical connections and reflector instrumentation, fall away from the reactor. Once ejected, the reflector halves will pivot until they contact the reactor support

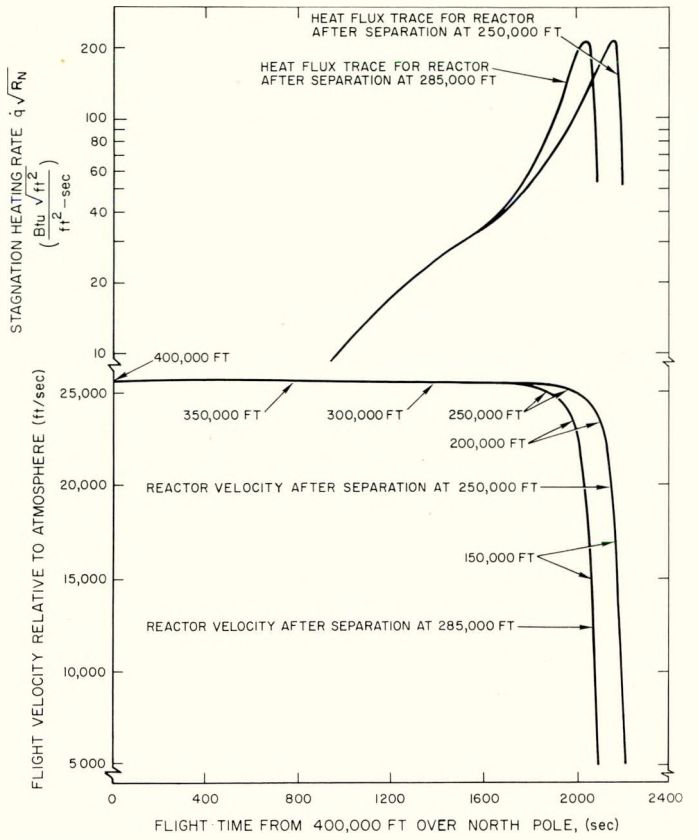

4-15-64 7623-0179

Figure 33. SNAP 10A Continuum Heating Rate and Flight Velocity Profile

legs and the tip of the shield. In this position, the cable harness is exposed to aerodynamic heating; complete release of the reflector is expected above 285,000 ft.

2. Thermoelectric Pump

The aluminum radiators of the thermoelectric pump will be completely ablated by 280,000 ft. The primary effect of this event is to increase the aerodynamic heating on the upper surface of the reactor vessel. The top surfaces of the magnets will have started to ablate by this altitude. However, the reactor vessel top will separate prior to complete magnet ablation.

3. Reactor Separation

Separation of the reactor from the SNAP 10A system depends on ablation of the four titanium support legs and the NaK inlet and outlet pipes. The forward portion of the NaK outlet pipe will receive the greatest heating rate of these

components during reentry and will melt through at 290,000 ft. During melting of the outlet pipes the reactor remains attached to the converter structure by four titanium support legs which follow the outline of the top of the shield. Shortly after the outlet pipes melt, the 0.032-in. thick titanium wall melts exposing the portion of the stainless steel NaK inlet lines where the walls are 0.020-in. thick. Ablation of the reactor inlet NaK lines is complete by 285,000 ft. At this point, the reactor will separate from the converter structure and begin to tumble. The reactor will continue toward earth on a trajectory dependent upon a ballistic parameter determined by the reactor weight, projected area to the air stream, and the drag coefficient of a tumbling cylinder.

4. Agena Separation

The converter structure-Agena complex remains aerodynamically stable after reactor separation and continues to reenter in an oscillating mode, nose forward. As shown in Figure 33 the aerodynamic heating rate continues to increase after reactor separation and results in the burning away of the converter structure and in severe heating at the SNAP 10A-Agena connector ring. The connector structure will fail by 245,000 ft, causing breakup of the vehicle into segments of questionable aerodynamic stability.

B. NaK-FILLED SYSTEM AT ENTRY

The presence of NaK in the SNAP 10A system will retard reentry ablation by absorbing a portion of the available aerodynamic heat production. A conservative analysis must therefore be based on a configuration with reflectors in place and a NaK system which has not been penetrated prior to reentry and has a flow rate in the reverse direction of operation. The flow in the reverse direction is a result of aerodynamic heating of the thermoelectric pump radiator fins and subsequent conduction of heat through the thermoelectric pump elements to the cooler NaK.

The NaK system will be simultaneously heated at four principal points: (1) the reactor outlet lines at the forward end of the power unit normal to the flight path, (2) the reactor outlet lines where they penetrate the vessel support legs, (3) the converter tubes, and (4) the upper converter manifold. Heating is greatest where the lines are aligned normal to the air stream. However, the entire reactor system will heat up as a result of NaK circulation transmitting

the heat from local hot points where aerodynamic heating supplies energy to the system. The average temperature of these parts of the system where NaK will flow is shown in Figure 34. The first penetration will be made at the outlet lines ahead of the reactor.

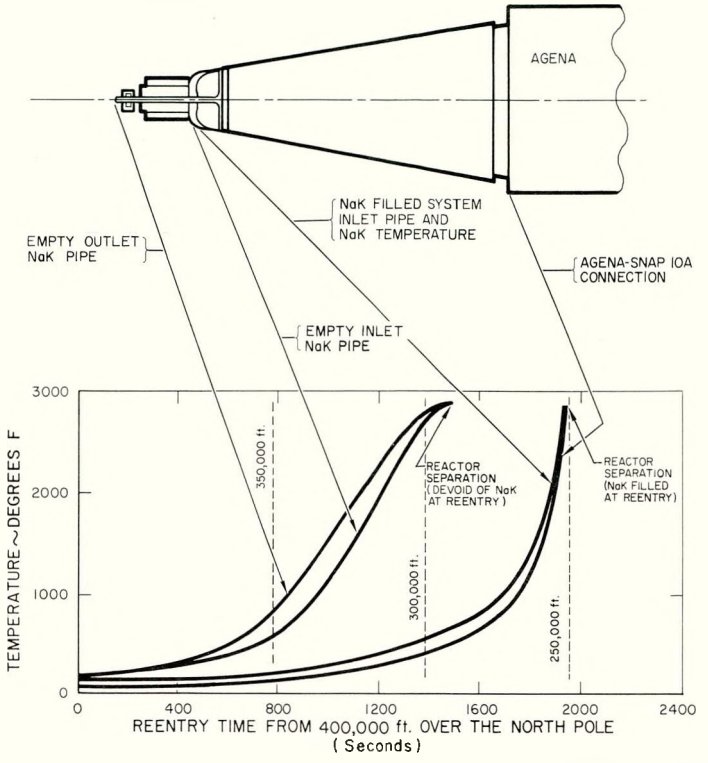

4-14-64 7623-0180

Figure 34. SNAP 10A Temperature Profiles During Reentry from Orbit

1. Reflector Retainer Band – Reflector Ejection

The NaK in the system has no effect on the reflector retainer band, and reflector ejection will occur above 285,000 ft as described for the system re-entering devoid of NaK.

2. Reactor Separation

Reactor separation from the remainder of the SNAP 10A system will be delayed due to the removal by the flowing NaK of the energy necessary to raise the NaK inlet and outlet pipes to their melting temperatures. The four titanium support legs will melt and expose the NaK inlet lines to the airstream thus resulting in NaK line ablation when the NaK system ruptures. As a result of

forward NaK pipe burnthrough, separation of the reactor from the remainder of the system is expected to occur by 250,000 ft. Complete ablation of the thermoelectric pump fins, and loss of magnetism in the pump by 280,000 ft, will result in termination of NaK flow. Since heat will no longer be carried away in quantity by the flowing NaK, the temperature of the NaK lines exposed to aerodynamic heating will rise sharply. The most probable point of first penetration will be at the forward NaK lines due to the magnitude of aerodynamic heating at this location. However, system rupture is assured by rupture of an expansion compensator at a pressure between 100 to 200 psi (1900 to 2200°F). NaK system rupture, followed by NaK line burnthrough and reactor separation, will therefore occur above 250,000 ft.

C. REACTOR VESSEL ABLATION

The free tumbling reactor vessel trajectories begin at 285,000 and 250,000 ft for the respective systems, devoid or filled with NaK. These trajectories are shown in Figure 30.

The heating of the reactor vessel during the tumbling mode will be greatest at the upper and lower circumferences of the vessel. Since the lip weld on the vessel head is exposed to aerodynamic heating from the beginning of reentry, it will be the first part of the vessel to experience complete peripheral melting. The reactor vessel completely ablates by 240,000 ft for both the cases of NaK in the core and the core devoid of NaK at the initiation of the reentry sequence. This is due to the respective energy (temperature) levels of the reactor, in each case, at separation. The interior of the reactor separated at 285,000 ft would be comparatively cool, approximately 200°F, while, due to NaK circulation, the temperature of the reactor separated at 250,000 ft would be in excess of 1200°F.

After melting of the reactor vessel, the core will be held together by only the grid plates. The upper grid plate will melt shortly after exposure to direct aerodynamic heating which will occur when adjacent sections of the vessel ablate. The fuel elements will continue to reenter as a single mass until disengaged from the lower grid plate by aerodynamic forces of ablation of the lower plate. Thereafter, the fuel elements will reenter individually.

Disengagement of the fuel from the grid plates immediately after reactor vessel ablation will allow the elements to separate and continue on independent trajectories from an altitude of approximately 240,000 ft. The release of fuel elements from this altitude in the reentry trajectory will expose the fuel to a major portion of the available aerodynamic heating. The ballistic parameter (W/C_DA) of an individual fuel element has a value between 20 and 30 for cross-flow orientation with oscillations. Therefore, deceleration will take place during a sufficiently long time interval to impart appreciable aerodynamic heating to a fuel element. This will result in a significant degree of fuel element burnup and is expected to cause complete ablation.

The separation sequences of the SNAP 10A (void and filled NaK systems at reentry) are summarized in Table 12.

TABLE 12

SNAP 10A-AGENA SEPARATION SUMMARY

Item	System Devoid of NaK at Reentry		System with NaK Circulation	
	Time* (sec)	Altitude (ft)	Time* (sec)	Altitude (ft)
NaK outlet pipe (front of reactor)	1540	290,000	1950	250,000
Retainer band rupture, reflector ejection†	1720	285,000	1720	285,000
Reactor support legs	1720	285,000	1720	285,000
NaK system loop rupture	—	—	1760	275,000
NaK inlet pipe (at support legs) reactor separation from SNAP 10A system	1720	285,000	1950	250,000
Agena separation	1890	245,000	1970	245,000
Reactor vessel ablation (fuel element release)	1900	240,000	1990	240,000
Impact	2260	Sea level	2370	Sea level

*Time zero at 400,000 ft over North Pole
†If not previously ejected at the time of reactor shutdown in orbit

X. STEADY-STATE OPERATION IN A RAIN-FILLING CRATER

If the SNAP 10A reactor core somehow survives the aerodynamic heating and impact reentry forces and remains in a configuration capable of criticality, the possibility of quasi-steady-state reactor operation on land exists under certain environmental conditions. Further, if the reactor survives the impact forces, some penetration of earth is probable, possibly leaving the reactor resting in a small crater. Under these conditions, it is possible that water could collect around the reactor to a sufficient degree for criticality to be regained. If the water input (most likely through rainfall) is of the proper rate, steady-state operation of the reactor could conceivably occur.

This situation has been analyzed under very conservative assumptions in order to determine an upper limit for possible steady-state power operation. The analytical model employed is based on the following assumptions: (1) The reactor survives reentry heating and the core impacts on land as a single intact entity; (2) The core survives the impact without disassembly; (3) The hydrogen content of the fuel is equal to the initial hydrogen loading; (4) Upon impact, the core digs a cylindrical crater and positions itself upright in the crater so that free convection circulation of water is possible through the lower end of the core; (5) The core vessel is open at both ends. This model is illustrated in Figure 35 and was investigated for various rain rates and crater radii.

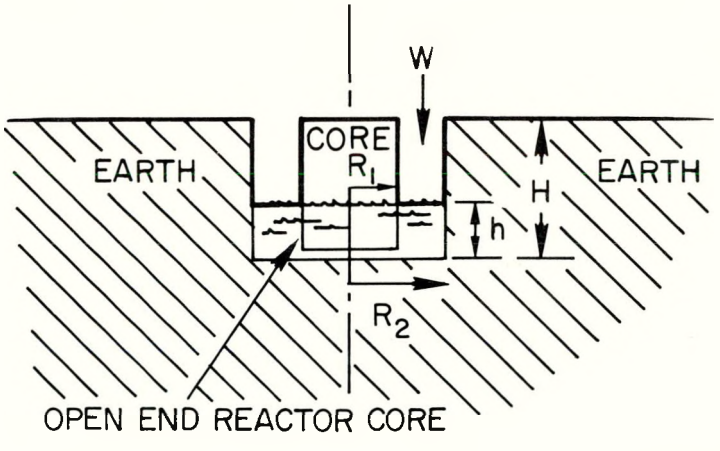

7-10-63 7623-0007

Figure 35. Core in Center of Cylindrical Crater During Rainstorm

An approximate relationship between reactivity insertion rate and rain rate may be developed for a specified crater size. An upper limit on rain rate for the approach to steady-state operation may then be set by consideration of the maximum reactivity insertion rate which would not cause fuel damage during the initial power pulse.

The rain rate may also be related to the steady-state power of the reactor. Under the condition that heat losses other than that resulting from boiling off of water are negligible, the steady-state reactor power must be equivalent to the water boil-off rate. The steady-state power level is limited to a value above which the corresponding temperature and hydrogen diffusion will cause cladding rupture. Hence, a second relationship limiting the rain rate for steady-state operation in various size craters may be obtained.

Both of these effects are illustrated in the curves of Figure 36 which shows the relationship between rain rate and crater size for various steady-state power levels. The highest steady-state power curve shown is 250 kw. Above this power level, damage to fuel occurs because heat removal under the boiling water heat transfer mode is not sufficient without increasing fuel temperature beyond the damage point. Therefore, steady-state operation certainly must lie below the 250 kw line.

The upper (or semi-horizontal) curve in Figure 36 represents the rain rate above which the initial power pulse associated with the rising water level will damage the rods. This curve was obtained using 0.9¢/sec as the maximum allowable reactivity insertion rate. This is a conservative ramp input with respect to providing an upper limit on steady-state operation, because information from this ramp indicated that smaller ramps will cause fuel damage and thus provide a lower limit line. The maximum transient energy pulse associated with this ramp at the various rain rates considered was 35 Mw-sec[13]. This value is approximately the energy released in the SNAPTRAN-3 destructive test, which further indicates conservatism for this use. The value of the rain rate must lie beneath the values of this curve and the 250 kw curve for possible steady-state power operation.

The third and final boundary limit is provided by the vertical line at $R_1/R_2 = 1.0$ which is a physical limit because the crater radius cannot be smaller than the core radius. The R_1/R_2 limit cannot be established at a value less than 1.0 because it has been shown that certain moisture-bearing soils can cause criticality. Thus, together these curves form a limiting area of conditions, outside of which steady-state power is not possible.

The curve to the extreme right in Figure 37 represents the steady-state power associated with the various maximum rain rates which would not cause

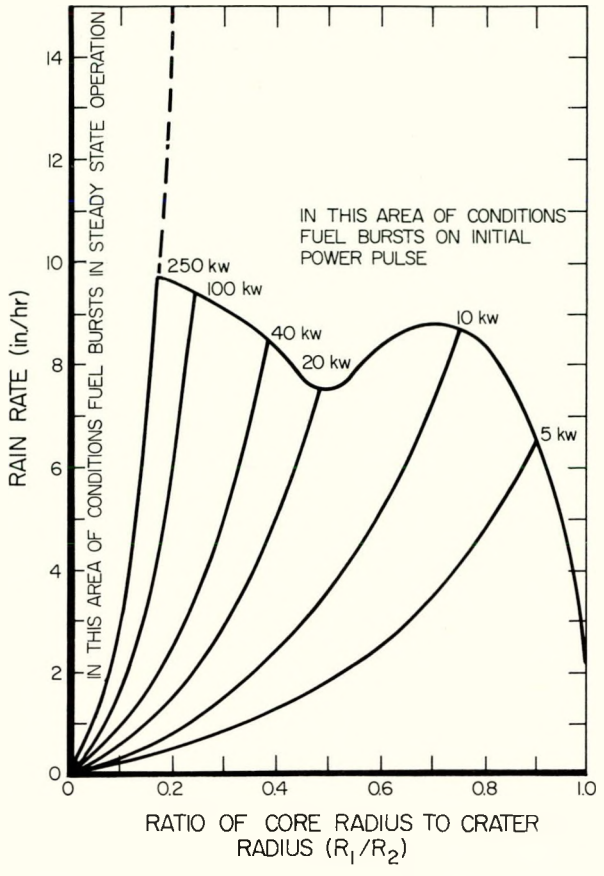

6-24-64 7623-0407

Figure 36. Effect of Rain Rate and Crater Size on Possible Steady-State Power Level

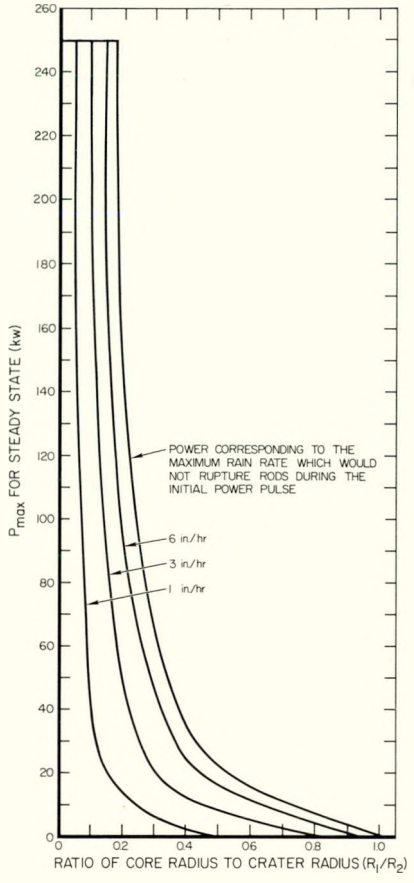

6-24-64 7623-0408

Figure 37. Maximum Steady-State Power as a Function of Crater Size for Various Rain Rates

rod damage on the first power pulse. The other curves on Figure 37 represent steady-state power levels associated with rain rates from 1 to 6 in./hr. If an upper limit could be set for rain rate and a lower limit could be set for the ratio R_1/R_2 the possible steady-state operation range would be limited accordingly. For example, assume that the crater formed is five times larger in radius than the reactor core. Further, assume that it is improbable to have rain rates exceeding say, 3 in./hr. Examination of Figure 37 would then lead to the conclusion that steady-state power operation at levels exceeding 50 kw would be very improbable.

Use has been made of a reactivity per inch change in water level rate applicable to the case of water levels about the center few inches of core height. This use is justified in the case of small (R_1/R_2) ratios in that the reactor core can go cold-critical when the water level reaches 6.85 in. As (R_2-R_1) decreases

below 4 in. the reflector no longer appears infinite and criticality would occur for higher water levels with a corresponding decrease in reactivity worth per unit change in water level.

In summary, by considering maximum power levels as limited by fuel rod damage, it is possible to predict the maximum steady-state power for a SNAP 10A reactor in a rain-filling crater. The model employed was very conservative and highly idealized. It is very unlikely that all of the conditions imposed on the system could occur simultaneously. For example, in all probability, the reactor, after impacting on soil, will be plugged with dirt at one end of the core, thus preventing water circulation. For this case the maximum power which can be generated in the core is 6 kw[12] before rupture of the fuel element occurs due to overheating. Consequently, it is highly improbable that steady-state operation will occur above the 5 kw curve shown in Figure 36. Furthermore, the hydrogen concentration will be lower than assumed due to reentry heating, and the rain rates studied are very high for any part of the world except under extreme short-term conditions.

XI. LONG-TERM OPERATION

Under design conditions the reactor will operate at full power for a period of 1-year at an expected average temperature in the range of 910 to 925°F. At the end of this period, which is the end of the design mission life, the reactor will be shut down by ejection of the reflector which is initiated by operation of the safety devices described in Section IV. Following shutdown, the reactor will continue in orbit for the design orbit lifetime of 3800 years, thus providing a sufficient decay period prior to reentry to preclude fission product hazards.

The safety devices have been designed and will be tested to acceptable reliability standards. Furthermore, two different initiating signals may actuate the EABRD while in orbit: an on-board low voltage signal and a telemetry command from ground. In addition, a backup device, the TABRD, is provided and is actuated inherently by the temperature reduction of the outlet NaK line. However, it has not been possible to test the safety devices after operation in a space and radiation environment for 1-year. Thus, the possibility of malfunction of the safety devices exists.

Failure of the safety devices could result in continuous reactor operation in orbit. If the reactor is not shut down by reflector ejection, power will gradually decay due to fuel depletion, fission product buildup, and hydrogen leakage. Since power decay and declining temperatures will diminish the rate of burnup and hydrogen loss, operation in a low power range can continue almost indefinitely. This section discusses this mode of operation and presents the results of a study of reactor behavior under such conditions.

Nearly every mode of system failure can be categorized as leading to one of two modes of circulation system failure, specifically, loss of flow or loss of NaK. Some of the causes of system failure are listed below.

a) Thermal and electrical degradation of the pump thermoelectric materials

b) Nuclear radiation damage to the pump thermoelectrics

c) High resistance film built up on the pump throat due to contamination of the NaK.

d) Breakdown of the high emissivity coating on the pump radiators

e) Loss of the bond between the thermoelectrics and the radiators in the pump

f) Loss of the bonds in the thermoelectric elements of the converter

g) Degradation of the high emissivity coating on the thermoelectric converter

h) Meteoroid puncture of the NaK line

i) Erosion of the NaK line walls or connections.

Items a through e will cause NaK stagnation in the core. Items f and g will reduce the system's heat rejection capability and produce stagnation as a secondary effect by increasing the rate of thermal degradation of the NaK pump. Items h and i will cause a loss of NaK from the system.

Based on these considerations, reactor performance was investigated from startup to the design orbit lifetime of 3800 years. As the various system failure modes can be represented by a decreasing flow and heat rejection capability, reactor power and temperature were determined as a function of time for different flow and TE converter emissivity coating degradation rates. The actual occurrence of stagnation and loss of NaK was treated separately at the time they occurred.

Available pump test data and consideration of probable pump degradation mechanisms indicated that pump degradation would most likely occur exponentially at a rate in the range of 5 to 20% per year. In addition to the pump degradation, flow would be further affected by the decreasing reactor coolant outlet temperature which reduces the efficiency of the pump thermoelectrics. Reactor outlet temperature is indirectly influenced by the T/E converter emissivity coating degradation, so that a complex relationship exists between flow decay and the factors causing it. Figure 38 shows the normalized flow rate as a function of time for exponential 5 and 10% per year pump and emissivity coating degradation rates.

The effect of pump degradation rate on power decay is illustrated in Figure 39. At any given time, the power levels for the pump degradation rates listed fall within the thick line. As this single curve shows, flow has a minor effect on power degradation. This is because power changes are initiated by

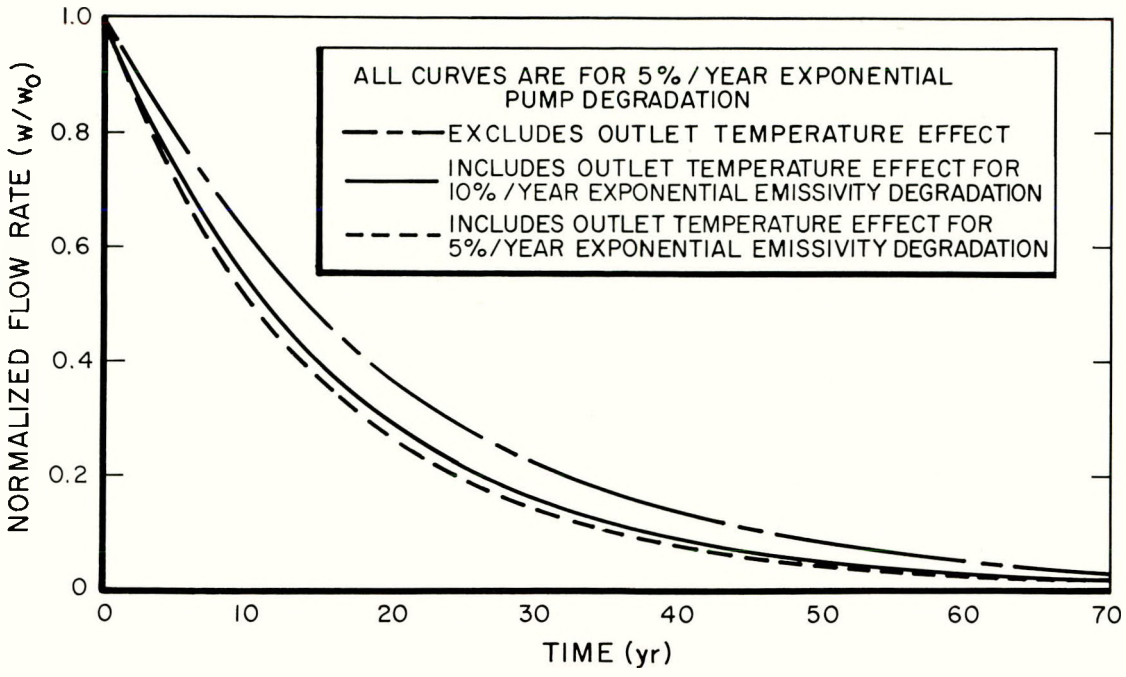

10-8-64 7623-0409-1

a. 5%/yr Pump Degradation

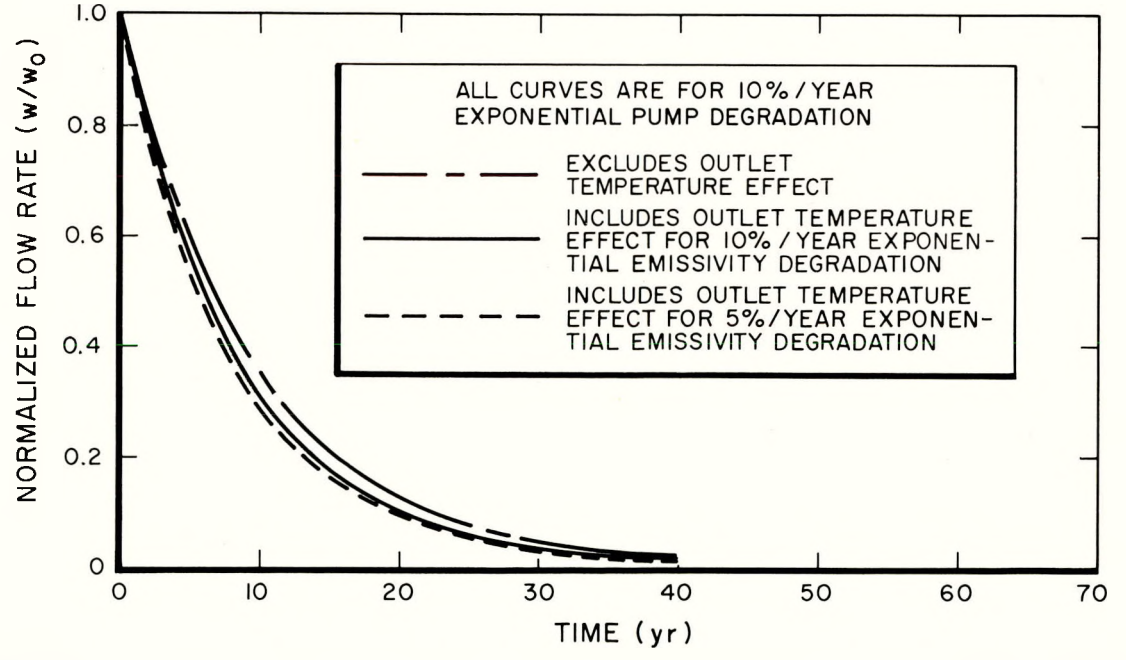

10-8-64 7623-04-9-2

b. 10%/yr Pump Degradation

Figure 38. Flow Rate Degradation

nuclear effects, such as fuel burnout, fission product poisoning, hydrogen losses and redistribution, etc. These mechanisms are not directly influenced by flow. However, to the extent that flow affects temperature or temperature distribution, an indirect effect is possible. For example, differences in flow will lead to a difference in core ΔT which would affect hydrogen losses and hydrogen redistribution. However, it takes time to establish a significantly different ΔT, and core temperature decreases with time. Hydrogen loss rates and redistribution become insignificant at low temperatures, thus vitiating the effect of flow rate degradation on power.

The thermoelectric converter aluminum radiators are coated with a thin layer of stannous oxide, with an emissivity of approximately 0.85 as compared to 0.2 for aluminum. Under the action of micrometeoroids impinging on the exposed radiator surface, the coating will be worn away, and thus the emissivity of the radiator will decrease and eventually approach that of the aluminum. The fraction of the coating lost in a given time interval is proportional to the surface area of exposed coating still remaining. Therefore, an exponential coating degradation was assumed, and rates between 0 and 10% per year were investigated. Figure 40 shows the effect of emissivity degradation rate on power decay, and although more pronounced than the effect of flow, it does not exhibit a strong dependence in the range of interest.

The crossover point of the 5 and 10% curves occurs because of the relative emissivity and temperature changes. In the early years the emissivity of the 10% case is substantially lower than the emissivity of the 5% case due to its faster degradation, while there is not much difference in NaK temperature at this time, although the NaK temperature of the 10% case is beginning to exceed that of the 5% case. Because, in both cases, the emissivity is degrading to the same value, the emissivities are very nearly equal after a substantial time. However, the NaK temperature of the 10% case becomes significantly higher than the 5% case, thus providing higher heat rejection capability and higher power. The 0% emissivity degradation case remains at a higher power throughout because it retains the higher emissivity of the stannous oxide.

Based on this information the parameters of interest for further investigation were established to be all combinations of the 5 and 10% pump and emissivity degradation rates. Analyses of the temperature and power behavior of the system in these various decay modes determined the feasible range of long

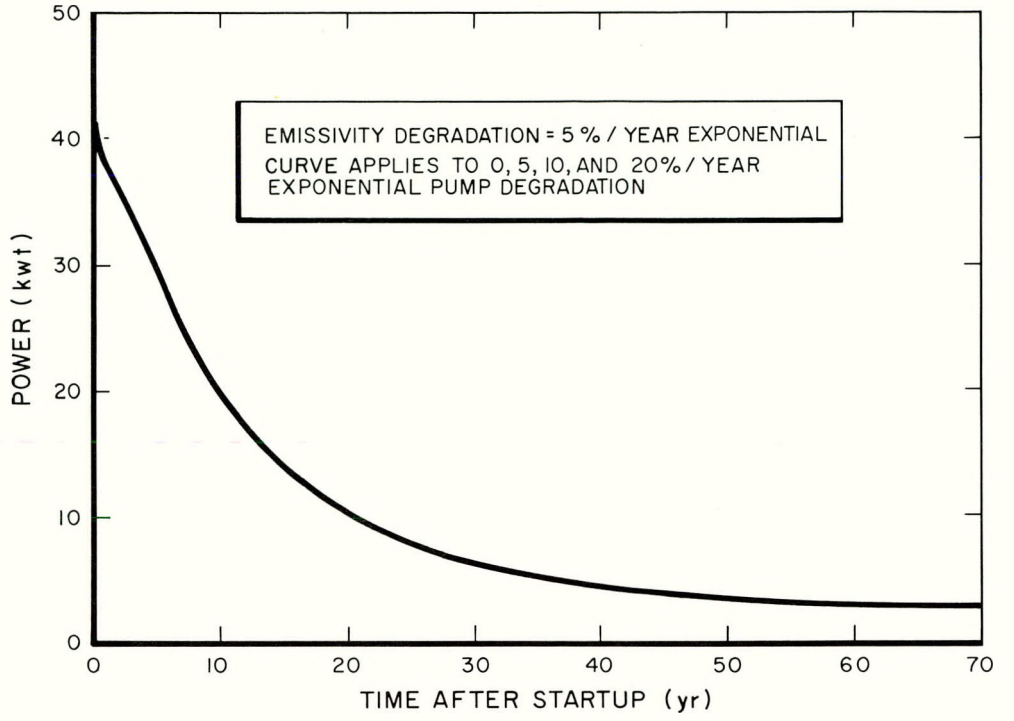

10-8-64 7623-0410

Figure 39. Effect of Pump Degradation on Power Decay

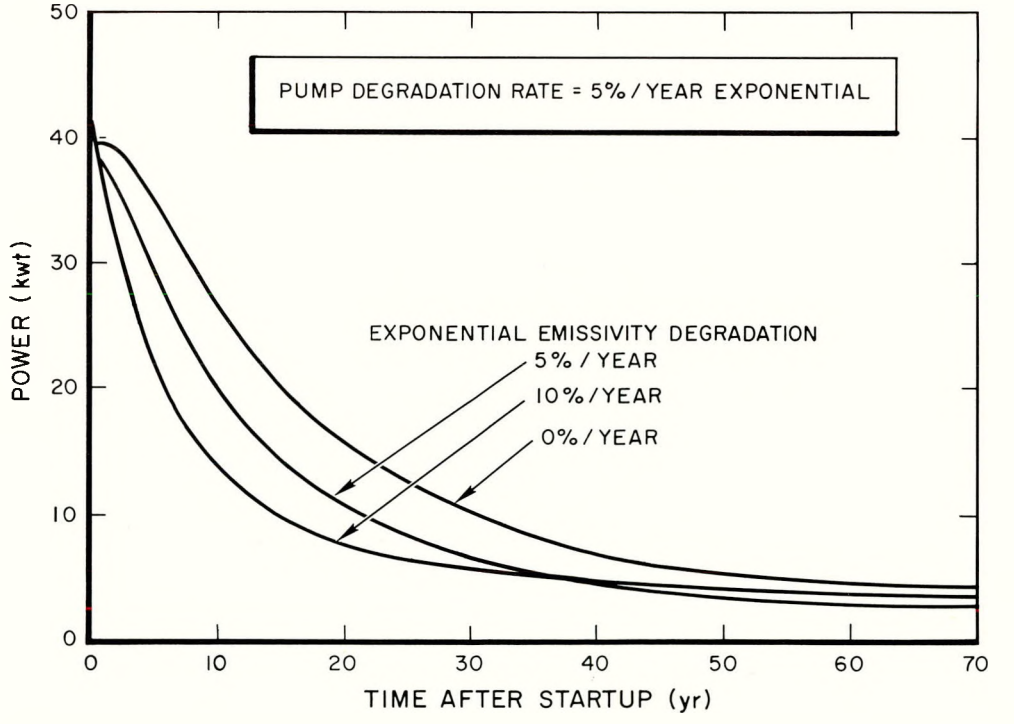

10-8-64 7623-0411

Figure 40. Effect of Emissivity Degradation on Power Decay

term reactor operation before loss of flow or loss of NaK. The results are shown in Figure 41 including the 3-day startup transient.

As discussed at the beginning of this section, there are numerous events which could cause loss of flow or loss of NaK, although it is difficult to specify at what point in time any one of these might occur. To be conservative in this study, loss of flow was assumed to occur when the flow rate had decayed to 2% of its initial value. At flow rates this low, heat transfer by conduction becomes as important as convection, so that the core heat transfer model would no longer be valid and would approach the no-flow model. The time at which stagnation (loss of flow) occurs thus depends on both the flow and emissivity degradation rates. Because the time of occurrence of the potential causes of loss of NaK (meteoroid puncture, erosion, etc.) cannot be reliably predicted, loss of NaK was assumed to occur at the same time as stagnation (but not simultaneously). Table 13 lists the time at which loss of flow and loss of NaK occurs and the reactor power and average temperature at that time. In one instance, the 10%/5% case (pump and emissivity degradation, respectively), stagnation occurred before 2% of initial flow was reached because the inlet temperature had decreased to the NaK freezing point.

TABLE 13

REACTOR CONDITIONS BEFORE AND AFTER LOSS OF FLOW OR NaK TRANSIENT

Exponential Degradation (%/yr)		Time At Which Transient Occurs (years after startup)	Loss of Flow				Loss of NaK			
			Before Transient		After Transient		Before Transient		After Transient	
Pump	Emissivity		Power (watts)	Temperature (°F)	Power (watts)	Temperature (°F)	Power (watts)	Temperature (°F)	Power (watts)	Temperature (°F)
5	5	67	2600	340	82	352	2600	340	5.5	343
5	10	70	3300	410	150	424	3300	410	27	414
10	5	32	6000	470	230	490	6000	470	70	475
10	10	38	4800	550	370	568	4800	550	170	554

The immediate or transient effect of loss of flow or loss of NaK is an abrupt change in power level and fuel temperatures. The power level will decline rather quickly due to the negative temperature coefficient. The fuel temperatures may increase initially and then decrease, or may decrease immediately depending on the power behavior and the heat transfer characteristics of the system

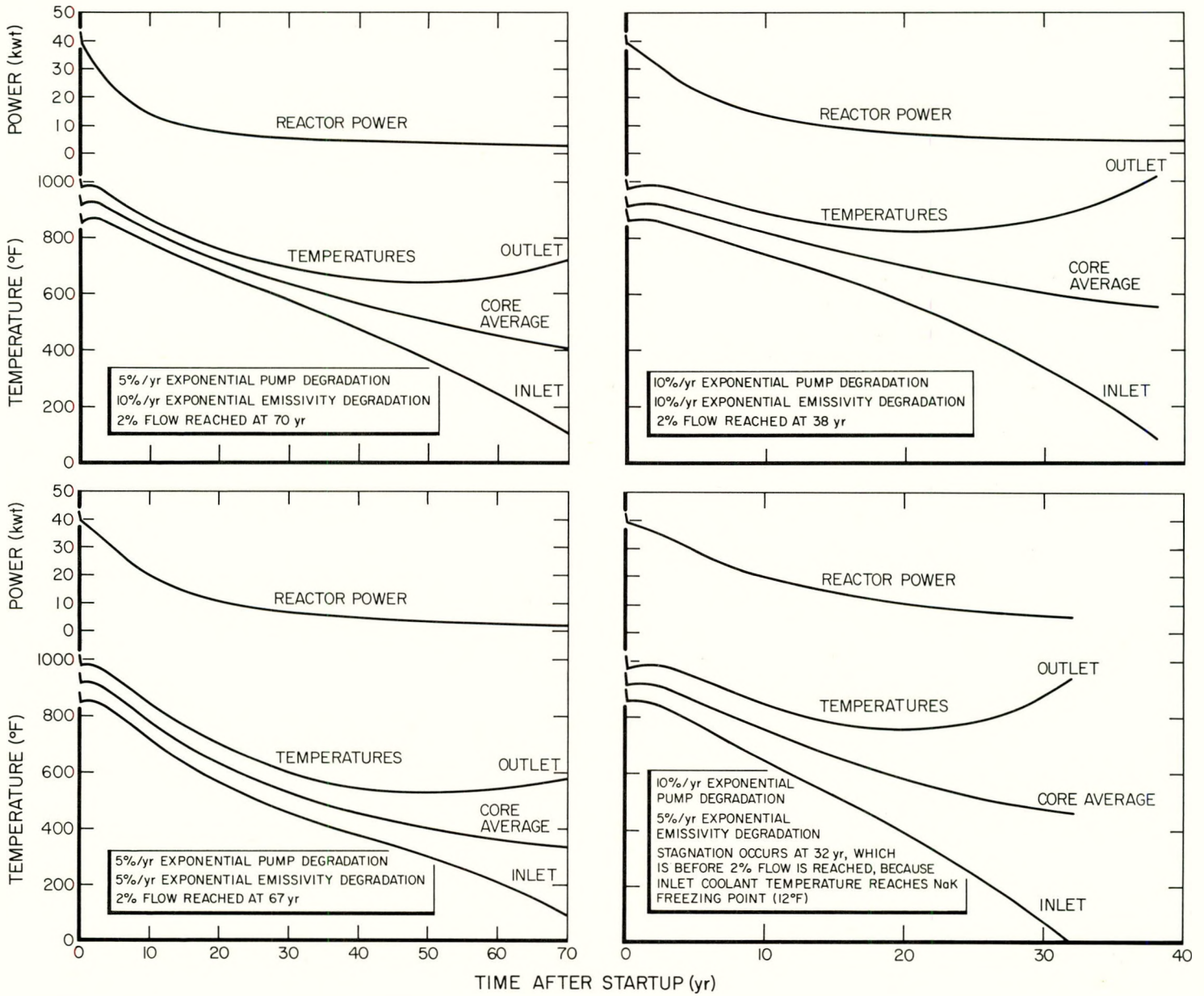

10-5-64

7623-0412

Figure 41. Operating Modes Before Loss of Flow or Loss of NaK

after the loss of flow or NaK. Following the transient, a quasi-equilibrium is reached at a power level consistent with the reactivity changes caused by the transient and the heat rejection capability of the altered system. Table 13 also lists the power level and core temperature reached after the transient for the various cases of interest. A very slow power decay then takes place from the quasi-equilibrium condition.

Figure 42(a) illustrates the power and maximum fuel temperature as a function of time during the loss of NaK transient initiated at the two percent flow conditions for the case of 10%/yr exponential pump and emissivity degradation. This case results in the highest fuel temperature of any of the end-of-life conditions considered. Loss of flow would result in a lower fuel temperature due to better heat transfer with NaK in the core. However, since the maximum fuel temperature attained during the transient is a function of the initial power level, the loss of NaK and flow transients were also analyzed from full power conditions. Figure 42(b) shows the loss of NaK transient from essentially full power after two years operation. Even under these conditions, the maximum fuel temperature is below the damaging level. Thus, in no case do the loss of NaK or flow transients result in conditions which would destroy the core; therefore, continued operation at very low power levels would occur as described below.

The power decay following the occurrence of loss of flow and loss of NaK was determined for each case of interest until the design orbit lifetime of 3800 years was reached. Gradual power reduction is caused by fuel burnup, fission product poisoning and hydrogen loss which would be very slow due to the reduced core temperature. The constantly declining core temperature compensates for the reactivity losses through the negative temperature coefficient. Figure 43 illustrates the complete power history from startup to design orbit lifetime for each case considered when loss of flow occurs; Figure 44 provides the same information for the loss of NaK situation. The power decay is based on radiation of heat from the reactor to space conditions averaged between full sun and dark sky.

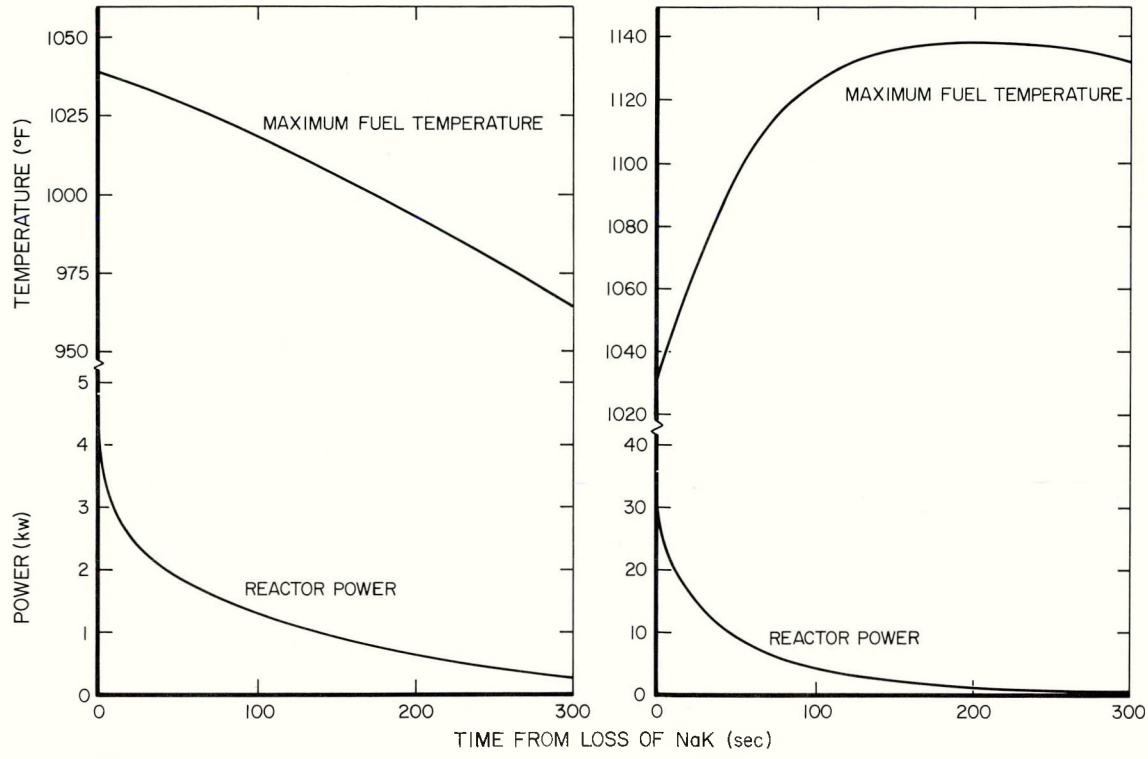

10-8-64 7623-0518-1-2

a. Loss From End of Life Conditions for 10%/yr Case

b. Loss From Full Power After 2-yr Operation

Figure 42. Transient Conditions Following Loss of NaK

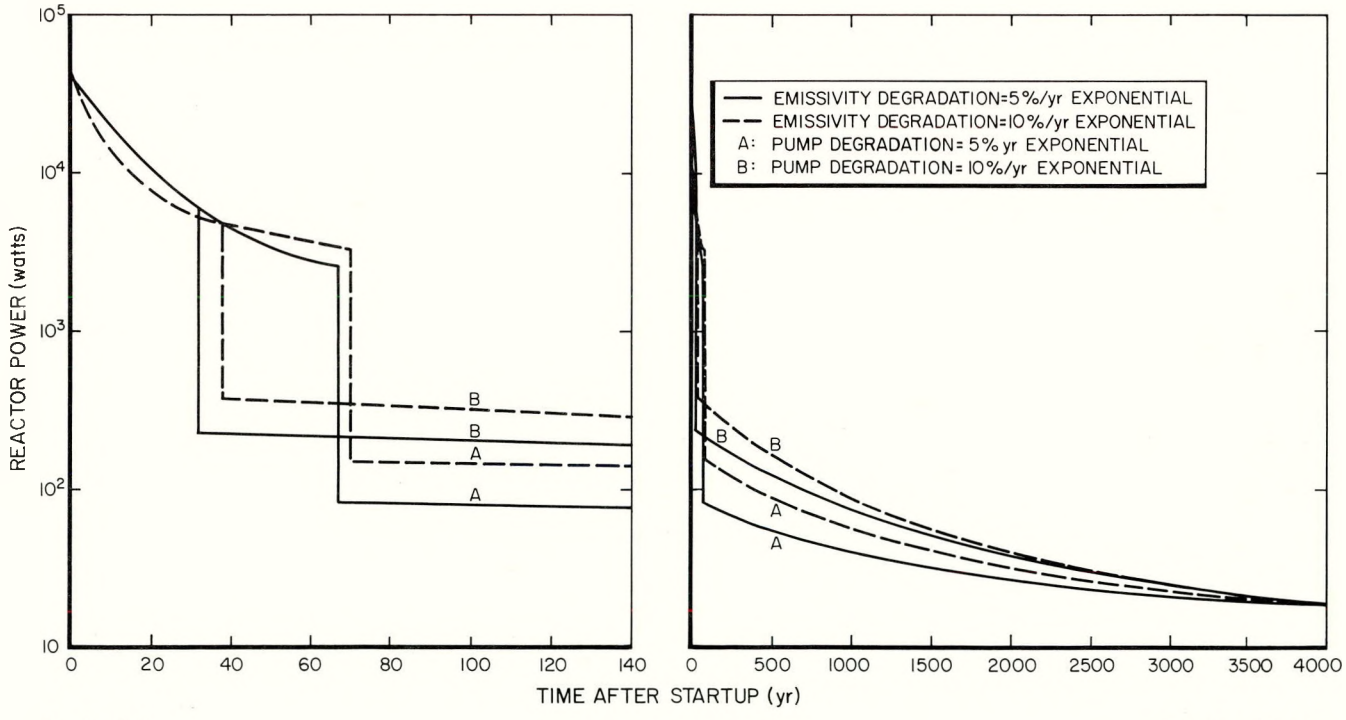

10-8-64 7623-0519

Figure 43. Long-Term Power Decay With Loss of Flow

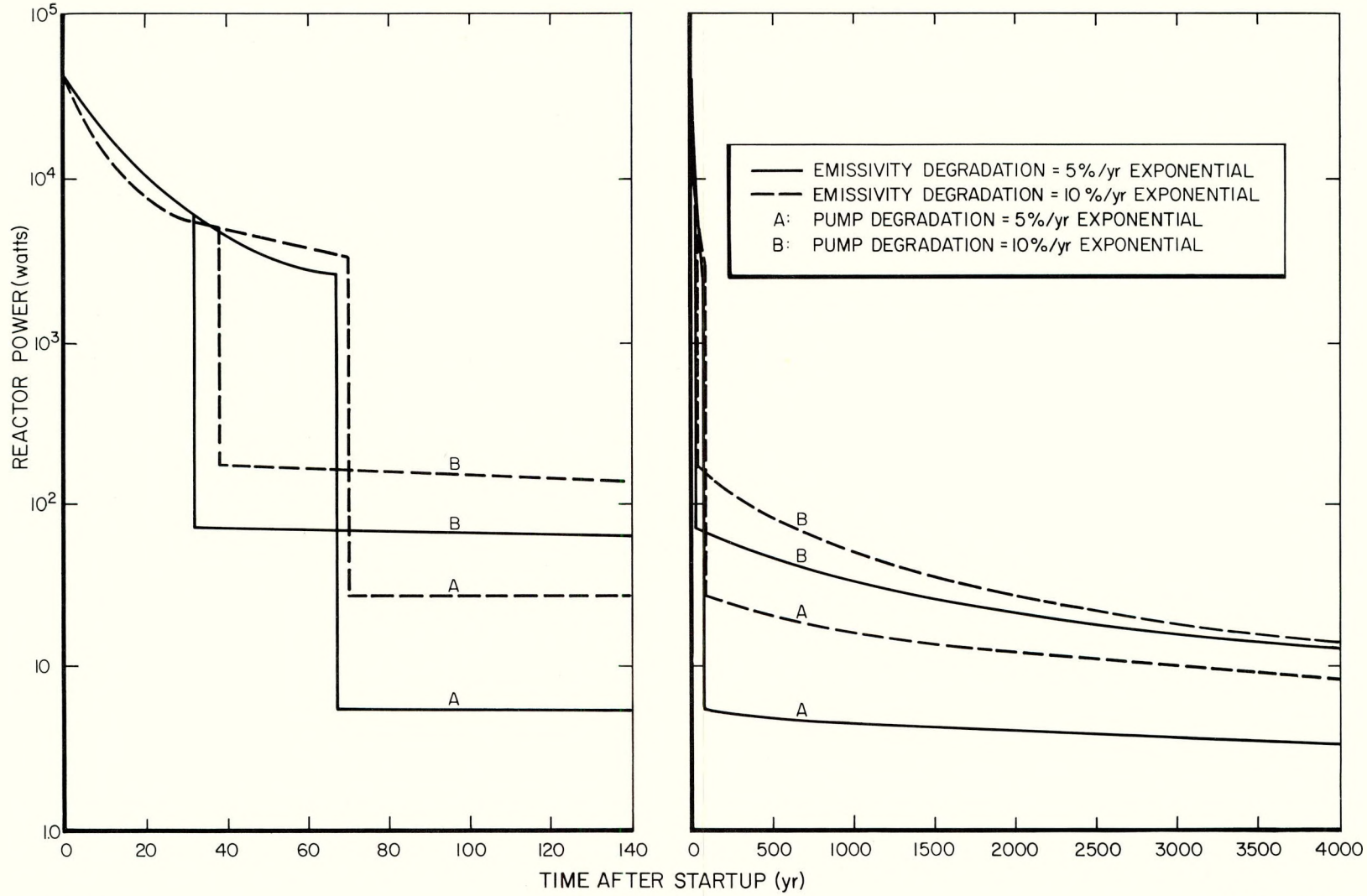

Figure 44. Long-Term Power Decay With Loss of NaK

REFERENCES

1. A. W. Thiele, and C. A. Guderjahn, "SNAP 2 Hydride-Moderated Critical Assembly," NAA-SR-3620 (1959) Secret

2. L. A. Wilson, "SNAP 2 Experimental Reactor Physics Analysis," NAA-SR-3607 (1959) Secret

3. F. H. Clark, et al., "Analysis of S2DR Design," NAA-SR-5890 (1961)

4. H. P. Flatt, and D. C. Baller, "The AIM-6 Code," NAA-SR-4694 Addendum (1960)

5. S. Stone, "ZOOM, A One-Dimensional Multi-Region, Multi-Group Diffusion Code for the 704," U. C. R. L. 5293 (1960)

6. E. L. Wachspress, "A Generalized Two-Space Dimension Multigroup Code for the IBM-704," KAPL-1724 (1957)

7. D. S. Vargofcak, "ULCER," NAA Program Description AMTD-123 (1962)

8. B. Lemke, "FORTRAN SNG Code," NAA Program Description (1959)

9. K. L. Rooney, "FARSE-1A, A Modification of FARSE to Include Angular Dependence of Shield Leakage," TDR 5954 (1960)

10. C. A. Goetz, "SCAR-1, Scattered Fast Neutron Current From an Ion Motor Ring," NAA-SR-6191 (1961)

11. General Electric Aircraft Nuclear Propulsion Department, "Shielding Computer Program 14-0 and 14-1 Reactor Shield Analysis," XDC59-2-16 (1959)

12. L. S. Mims, "Analysis of SNAP 10A Reactor Immersed in Slowly Rising Water," NAA-SR-MEMO-8271 (1963)

13. D. F. Paddleford, and R. W. Winson, "10FS-1 Accident Analysis," NAA-SR-MEMO-8325 (1963) Confidential